

QUANTUM DIFFUSION AND SPIN DYNAMICS OF MUONS IN COPPER

Graeme Luke

B.Sc., Queen's University, 1984

A THESIS SUBMITTED IN PARTIAL FULFILLMENT OF
THE REQUIREMENTS FOR THE DEGREE OF
DOCTOR OF PHILOSOPHY

in

THE FACULTY OF GRADUATE STUDIES
DEPARTMENT OF PHYSICS

We accept this thesis as conforming
to the required standard

THE UNIVERSITY OF BRITISH COLUMBIA

September 1988

© Graeme Luke , 1988

In presenting this thesis in partial fulfilment of the requirements for an advanced degree at the University of British Columbia, I agree that the Library shall make it freely available for reference and study. I further agree that permission for extensive copying of this thesis for scholarly purposes may be granted by the head of my department or by his or her representatives. It is understood that copying or publication of this thesis for financial gain shall not be allowed without my written permission.

Department of physics
The University of British Columbia
1956 Main Mall
Vancouver, Canada

Date:

16/9/88

Abstract

We have studied the quantum diffusion of positive muons in pure copper over the temperature range $20 \text{ mK} \leq T \leq 200 \text{ K}$ using the technique of muon spin relaxation (μSR). The rate of diffusion has been deduced from its effect upon the muon polarization function. The measurements were made in a weak longitudinal external magnetic field, where the spin relaxation has proved to be the most sensitive to the muon hop rate below 150 K.

Our results for the behaviour of the muon hop rate are well explained by the recently developed theories of the quantum diffusion of light interstitials in metals by Kondo, Yamada and others. These theories stress the effects of the conduction electrons in the metal in providing a form of “friction”, retarding the diffusion process.

In addition we have utilized the technique of level-crossing resonance spectroscopy, in its first application to μSR measuring the electric quadrupole interaction strength of the copper nuclei. These results have enabled us to show that the muon occupies the same octahedral site at all the temperatures studied. This allows one to rule out the possibility of metastable muon sites contributing to any significant portion of the muon polarization.

Contents

Abstract	ii
List of Tables	vi
List of Figures	viii
Acknowledgement	ix
1 Introduction	1
1.1 History of the Study of Muons in Copper	3
1.2 Muons	6
1.3 Muon Spin Research	8
1.4 μ SR Techniques	10
1.4.1 Time-Differential μ SR	11
1.4.2 Time-Integral μ SR	13
1.5 μ SR Facilities	13
1.6 μ^+ in Copper—Previous Work	16
1.6.1 Transverse Field Experiments	18
1.6.2 Zero Field Experiments	20
1.6.3 Level-Crossing Resonance	21
1.6.4 Pion Decay-Site Spectroscopy	22

1.7	Muon Diffusion	23
1.7.1	Diffusion in Copper	23
1.7.2	Diffusion in other Metals	26
2	Relaxation Functions	35
2.1	Kubo-Toyabe Theory	36
2.1.1	Zero Field	36
2.1.2	Longitudinal Field	37
2.2	Quantum Mechanical Zero Field Calculations	39
2.3	Exact Static Theory	42
2.4	Level-Crossing Resonance	46
2.5	Strong Collision Model for Diffusion	48
3	Diffusion Theories	58
3.1	Flynn and Stoneham Theory	58
3.2	Teichler Theory	60
3.3	Kagan-Klinger Theory	61
3.4	Kondo Theory	62
3.5	Yamada Theory	68
4	Experimental Techniques	71
4.1	Time-Differential μ SR	72
4.1.1	Transverse Field	74
4.1.2	Longitudinal and Zero field	76
4.2	Integral μ SR	77
4.3	Experimental Apparatus	79
4.3.1	Muon Beamlines	79

4.3.2	μ SR Spectrometers	81
4.3.3	Data Acquisition System	83
4.3.4	Cryogenics — Above 4.2 K	84
4.3.5	Cryogenics — Dilution Refrigerator	85
4.3.6	Data Analysis	87
4.4	Samples	87
5	Results	96
5.1	Quadrupolar LCR	96
5.1.1	Quadrupolar Interaction	97
5.1.2	Muon Site	98
5.2	Hop Rate	101
6	Conclusions	117
	Bibliography	119
A	Muon Diffusion Rates in Copper	133

List of Tables

1.1	Selected properties of muons	7
1.2	Selected properties of metals	17
5.1	Parameters extracted from hop rate results, for Kondo's model for the muon hop rate.	108

List of Figures

1.1	Schematic representation of various diffusion processes	30
1.2	Radial plot of positron emission probability	31
1.3	Raw spectrum in transverse field geometry, showing muon precession and lifetime.	32
1.4	Muon Site in Copper Lattice, also shown is tetrahedral site	33
1.5	Calculated linewidths of muon precession signals for applied fields trans- verse to the $\langle 100 \rangle$, $\langle 110 \rangle$, and $\langle 111 \rangle$ crystal orientations. (From refer- ence [1])	34
2.1	Kubo-Toyabe Theory– Static Muon Polarization vs. Time, in zero field and several longitudinal fields ω_0/Δ	38
2.2	Zero field relaxation of muons in NaF, caused by dipolar interactions . .	52
2.3	Exact Muon Polarization function — 6 nn Cu atoms, $\langle 110 \rangle$ orientation .	53
2.4	Comparison between KT and Exact Theory	54
2.5	Portion of Hamiltonian matrix for muon interacting with spin-3/2 nucleus	55
2.6	Copper energy level diagram for electric quadrupolar and Zeeman inter- action.	55
2.7	Muon Polarization in ZF with hopping	56
2.8	Muon Polarization Function in WLF with hopping.	57

3.1	Kondo Theory — Hop rate versus temperature.	68
4.1	Corrected asymmetry for a typical transverse field experiment, showing muon precession as well as relaxation.	89
4.2	Weak transverse field geometry.	90
4.3	Longitudinal and zero field geometry	91
4.4	Omni – μ SR spectrometer, showing counter-cryostat geometry used for ZF and LF measurements.	92
4.5	Electronics arrangement for time-differential μ SR experiments	93
4.6	Timing of data acquisition events	94
4.7	Oxford Dilution Refrigerator	95
5.1	Integral measurement of longitudinal relaxation. Field applied along the $\langle 110 \rangle$ direction. Inset: expanded vertical scale	111
5.2	Time-differential spectra at level-crossing resonance	112
5.3	WLF TD- μ SR spectra at low hop rate	113
5.4	WLF TD- μ SR spectra for rapidly hopping muons	114
5.5	Dynamic relaxation functions in ZF and 15 G longitudinal field, with hop rate ν_{hop} between 0 and $3 \mu s^{-1}$	115
5.6	Muon hop rate over the temperature range $20 \text{ mK} < T < 200 \text{ K}$	116

Acknowledgement

Experiments at an accelerator necessarily involve the efforts of a relatively large group of people to ensure their success. As a result of this, I have been fortunate to have been able to work with other members of the TRIUMF μ SR group on a number of research projects outside of this thesis, all of which I have enjoyed immensely. Syd Kreitzman and Rob Kiefl have both been extremely good teachers over the years and have always taken the time to discuss and explain the physics of their respective experiments. I would also like to express my thanks to the other scientists who assisted in these experiments including Eduardo Ansaldo, Stan Dodds, Tanya Riseman and Dale Harshman. The contributions and guidance of my supervisor Jess Brewer, who has realized the importance of my being able to work on a number of experiments, as well as travel to conferences, while retaining some focus on this thesis have been greatly appreciated. Finally, the technical assistance which has been provided by John Worden, Keith Hoyle and Curtis Ballard has been invaluable in carrying out the experiments described in this thesis.

Chapter 1

Introduction

This thesis deals with the properties of positive muons implanted into copper. Of primary interest is the diffusive behaviour these muons exhibit as a function of temperature. In the course of studying the muon diffusion, we have also studied the muon site in the copper lattice, since the nature of this site affects the interpretation of the diffusion results.

The study of diffusion of light interstitials in metals has generated intense theoretical and experimental interest, primarily because various quantum effects are expected and have in fact been observed. Light interstitials are also the most likely to exhibit anomalous behaviour at low temperatures, as a result of their low mass. The field of hydrogen in metals has been extensively studied; hydrogen isotopes diffuse the most quickly of all atomic interstitials and offer a wide range of masses (factor of 3) with which to test theories concerning diffusion. In addition, hydrogen isotopes are the simplest impurities and therefore the most tractable theoretically.

Various authors, including Kehr [2] and Fukai and Sugimoto [3], have described four different mechanisms for the diffusion of hydrogen isotopes in metals, each of which may be operative at various temperatures. These are shown schematically in Figure 1.1. At the lowest temperatures, no phonons are present and either coherent

tunnelling or hopping dominates the diffusion. Here, the interstitial is in a self-trapped state (*i.e.* localized in a potential created by its presence) and quantum mechanically tunnels to a neighbouring site (along with any lattice distortion field it may cause) with no change in the phonon system.

At higher temperatures, few-phonon processes will become important. Lattice vibrations can bring the energy levels of two neighbouring self-trapped sites to the same value, allowing tunnelling. This process is referred to as thermally activated tunnelling.

At even higher temperatures thermally activated over-barrier hopping is possible. The energy for these over-barrier hops is provided by phonons. At the highest temperatures, the diffusing particle is no longer self-trapped in the interstitial potential and undergoes free motion, similar to atomic motion in gases.

The positive muon μ^+ , with its mass approximately 1/9th that of a proton, can also be implanted into metals, extending the mass range of hydrogen-like impurities an order of magnitude lower. As a result of its low mass, the muon provides a severe test for theories of quantum diffusion.

Many of the muon's interactions in matter may be observed through their effects on the muon's spin. That the time development of the muon spin can be observed is a consequence of the parity-violation of the weak interaction, which causes the muons to be produced in a 100% spin-polarized state and to subsequently decay, emitting a positron preferentially along the direction of the muon spin. As will be discussed in detail, this parity violation makes it possible to study muon spin relaxation. Through this relaxation, the muon's diffusive behaviour may be deduced in a manner similar to that of other magnetic resonance spectroscopies, such as NMR.

This thesis is divided into a number of sections. First a general introduction will be given, both to the experimental field of μ SR and also to some of the previous work in the field of quantum diffusion of muons in copper. Some theoretical background will be

described, concerning both the interpretation of the μ SR data and the understanding of the mechanisms important in light interstitial diffusion. Finally, there will be a detailed description of our experiments performed at TRIUMF¹ and their results, which are interpreted in terms of recent theories for quantum diffusion.

1.1 History of the Study of Muons in Copper

If one starts with initially spin-polarized muons and applies a magnetic field perpendicular to that polarization, the subsequent muon precession will be observed in the angular distribution of emitted positrons. Different muons throughout the sample may experience slightly different fields, due perhaps to random dipolar fields from the host nuclei. As a result, there will be some dephasing of the spins, resulting in relaxation of the polarization. This is the familiar “ T_2 ” relaxation seen in nuclear magnetic resonance (NMR). If the muons diffuse within their lifetime the effects of these random fields will tend to be averaged out and the relaxation rate will decrease, as the signal is “motionally narrowed”. The amount of narrowing of the precession line (the Fourier transform of the polarization function) can then be used to infer the diffusion rate. This was the basis of the first experiment on muons in copper [4], where the muon hop rate was seen to decrease with decreasing temperature from room temperature down to approximately 80 K, below which it appeared that the muons were completely static.

The muon site was a matter of interest in the study of the properties of muons in materials as the choice of sites affected the interpretation of the diffusion results. Hartmann [1] showed that the relaxation rate of the muon polarization was both field

¹Meson facility of the University of British Columbia, University of Victoria, Simon Fraser University and University of Alberta

and orientation dependent, and that this dependence was a characteristic of the symmetry of the muon site. As a result, Camani *et al.* [5] were able to show that the muon primarily occupied the site with octahedral symmetry, at the center of the copper face-centered cubic unit cell. They found better agreement between the calculated relaxation rates and their measured values if they assumed that the muons caused a local deformation of the lattice, pushing away their nearest neighbours by $\sim 5\%$ of their unperturbed separation.

The μ^+ , being a positively charged particle, attracts a screening cloud of conduction electrons around it after it stops in a metal. The fractional difference of the muon precession frequency in media from its vacuum value, a result of paramagnetic screening by nearby electrons, is called the Knight shift. Its value for muons in copper has been measured to be approximately 60 ppm [6]. These electrons do not form a muonium (μ^+e^-) state in metals since there is such a rapid exchange of electrons around the muon that the effects of each individual electron are averaged to zero. In other words, the electron exchange rate is much greater than the hyperfine frequency, hence the muon precession is essentially unaffected by the nearby electrons.

At this point (in 1981) it appeared that a complete understanding of the diffusion of muons in copper had been reached, until it was discovered [7,8] at CERN that at even lower temperatures, below 20 K, there was a decrease in the rate of relaxation of the spin polarization. Thus it appeared that the muons were diffusing again, with the hop rate increasing with decreasing temperature. Other explanations, however, such as a change in the muon site, were also consistent with the data, and thus another technique became necessary to differentiate between the various possibilities.

Since the muons are initially highly (often 100%) polarized, a large static field is not needed to generate a measurable polarization as is the case in many other types of spectroscopy, such as NMR. It is therefore possible to observe the evolution of the

polarization in zero applied field (ZF). The ZF measurements of Clawson [9,10] and Kadono [11,12] were used to extract the muon hop rate and found to be more sensitive than the transverse field (TF) method in the limit of slow hopping. Their results also showed that the hop rate was increasing with decreasing temperature below 20 K. Although these measurements were consistent with an unchanged muon octahedral site, it was still possible to construct models involving metastable sites [13,14] of different symmetry which would cause spin relaxation which closely resembled that at the octahedral site.

The application of a weak longitudinal field (WLF) provided further confirmation that in fact the muon diffusion rate was increasing with decreasing temperature below 20 K [15,16]. It also demonstrated that the changes in the polarization could not be due to the partial occupation of various metastable sites. The WLF method has also proved to be the inherently most sensitive technique for the extraction of hop rates from the spin relaxation functions, as will be discussed later.

Most recently, the level-crossing resonance (LCR) technique [17] has been applied to the system of muons in copper. Level-crossing, discussed in detail in a later section, is a double resonance technique allowing the direct measurement of the copper electric quadrupole interaction strength. This interaction is caused by the electric field gradient (EFG) from the muon acting on the spin-3/2 copper nuclei and is sensitive to the microscopic arrangement of those nuclei around the muon. These measurements demonstrate that the muon site remains unchanged over all temperatures studied to date.

1.2 Muons

Muons were first observed in cosmic ray experiments in 1937 [18,19]. Their parity-violating decay was predicted by Lee and Yang [20] and first observed in 1957 [21,22] in two different experiments, one of which [21] was in effect the first muon spin rotation experiment.

The μ SR technique relies upon the parity violation of the weak interaction. Muons (which are leptons) exist as both positively and negatively charged particles, with properties which are essentially identical to those of electrons (except for a larger mass and the fact that they decay). Muons are created from pions in the weak decays

$$\begin{aligned}\pi^+ &\rightarrow \mu^+ + \nu_\mu \\ \pi^- &\rightarrow \mu^- + \bar{\nu}_\mu\end{aligned}\tag{1.1}$$

with an average pion lifetime $\tau_\pi = 26.03$ ns. In the pion rest frame, muons are emitted isotropically in pion decay as there is no preferred direction (since pions have spin 0). Because only left handed neutrinos exist, the positive muons must also be emitted with negative helicity in order to conserve both angular and linear momentum. This means that in the pion rest frame the muons are created 100% spin polarized, with their spins antiparallel to their momentum. Some of the important properties of the muon are given in table 1.1.

Muons themselves decay weakly, into a three-body final state.

$$\begin{aligned}\mu^+ &\rightarrow e^+ + \nu_e + \bar{\nu}_\mu \\ \mu^- &\rightarrow e^- + \bar{\nu}_e + \nu_\mu\end{aligned}\tag{1.2}$$

Whereas muons are emitted isotropically in pion decay, the muon spin provides a preferred direction for the decay positrons. Energy and momentum conservation causes

Table 1.1: Selected properties of muons

Mass	105.6595 MeV/c ² = 206.77 × m _e = 0.1126 × m _p
Charge	±e
Spin	I = $\frac{1}{2}\hbar$
Magnetic Moment	3.183452(10) × μ _p
Gyromagnetic Ratio (γ _μ /2π)	13.55342 kHz/G
Lifetime τ _μ	2.19714(7) μs
Direction of Moment	μ _μ = ± γ _μ I for μ [±]

the direction of the emitted positron to be correlated with the direction of the muon spin. This parity violation is also a consequence of the fact that only left-handed neutrinos exist. The positron need not be emitted exactly along the muon spin direction; the angular dependence of the decay probability is a function of the positron energy, as shown in equation 1.3. There is, however, a sufficient correlation between the muon spin and the direction of emission of the positron to allow the measurement of the muon polarization after averaging over a number of decays.

Neglecting the rest energy of the positron (511 keV), the probability p per unit time of an e^+ being emitted into solid angle $d\Omega$ at an angle θ from the muon spin is given by:

$$dp(\epsilon, \theta) = \frac{1}{\tau_\mu} [1 + a(\epsilon) \cos \theta] n(\epsilon) d\epsilon d\Omega \quad (1.3)$$

where

$$\epsilon = \frac{E(e^+)}{E_{max}(e^+)},$$

$$n(\epsilon) = \frac{1}{2}\epsilon^2(3 - 2\epsilon),$$

$$\text{and} \quad a(\epsilon) = \frac{2\epsilon - 1}{3 - 2\epsilon} \quad (1.4)$$

This probability, integrated over all positron energies, is shown in figure 1.2 as a function of the polar angle θ . The reduced positron kinetic energy is ϵ , with the maximum positron energy $E_{max} = 52.8$ MeV. The average positron energy $\bar{E} = 36$ MeV is found by integrating over the probability distribution in equation 1.3. Similarly, the average asymmetry $\bar{a} = 1/3$. The asymmetry factor $a(\epsilon)$ in equation 1.4 is actually negative at the lowest positron energies, and equal to 1.0 at the maximum energy. A positron with 52.8 MeV kinetic energy will have zero probability of having been emitted exactly opposite to the muon spin direction at the time of the decay.

1.3 Muon Spin Research

Muon Spin Relaxation/Rotation/Resonance (μ SR) refers to a collection of techniques in which positive muons are injected into a target material of interest, with which they interact electromagnetically [23,24,25,26]. The *μ SR Newsletter* in its definition of μ SR states

μ SR stands for Muon Spin Relaxation, Rotation, Resonance, Research, or what have you. The intention of the mnemonic acronym is to draw attention to the analogy with NMR and ESR, the range of whose applications is well known. Any study of the interactions of the muon spin by virtue of the asymmetric decay is considered μ SR, but this is not intended to exclude any peripherally related phenomena, especially if relevant to the use of the muon's magnetic moment as a delicate probe of matter.

These interactions allow the microscopic properties of the material be probed on the timescale of the 2.2 μ s muon lifetime. All of the experiments discussed in this thesis

involve positive muons. Negative muons behave rather differently in condensed media, where they immediately become tightly bound to the host nuclei, and effectively give rise to substitutional impurities, rather than interstitial ones.

A number of germinal μ SR studies were conducted in the 1960's following the discovery of parity violation. Some of these first experiments were actually experimental tests of quantum electrodynamics (QED). Three principal experimental measurements — the muonium (μ^+e^-) hyperfine splitting (ν_0) [27], the muon magnetic moment (μ_μ) [28] and the muon anomalous magnetic moment ($g_\mu - 2$) [29] — together provided excellent agreement with the predictions of QED, and were considered one of the most stringent tests of the theory.

It was, however, not until the 1970's that μ SR became widely applied to problems in condensed matter physics and chemistry following the development of so-called “meson factories” such as TRIUMF, PSI²(formerly SIN) and LAMPF³, which were able to produce large fluxes of spin-polarized positive muons.

A great number of systems in both chemistry and physics have been studied with the μ SR technique. Significant contributions have been made to the study of dilute magnetic systems, such as spin glasses [30], as well as to the study of muonic radicals (paramagnetic molecules incorporating muonium as the chemical analogue of hydrogen) in liquids, solids and gases [31,32]. Muon defect centers have been studied in semiconductors [33,34], where the analogous hydrogen centers are either very difficult to study or too difficult to form. Recently, μ SR has been used to study the magnetic properties of the new high- T_c superconductors [35,36] and their related magnetic materials[37,38].

The area which has perhaps been most extensively studied with μ SR has been the diffusion of light interstitials in metals, where muons can be considered an extremely

²Paul Scherrer Institute, at Villigen Switzerland

³Los Alamos Meson Physics Facility

light isotope of hydrogen. This has allowed the testing of models for diffusion over an isotopic mass range of approximately $0.1m_p$ to $3m_p$ (for μ^+ , p , d , t) with singly charged impurities. Although from a fundamental point of view, the positive muon is most similar to a positron, in condensed matter its behaviour is strongly affected by its mass, with the result that its interactions more closely resemble those of the proton.

One of the most attractive features of μ SR is that usually only one μ^+ is in the sample at any time, making it an infinitely dilute probe. As a result, probe-probe interactions, which must be carefully considered when studying implanted hydrogen in metals, can be completely ignored in μ SR. Additionally, since the muons generally start out 100% polarized, one is able to perform an experiment on a small ensemble of muons, whereas other spectroscopies with smaller levels of polarization require many more spins to obtain a signal. A typical μ SR spectrum will contain the information from a few million muons, whereas an NMR spectrum might require 10^{18} spins.

It should be pointed out that although samples are exposed to ionizing radiation both through the initial implantation of the muons and through the subsequent muon-decay positrons, radiation damage to the sample is negligible.

1.4 μ SR Techniques

A μ SR experiment involves the implanting, generally one at a time, of highly polarized positive muons. These muons come to rest in the target and sample the local magnetic environment through their spin. The decay positrons are monitored to give information on how the muon spin evolved before decaying.

There are a number of experimental techniques which are used in μ SR experiments. The most widely used is the time-differential experiment, used to measure the time-development of the muon polarization function. Integral μ SR experiments have

recently become widely used for double-resonance or level-crossing experiments. Other techniques such as stroboscopic μ SR and muon channeling were not used in this work and are described elsewhere (see for example reference [25]).

1.4.1 Time-Differential μ SR

In a time-differential μ SR experiment the polarization of a muon ensemble is measured as a function of the time after its implantation in a sample. A direct result of the requirement to measure this time difference is that at a continuous beam facility such as TRIUMF, where the muons arrive more or less at random, only a single muon can be allowed in the sample at a time. This is so that a detected decay positron can be unambiguously associated with the muon whose spin direction it reflects. At pulsed beam facilities, such as RAL⁴ and BOOM⁵, each beam pulse contains a large number of muons, all of which arrive at approximately the same time, and it is therefore unnecessary to be able to associate a given positron with an individual muon; such pulsed facilities, of course, have a time resolution limited by the width of the beam pulse.

Typically, a muon enters the sample after passing through a thin scintillation counter, which signals the start of an event. After some length of time the muon decays, emitting two neutrinos (which are not observed) and a positron which is detected in another scintillation counter. For each detector, a histogram of detected positrons is kept as a function of the time difference between when the muon enters the sample and when it decays. After a macroscopic period of time, the number of detected positrons in a given histogram, (for example, that corresponding to the back (*B*) counter), will

⁴Rutherford Appleton Laboratory at Chilton, United Kingdom

⁵Booster Muon Facility at Ko-Energie Kenkyujo (High Energy Laboratory), Japan's national accelerator laboratory in Tsukuba, Japan.

be:

$$N_B(t) = N_0^B \left(B_B + e^{-t/\tau_\mu} \left[1 + A_0^B \mathcal{P}(t) \right] \right) \quad (1.5)$$

where B_B corresponds to the fraction of time-independent background events, A_0^B is the asymmetry of the B counter and \mathcal{P} is the muon polarization function. The asymmetry of a given counter can be found by integrating the product of the detector efficiency, the positron energy spectrum $n(\epsilon)$ and the asymmetry $a(\epsilon)$ given in equation 1.4 over the positron energy ϵ and the solid angle subtended by the counter. If all positrons were detected with 100% efficiency in a counter with infinitesimal solid angle, its asymmetry would be exactly 1/3; typically, actual values of the asymmetry lie in the range $0.2 \leq A_0 \leq 0.4$. The raw spectrum for a single counter in a transverse applied field is shown in figure 1.3.

Generally counters are arranged in opposing pairs, 180° to each other. Signals from these two counters, say F and B , corresponding to forwards and backwards, have their time-independent background subtracted to give the signals $\mathcal{F}(t)$ and $\mathcal{B}(t)$. An experimental asymmetry is then defined:

$$\mathcal{A}(t) \equiv \frac{\mathcal{B}(t) - \mathcal{F}(t)}{\mathcal{B}(t) + \mathcal{F}(t)} \quad (1.6)$$

In the case where the counters are identical and symmetric, then the asymmetry $\mathcal{A}(t)$ is simply proportional to the muon polarization $\mathcal{P}(t)$. Otherwise, small corrections are needed to extract the polarization function, as shown in chapter 2.

Two useful experimental geometries are possible, depending on the relative orientations of the initial muon polarization and the applied field (if any). In the transverse field (TF) geometry, the muon spins are initially perpendicular to the applied field, about which they precess. In the zero/longitudinal field (ZF/LF) geometry, the muon spins are initially polarized along the direction of any applied field, normal to the planes of the positron detectors.

1.4.2 Time-Integral μ SR

It is not always necessary to completely determine the entire muon polarization function. In some instances it is sufficient to measure only its integrated value over some length of time (which is long relative to the muon lifetime). In this case, one is no longer restricted to have only one muon in the sample at a time. This allows the use of greatly increased muon count rates, which provides increased sensitivity in some types of experiments. Integral experiments, which can be performed in an essentially similar manner at continuous or pulsed facilities, will be discussed in greater detail in a later section.

1.5 μ SR Facilities

At present, there are facilities at TRIUMF, PSI, LAMPF, BOOM, RAL, Brookhaven, Gatchina, Dubna and CERN where μ SR experiments are carried out. Of these laboratories, some (for example TRIUMF, PSI and Brookhaven) are essentially dc beams – *i.e.*, the muons arrive more or less continuously, at random intervals – whereas others are pulsed – *i.e.*, a large number of muons arrive at once, then there is a large delay before the next pulse arrives. The muons are all created by pion decay. The pions themselves are created when a primary beam (generally protons) is focussed on a fixed target (typically carbon or beryllium). At TRIUMF, the initial proton energy is 500 MeV, with proton currents between 100–200 μ A. An upgrading of the PSI accelerator will increase its current capability to ~ 1 mA, which will provide a corresponding increase in the beam rates in the secondary channels. Increased pion (and therefore muon) fluxes are also possible by increasing the proton energy, as the rate of pion production is roughly proportional to the beam power for proton energies above ~ 700

MeV.

As previously mentioned, the development of meson factories has provided the large fluxes of muons which make μ SR experiments practical. The initial beamlines developed for μ SR provided so-called “backward” muons, created from pions in flight, and traveling backwards in the pion rest frame with typical lab-frame momenta of 86 MeV/c. A backward beam consists of three distinct segments. The first collects pions of a given momentum from the production target. Following this is the decay section, either a long series of quadrupole magnets or a solenoid in which the pions decay and the subsequent muons are focussed down the channel. Finally, there is the muon segment, which is tuned to the momentum of the desired muons from the decay section. Because the beam optics select muons with a fairly small angular acceptance (along the beam direction) the beam is generally quite highly polarized ($\sim 85\%$). However, such beams are also quite energetic, with a typical stopping range of 1-2 g/cm². This necessitates the use of rather thick samples in order to stop the beam. Frequently, a degrader is placed in front of the target to slow down the incident beam; however, this also degrades the (already poor) luminosity of the resultant beam.

The decay μ beam exhibits rather poor luminosity, (*i.e.*, it has a large spot size), as the pions decay over a long distance (a typical decay section is 6 m long) and across the diameter of the pion beam. This makes it impossible to focus the beam onto a small spot, as there is no imagable point-like source of the muons. The poor luminosity requires that large targets be used in experiments, making it difficult to always study the best samples (for example the most pure, or homogeneous), as they are typically available only in small amounts.

Typical backgrounds due to scattered positrons and muons stopping outside of the sample (perhaps 10% of the muon stops) with a backward beam also contribute to making the study of subtle effects, such as slow relaxation rates, quite difficult. A

further complication is the need for electronics and detectors to veto muons which pass through the sample entirely.

Instead of collecting muons from pions which decay in flight, one can make a beam of muons which come from pions which decay at rest. Such a beam is called a surface beam [39,40], as the muons come from pions which were at rest on or near the surface of the production target. Surface muons have a momentum of $29.8 \text{ MeV}/c$, corresponding to a kinetic energy of 4.1 MeV . Their range is approximately $140 \text{ mg}/\text{cm}^2$ in water or CH_2 , or approximately 0.2 mm in copper, so that they penetrate well into the bulk. Surface muons have a number of properties which make their use especially attractive for μSR experiments. They are created 100% spin polarized, which results in the highest possible experimental asymmetry. A further advantage is that the source of the muons is the imaged spot on the production target where the pions were produced, rather than a large volume of a decay section as in the backward beam. This allows the resulting beam to be focussed down to a small spot. As a result, the luminosity of a surface beam is much greater than that of a corresponding decay beam. Finally, the smaller range of surface muons means that less mass is needed to stop the beam. The higher luminosity and smaller stopping range has allowed the study of much smaller samples than possible with the decay beams.

One potential disadvantage of the surface beam comes from its small stopping range. This requires that a minimum of mass be placed in the beam upstream from the sample. As a result, beamline windows and scintillation counters in the path of the beam must be as thin as possible, and as close as possible to the sample, so that any scattered muons stop in the sample, rather than in the cryostat. Muons which stop outside of the sample can cause a background which may be impossible to separate from the signal originating in the sample.

Only positive surface muon beams are possible, as stopped negative pions quickly

undergo nuclear capture in the production target before they can decay into negative muons.

1.6 μ^+ in Copper—Previous Work

Copper was one of the first materials to be studied using μ SR [4]. There have been more μ SR experiments on copper than on any other material, with the possible recent exception of high- T_c superconductors. Studies involving copper have provided examples of a rich collection of phenomena, including localization through small polaron formation, classical thermally-activated over-barrier hopping, sub-barrier tunnelling, quantum diffusion and, most recently, level-crossing resonance.

It is extremely difficult to study the diffusion of hydrogen in copper, as hydrogen is not very soluble in Cu. As a result, the only diffusion studies of hydrogen in copper have been performed at high temperatures. Studies of muon diffusion can therefore provide some unique information about the diffusion of light interstitials in copper at low temperatures.

Copper is well suited for μ SR studies; among the reasons is that it has a face-centered cubic (fcc) lattice, in which the muon occupies a unique site. Both copper isotopes, ^{63}Cu and ^{65}Cu , have large nuclear moments with which the muon spin can interact, leading to strong depolarization effects when the muon is slowly moving. Muons, as will be shown, diffuse fairly slowly in copper over a large range of temperatures (relative to their lifetime). This allows the study of the muon's interactions at a given site, without those interactions being averaged over a large number of sites.

Some of the properties of copper are given in table 1.2, along with similar information for a number of other metals for comparison. When a positive muon is stopped in a metal, it comes to rest in an interstitial site at a minimum of the local electrostatic

Table 1.2: Selected properties of metals

Metal	Crystal Structure	Θ_D	Isotope	Abundance	Spin I	$\gamma/2\pi$ (kHz/G)
Copper	fcc	315 K	^{63}Cu	69.09%	3/2	1.13
			^{65}Cu	30.91%	3/2	1.21
Aluminum	fcc	394 K	^{27}Al	100%	5/2	1.11
Silver	fcc	215 K	^{107}Ag	51.8%	1/2	0.17
			^{109}Ag	48.2%	1/2	0.20
Gold	fcc	170 K	^{197}Au	100%	3/2	0.10

potential. The time required for it to stop is typically 10^{-10} to 10^{-9} s. Energy is first lost through scattering with electrons until the muon has reached energies of 2–3 keV, after which it loses energy through cycles of muonium formation and ionization. In solids, this stage takes approximately 5×10^{-13} s [41]. There is no loss of polarization during the slowing down process since the total time involved is even shorter than the hyperfine period of the muon in the muonium state. Because of its charge, the μ^+ attracts a screening cloud of conduction electrons to it and pushes away the neighbouring positive ions, thus polarizing the lattice. The lattice distortion can actually cause a deepening of the potential minimum at the muon site, in which case the muon is said to be self-trapped. The combination of the muon, screening cloud of electrons and lattice distortion should be considered as a composite particle, often referred to as a small polaron [42] (by analogy with electrons) with an effective mass *etc.* When considering the diffusive properties of the muon, one must actually consider the motion of the small polaron state [42,43,44], as the polarization and phonon clouds accompany the muon as it diffuses.

1.6.1 Transverse Field Experiments

Transverse field measurements are analogous to simple “ T_2 ” measurements in nuclear magnetic resonance (NMR) experiments [45], where the relaxation envelope of the muon precession signal (in μ SR) corresponds to NMR’s free induction decay (FID). Spin relaxation, as in NMR, can be from both dynamical and static effects. Inhomogeneous broadening is an example of a static relaxation mechanism where an inhomogeneity in the applied field causes dephasing of spins across the sample volume. Similarly, static dipolar fields from the neighbouring spins also can cause a broadening of the signal. Broadening refers to an increase in the linewidth in frequency (or Fourier) space, corresponding to an increased rate of relaxation of the precession signal in time space. A non-relaxing, long-lived signal is said to be narrow, whereas a broadened line means that the time spectrum is quickly relaxed. Dynamical effects, such as fluctuating moments, can also cause relaxation, and are referred to as “ T_1 ” processes. As in NMR, it can be difficult to differentiate between the two types of relaxation in a straightforward transverse field measurement; other techniques must be used, such as spin echoes in both NMR and μ SR [46], or longitudinal and zero field measurements in μ SR.

The site of muon localization in the copper lattice was first determined by Camani *et al.* using transverse field measurements[5]. They found that the muon occupies the site where it has 6 nearest neighbour copper atoms, at the center of an octahedron. This is the same site which protons have been found to occupy [47] in fcc metals. This octahedral site, or o-site, as well as a hypothetical t-site, with tetrahedral symmetry, is shown in figure 1.4. The possibility of the muon occupying this tetrahedral or t-site site has been postulated by a number of authors and will be discussed later. Essentially, Camani *et al.* showed that the orientation dependence of the second moment of the

dipolar local-field distribution (dipolar width Δ) was the same as would be expected for the octahedral interstitial site, and inconsistent with other site assignments.

Van Vleck[48] showed that the broadening of magnetic resonance lines due to dipolar coupling of nuclear spins \mathbf{I} to unlike spins \mathbf{J} can be considered to be the sum of random dipolar fields whose distribution has second moment:

$$M_2 = \frac{1}{3} \gamma_I^2 \hbar^2 J(J+1) \sum_{\text{spins } J} \frac{(3 \cos^2 \theta - 1)^2}{r^6} \quad (1.7)$$

when the spins are subject to a transverse applied static field substantially larger than the dipolar fields.

However, in the case of an interstitial muon, which is a charged impurity, and neighbouring nuclei with spin $I \geq 1$, equation 1.7 is no longer valid until sufficiently high field when the Zeeman interaction of the nuclei is substantially larger than their quadrupolar interaction — the so-called “Van-Vleck limit”. In copper, this limit is essentially reached by 5 kG. However, one may calculate the second moment including quadrupole effects even in lower fields [1], and one finds that there is a characteristic step in M_2 as a function of applied field. The magnitude and direction of the step are different for different orientations of the crystal in the external field and for interstitial sites of different symmetry, thus allowing determination of the muon site. The location of the step gives an estimate of the magnitude of the quadrupole interaction strength, which Camani *et al.* [6] found to be

$$|\omega^Q| = 3.02 \pm 0.4 \mu\text{s}^{-1} \quad (1.8)$$

where $2\hbar\omega^Q$ is the energy splitting of the copper quadrupolar energy levels (with $J^z = \pm\frac{3}{2}$ and $J^z = \pm\frac{1}{2}$). The field-dependence of the relaxation rate is shown in figure 1.5 for the $\langle 100 \rangle$, $\langle 110 \rangle$, and $\langle 111 \rangle$ crystal orientations.

Camani *et al.* found no difference in their data taken at 20 K and 80 K, which they took to indicate that the muons were static below 80 K. They also found that the

calculated values for the second moment were only approximately in agreement with their measured values, although the location of the step occurred at the correct field, assuming that the muon is in the octahedral site. They discovered that if they assumed a dilation of the nearest neighbours of 5%, much better agreement was obtained and at high field the relaxation rate took on the Van-Vleck value.

1.6.2 Zero Field Experiments

The zero-field μ SR technique was first demonstrated by Hayano *et al.* [49] who observed the dipolar relaxation of muons in MnSi and ZrH₂. They showed that the non-secular parts of the dipolar interaction (those terms in the dipolar Hamiltonian which don't commute with the Zeeman interaction) contributed greatly to the relaxation of the muon polarization in zero field, causing an increase in the initial gaussian relaxation rate by a factor of $\sqrt{5}$ relative to that in high transverse field, as long as the muons were static. Furthermore, they discussed the sensitivity of ZF- μ SR to the effects of slow hopping, contrasting the relative lack of sensitivity in transverse field.

Experiments by Clawson *et al.* [9,10,50] and Kadono *et al.* [12,11,51] showed that the static dipolar width Δ , which characterizes the strength of the dipolar fields from the neighbouring copper nuclei on the muon, was independent of temperature, over the range $100 \text{ mK} < T < 100 \text{ K}$. This was taken as strong evidence that the muon site remained the same over that temperature range, since a different site, (*e.g.*, tetrahedral) would likely be characterized by a different dipolar width. Such a change in the dipolar width, corresponding to a different site occupation, has been observed in Bismuth [52]. The more recent results of Kadono *et al.* were also compared to the zero-field theoretical relaxation functions calculated by Holzschuh and Meier[53]. These calculations, which were fully quantum mechanical and exact in the limit of a strong copper quadrupolar

interaction, showed excellent agreement with the data, even in the long time ($t > 10\mu s$) region, in the case of the o-site, and poor agreement for the t-site.

1.6.3 Level-Crossing Resonance

Copper also provided the first demonstration of level-crossing resonance (LCR) in μ SR. The application of LCR was first proposed by Abragam [54]; since then, experiments in copper [17], free radicals [31,56,32] (in liquid, solid and gas phases), and both elemental and compound semiconductors [33] have quickly made it one of the most valuable μ SR techniques. LCR is now making the same contributions to μ SR that ENDOR (electron nuclear double resonance) has made to EPR (electron paramagnetic resonance).

The level-crossing occurs when there is an accidental degeneracy (in first order) between two spin states with different muon spins. Under these circumstances, a resonant exchange of polarization between the muon and nuclear spins can take place. In copper, this occurs when the copper quadrupole level splitting approximately matches the muon Zeeman splitting. The first LCR measurement in copper [17] was performed at 20 K, where the muon is diffusing slowly. The resonance was seen to be centered at $B_{\text{res}} = 80.9(4)$ G and was approximately 20 G wide. The longitudinal field was applied along the $\langle 111 \rangle$ direction. Some of the features which make LCR experiments so powerful include the fact that the relaxation function is independent of the number of nuclei which are off resonance, since they are essentially decoupled by the application of the longitudinal field. This allows the separation of the effects of each non-equivalent species of nuclei with which the muon interacts.

The term LCR is actually a slight misnomer. There is only a visible effect at the level-crossing if there is some coupling between the different states which cross. In this case, the levels repel each other and don't actually cross. For this reason, the technique

is occasionally referred to as avoided level-crossing (ALC). Here, we will still refer to level-crossing, even though this is not strictly the case.

1.6.4 Pion Decay-Site Spectroscopy

Positive pions (π^+) have a mass ($m_\pi = 139.6 \text{ MeV}/c^2$) which is only slightly greater than that of positive muons ($m_\mu = 105.7 \text{ MeV}/c^2$), and can also be implanted in materials. One can then observe the muons formed by pion decay. Since the muons are emitted isotropically when the pion is at rest, any anisotropy in the observed muon angular distribution is due to the interactions of the muons with the sample. In directions where the muons can pass without having to pass through lattice sites there is a maximum in their rate. The use of this orientation dependence, which is known as “channeling” (or “blocking” for the opposite effect), can then be used to determine the symmetry of the pion decay site, which is frequently sufficient to uniquely determine that site.

Pion decay-site spectroscopy has been applied to copper by Flik *et al.* [57] over a range of temperatures. Their result is that they observe the pion to decay mainly from the octahedral site, but at some temperatures they observe some occupation of the tetrahedral site. At room temperature, they find that both sites are significantly occupied, but by 80 K, the o-sites are preferentially occupied by a factor of at least one order of magnitude. They therefore conclude that the t-site is metastable for the pion, and therefore presumably also for the muon, since they should behave similarly in condensed matter. They predict that evidence of muon occupation of the t-site would occur at lower temperatures, where the muon would stay at the metastable site for a length of time comparable to the muon’s much longer lifetime.

1.7 Muon Diffusion

1.7.1 Diffusion in Copper

The first measurements of muon diffusion in metals were made by Gurevich *et al.* [4] and Grebinnik *et al.* [58] in transverse field. The μ^+ hop rate in Cu was determined by the motional narrowing of the dipolar relaxation of the transverse precession signal, whose second moment is given in equation 1.7. Abragam [59] showed that the polarization function in the presence of diffusion is given by:

$$\mathcal{P}(t) = \exp\left(-2\sigma^2\tau^2\left[e^{-t/\tau} - 1 + t/\tau\right]\right) \cos\omega t \quad (1.9)$$

where τ is the mean time between hops (*i.e.*, $1/\nu_{\text{hop}}$) and σ is the (gaussian) relaxation rate in the absence of motion. The Soviet group found that the effective muon spin relaxation rate in copper increased with decreasing temperature, reaching a maximum value corresponding to $\sigma = 0.252 \mu\text{s}^{-1}$ in their polycrystalline sample at temperatures below 80 K. The minimum temperature they reached was approximately 20 K.

They found that the hop rate displayed a temperature dependence which resembled that of an activated or ‘‘Arrhenius’’ process. The parameters which were extracted for the activation energy ($E_a/k_B = 560$ K) and the corresponding barrier height were too small to be attributed to phonon-assisted over-barrier hopping. Their results were interpreted in terms of sub-barrier diffusion at temperatures below 250 K. Deviation from the Arrhenius behaviour at higher ($T > 250$ K) temperatures was attributed to above-barrier diffusion.

Teichler [60] calculated the hop rate assuming that the dominant process in the hopping was phonon-assisted tunnelling, where the phonons only have to provide the energy necessary for the muon levels at adjacent sites to be equal, instead of actually lifting the muon over the barrier; he obtained good agreement with the experimental

results. At this point, it was thought that a consistent understanding of the self-trapping and diffusion of the muon in copper had been reached, with the muon being self-trapped below 80 K and with small polaron phonon-assisted tunnelling at higher temperatures.

Subsequent transverse field measurements[7,8,61] at temperatures below 20 K found that the muon spin relaxation rate started to decrease again with decreasing temperature. The most likely interpretation was an increase in the muon hop rate with decreasing temperature, causing motional narrowing as at higher temperatures. The field and orientation dependence of the relaxation rate were consistent with an unchanged octahedral muon site, with an unchanged electric field gradient, implying that the decreased depolarization rate was in fact due to increased hopping.

There were, however, a number of other possible causes which could not be distinguished in the transverse field measurements from an increase in the hop rate. This was because it is difficult to distinguish changes in the depolarization rate due to changes in the correlation time τ from changes due to a smaller static relaxation rate σ in equation 1.9. Some of these possibilities included the muon occupying a different site in the lattice, perhaps the tetrahedral site, as well as trapping at defects or impurities. A number of experiments investigated the effects of defects by deliberately introducing them into the samples, through radiation damage [62] and by mechanical deformation to introduce dislocations [63]. In both experiments, the introduction of large numbers of defects did not appreciably alter the TF relaxation rate, implying that the small number of these defects present in annealed crystals and polycrystals could not be responsible for the changes with temperature of the relaxation rate (and thus the inferred muon hop rate). Experiments on isotopically enriched samples containing over 99% of either ^{63}Cu or ^{65}Cu also yielded essentially the same results as the natural composition samples [8,61].

The narrowing was studied down to 50 mK [8,61]; the hop rate was observed to reach a plateau at approximately 500 mK, below which it remained constant. The authors claimed to be able to rule out a number of models which proposed alternate explanations for the effects on the relaxation functions, including metastable tetrahedral site occupation and trapping at impurities. They also claimed that the diffusion was due to a coherent tunnelling process. However, the TF experiments were not sufficient to completely rule out all other interpretations.

Zero-field measurements [9,64,12,11] displayed a dynamically-narrowed Kubo-Toyabe relaxation behaviour, also indicating an increase in hop rate with decreasing temperature. The semi-classical Kubo-Toyabe theory, discussed in chapter 2, shows that in zero field the polarization of static muons interacting with gaussian random dipolar fields evolves as

$$\mathcal{P}(t) = \frac{1}{3} + \frac{2}{3} (1 - \Delta^2 t^2) \exp \left[-\frac{1}{2} \Delta^2 t^2 \right]. \quad (1.10)$$

where Δ is the width of the dipolar field distribution. The effects of slow diffusion (relative to the muon lifetime and Δ) are clearly seen as a relaxation of the “ $\frac{1}{3}$ tail”.

Petzinger [65,66] considered the effects of muons diffusing to impurities or other sites where the muon is trapped and subsequently becomes depolarized. He showed that the zero-field and low longitudinal field relaxation functions had a behaviour which could distinguish the effects of trapping. The essential feature is that if the depolarization of the spin takes place while the muon is static in a trap site, then there will be a characteristic long-lived tail in the polarization, even if a minimum in the so-called Kubo-Toyabe relaxation function is not observed.

The fact that these experiments all displayed a relaxation of the long-time tail proved that the increase in the relaxation rate seen in transverse field was not an effect of impurity trapping but was rather a dynamical effect. The zero-field measurements all

exhibit a minimum in the muon hop rate around 40 K. There is a large variation in the absolute (fitted) value of the hop rate at this minimum, however, which demonstrates the difficulty of extracting very small hop rates from zero field data. The most recent results of Kadono *et al.* [11,12] indicate that muons are completely static around 40 K. The actual range extracted for static behaviour was found to vary with the form of the static function used to fit the data. Use of the Kubo-Toyabe function resulted in a static range from 20 K to 80 K, whereas use of the results of Celio and Meier [67] gave a narrower range of temperatures. The maximum value (within one standard deviation) of the hop rate at the minimum was approximately $10^{-2} \mu\text{s}^{-1}$. Earlier results [51,9] gave the value of ν_{hop} at the minimum to be $\sim 10^{-1} \mu\text{s}^{-1}$.

At higher temperatures (100 K and higher) the hop rates extracted from the ZF data are consistent with each other, as well as with the various transverse field results [4,58,6] up to ~ 140 K.

Below the minimum, an increasing hop rate was seen, down to 0.5 K. The hop rate was seen to obey a power law in this range of the form

$$\nu_{\text{hop}} \sim T^{-\alpha} \quad (1.11)$$

where estimated values for the exponent varied from $\alpha \sim 0.4$ [51] to $\alpha = 0.67 \pm 0.03$ in the most recent results [12]. The value of α depended on the range of temperatures used to extract it; deviations from the power law were around .5 K and 15 K. Below $T=0.5$ K the hop rate was observed to level out, reaching a constant value in the range $0.5 \mu\text{s}^{-1} \rightarrow 0.8 \mu\text{s}^{-1}$. These measurements were made down to ~ 70 mK.

1.7.2 Diffusion in other Metals

Aluminum is quite similar to copper in a number of respects, as can be seen in table 1.2. However, studies of muon diffusion in Al [68,69] show that muons are moving

much faster (by approximately 3 orders of magnitude) than they do in copper. This fast diffusion means that the methods used in copper, such as motional narrowing in transverse field, are ineffective in determining the diffusion rate in aluminum. The fact that the hopping frequency is much greater than the frequency of the muon-nuclear spin-spin interaction means that the TF signals are fully narrowed (*i.e.*, no relaxation) and similarly there is essentially no relaxation in longitudinal field or zero field.

Hop rates in aluminum have been deduced from trapping studies, where the muons diffuse to impurities which have been deliberately introduced into the sample. There are a number of temperature regimes in such studies. At lowest hop rates, the muon is diffusing slowly enough that it doesn't generally reach a trap before decaying. In this range, there is no relaxation of the transverse field signal since the diffusion is still fast enough to fully narrow the dipolar relaxation. As the muon hop rate increases, a significant fraction of the muons diffuse far enough during their lifetime that they reach a trap. Once they are trapped, their spins are quickly depolarized by the nearby static dipoles, and an increase is seen in the total depolarization rate. At high temperatures, where the muons are diffusing fast enough to reach traps almost immediately, a point is reached where thermal activation causes detrapping, and a corresponding decrease in the depolarization. The diffusion rate is deduced from the time required for the muon to diffuse to a trap, whose concentration has been controlled in the sample preparation.

Experiments in aluminum have used a range of dopants, including Li, Mg, Si, Ga, Ge, Mn and Ag; typical concentrations are 50 – 100 ppm. A number of difficulties are encountered in extracting hop rates from trapping studies. First, there is the difficulty in relating the hop rates extracted from the impure system to the pure material. It is also difficult to determine the absolute hop rate, as one must make some assumptions about the range of the trap effectiveness, based on the range of the elastic distortions and electronic density changes caused by the traps. This difficulty does not prevent one

from measuring the temperature dependence of the hop rate; just its absolute value.

The diffusion results for aluminum have been described by Hartmann *et al.* [68,69] in terms of the same quantum diffusion theories of Kondo and Yamada (discussed in chapter 3) used to describe the diffusion rates in copper. They observe that the hop rate decreases with decreasing temperature at high temperatures, reaching a minimum at approximately 5 K, where the hop rate $\nu_{\text{hop}} \sim 10^2 \mu\text{s}^{-1}$. Below this temperature, the hop rate follows a power law as in equation 1.11. A value of 0.7 for α (the exponent of the temperature) is obtained in the temperature range 0.05 K \rightarrow 2 K. In the temperature range 2 K \rightarrow 20 K, there is an approximately linear temperature dependence, followed by an exponential (activated) behaviour at higher temperatures.

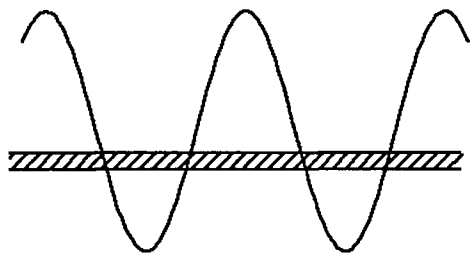
Silver and gold, like copper, have an fcc crystal structure. However, they have very small nuclear dipole moments, which means that there is very little relaxation in either transverse or longitudinal field. The diffusion rates have been measured [70] using magnetic impurities such as Gd and Er which depolarize the muons as they diffuse past. It is found that the muon is essentially immobile below 75 K, as in copper. Fitting these results in terms of an activated process, the authors find that the values of the preexponential factor and activation energy seem to indicate that the muons diffuse through an over-the-barrier hopping process.

The diffusion of muons and protons in bcc metals is generally much faster than in those with fcc structure. This is a result of the fact that the bcc unit cell has two nearly equivalent interstitial sites, with a small barrier between them. In the fcc crystal structure, there is a significantly larger barrier between interstitial sites.

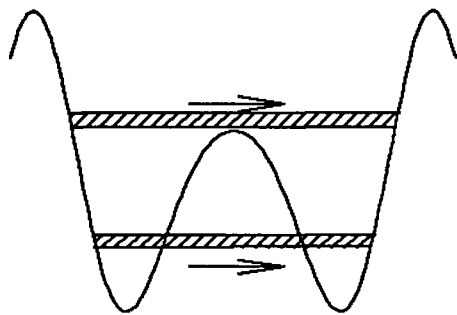
In niobium and vanadium, trapping at various impurities is apparently the dominant effect in the depolarization over the range of temperatures studied [71]. A complicated temperature dependence of the transverse field relaxation rate has been interpreted in

terms of trapping and detrapping from traps of different depths near different impurities. The details of the structure seen depends upon the precise amount and type of dopants used. The overall diffusion rates are much greater than in copper. The diffusion in pure niobium has been studied in the superconducting mixed state in transverse field [72]. The strong magnetic field gradients which exist due to the flux lattice provide a source of broadening in the muon precession which can be narrowed through diffusion. This method has the potential to differentiate between muons which are in the centers of flux lines (*i.e.* those in the normal state) and those which are in superconducting material due to the shift in the precession frequency which accompany the superconducting state. However, the role of flux-pinning in these studies is still not fully understood; changes in the flux-pinning as a function of temperature affect the precession lineshape in the same manner as muon diffusion [73].

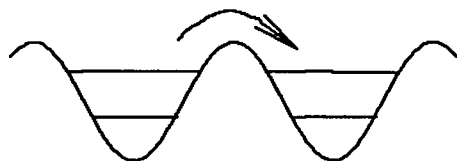
Iron is another bcc metal, but the fact that it is ferromagnetic allows the diffusion to be studied in both transverse [74] and longitudinal [75,76] fields. Two electrostatically identical but magnetically inequivalent muon sites are seen, with dipolar fields of 2.6 kG and -5.2 kG. These large dipolar fields mean that longitudinal field measurements as in copper (except with much larger applied fields) can be used to distinguish between intrinsic diffusion and the effects of traps. These differences show up above 70 K, where some trapping is seen in transverse field measurements. In addition, larger hop rates than in copper may be studied; in iron the hop rate varies between $\sim 10^9 \text{ s}^{-1}$ at 1 K and 10^{12} s^{-1} at 100 K. Recently, Kondo [77] was able to give a reasonable fit to the extracted hop rates in terms of the same model of quantum diffusion used to describe results in copper and aluminum.



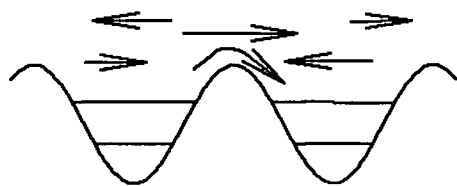
Coherent Tunneling
or Hopping



Incoherent Transition
Phonon-Assisted
Tunneling



Over-Barrier Jump



Fluid-Like
"Free Motion"

Figure 1.1: Schematic representation of various diffusion processes

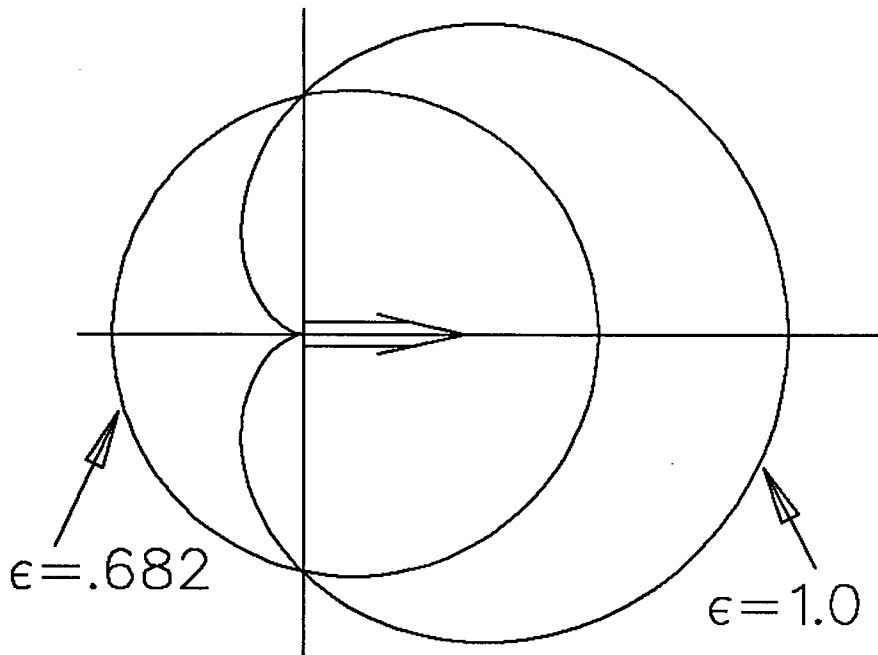


Figure 1.2: Radial plot of positron emission probability for $\epsilon = 1.0, \epsilon = \bar{\epsilon}$

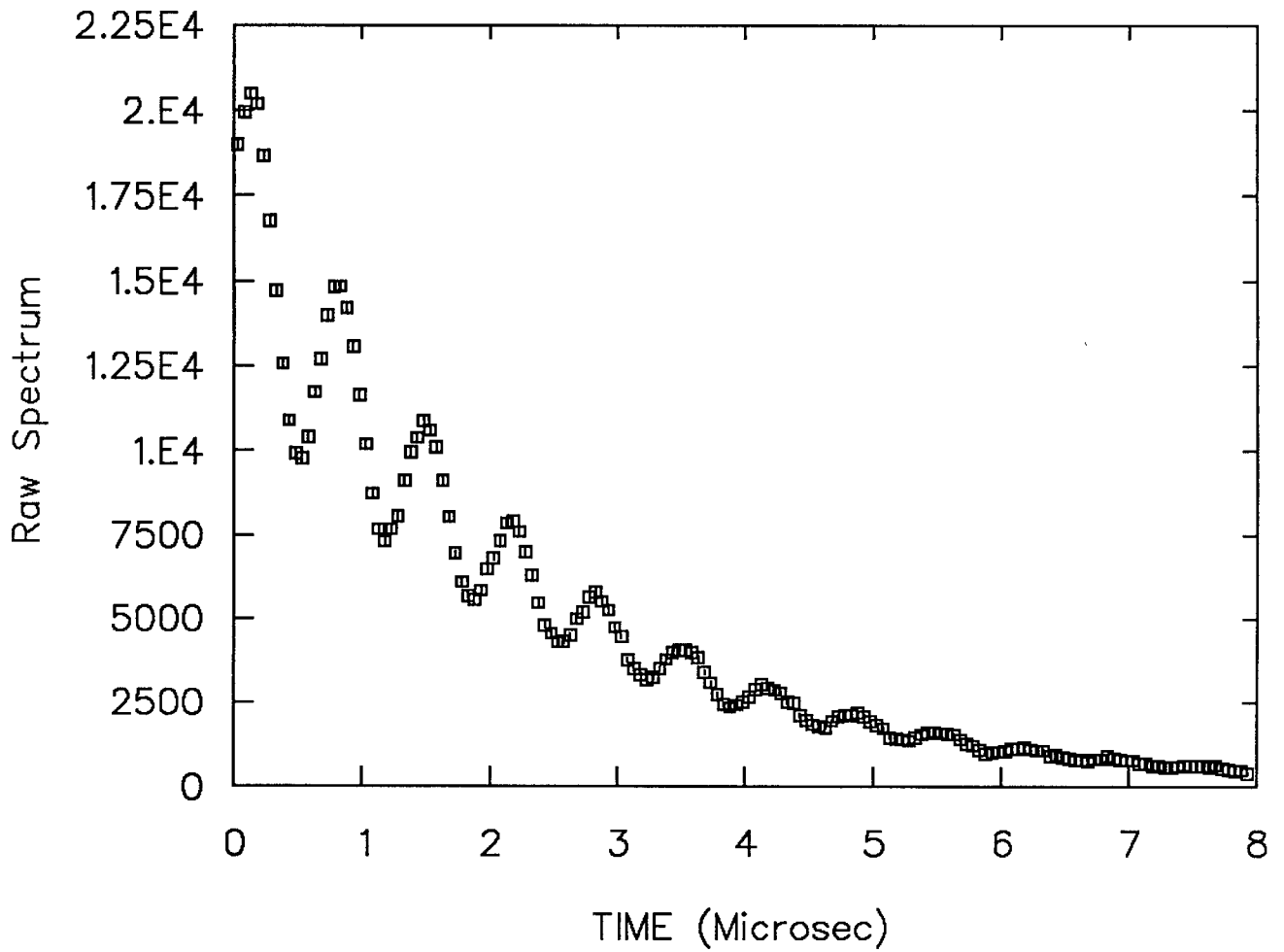


Figure 1.3: Raw spectrum in transverse field geometry, showing muon precession and lifetime.

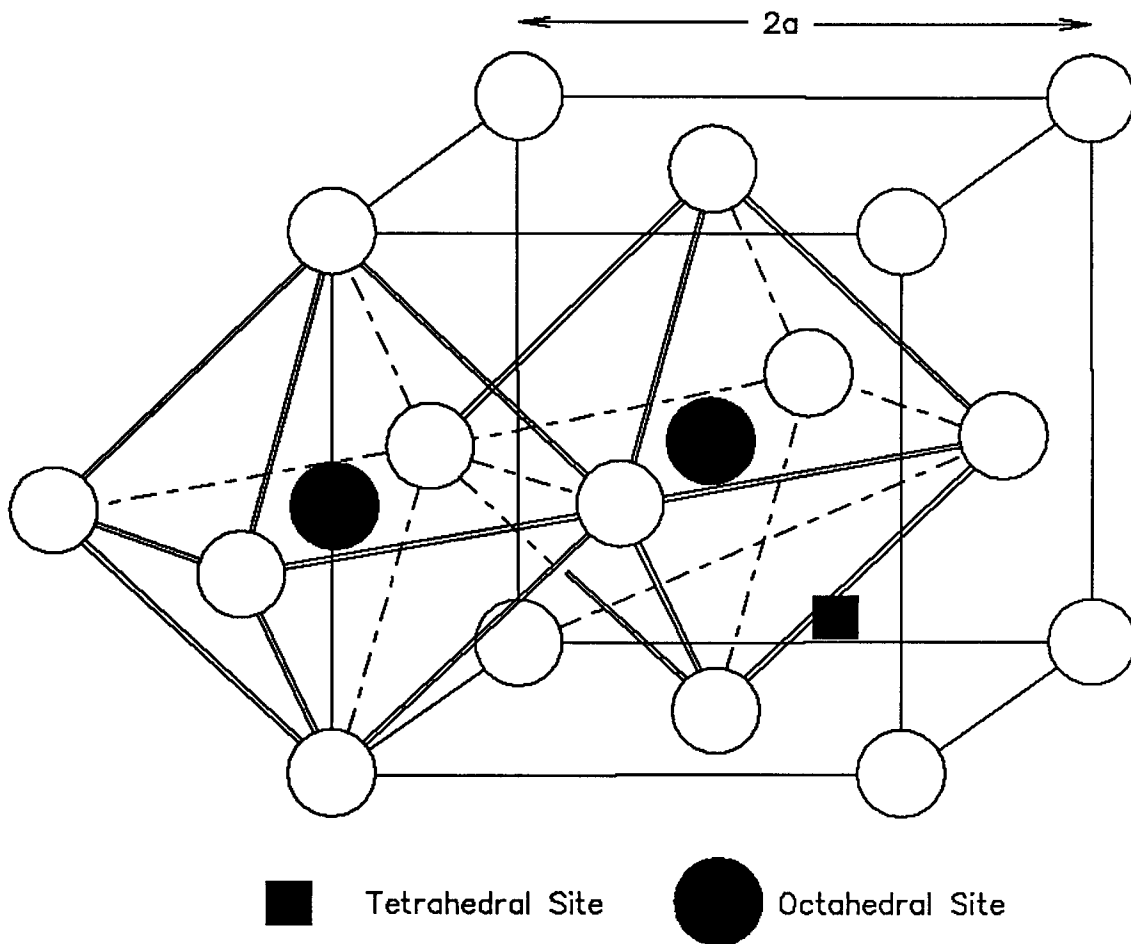


Figure 1.4: Muon Site in Copper Lattice, also shown is tetrahedral site

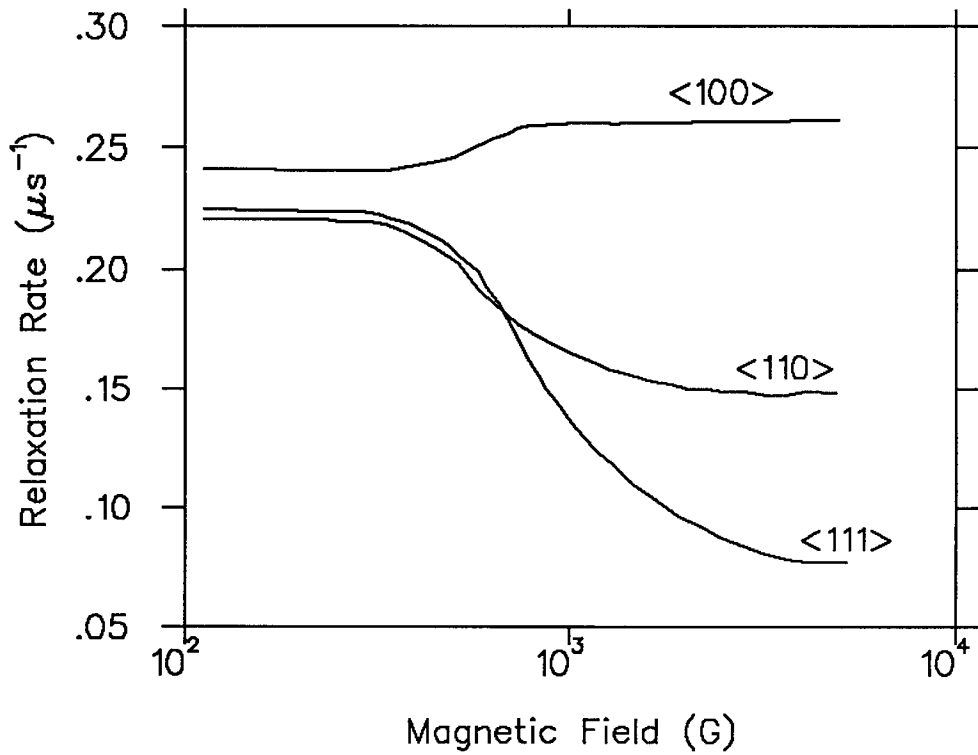


Figure 1.5: Calculated linewidths of muon precession signals for applied fields transverse to the $\langle 100 \rangle$, $\langle 110 \rangle$, and $\langle 111 \rangle$ crystal orientations. (From reference [1])

Chapter 2

Relaxation Functions

Most of the work in time-differential μ SR involves the measurement of what are loosely referred to as “relaxation functions”. Here, the term relaxation is used to describe changes in the muon asymmetry — in other words, the time development of the muon polarization — whether they are caused by reversible processes or not. These relaxation functions are then interpreted to relate them to the underlying physical mechanisms causing them.

Clearly, if one wishes to extract microscopic information about a system of interest, one must have some method of calculating theoretical relaxation functions with which to compare one’s data. The first theoretical calculations for zero and longitudinal field were semi-classical ones, introduced by Kubo and Toyabe, originally with respect to NMR. More recently, analytic quantum mechanical calculations have been performed in the zero field case, employing a number of approximations, and finally an expansion technique has been developed which allows arbitrarily exact calculations of the static polarization function in any applied field.

2.1 Kubo-Toyabe Theory

When any applied fields are weak compared to the local fields in a material, perturbational methods break down for evaluating relaxation functions. The theory of Kubo and Toyabe [78,49] gives an approximate method for evaluating the time evolution of a classical spin ensemble, in zero and low longitudinal field. In both cases, the local fields are assumed to be static and random with a gaussian distribution. In particular, the evolution of the host spins due to their interaction with the magnetic field produced by the interstitial magnetic moment is explicitly neglected. Since this is a classical theory, it ignores any noncommutivity of various parts of the Hamiltonian with each other.

2.1.1 Zero Field

For a local magnetic field given by

$$\mathbf{H} = (H_x, H_y, H_z) \quad (2.1)$$

the muon spin (initially polarized along \hat{z}) evolves as

$$\mathcal{P}_z^\mu = \frac{H_z^2}{H^2} + \frac{H_x^2 + H_y^2}{H^2} \cos(\gamma_\mu H t) \quad (2.2)$$

$$= \cos^2 \theta + \sin^2 \theta \cos(\gamma_\mu H t) \quad (2.3)$$

where θ is the angle between \mathbf{H} and the \hat{z} direction.

The sum of the various dipolar fields on the muon from its neighbouring nuclei is taken to be given by a gaussian field distribution

$$P(H_i) = \frac{\gamma_\mu}{\sqrt{2\pi}\Delta} \exp\left[\frac{-\gamma_\mu^2 H_i^2}{2\Delta^2}\right] \quad i = x, y, z \quad (2.4)$$

which has a second moment given by the dipolar width Δ

$$\frac{\Delta^2}{\gamma_\mu^2} = \langle H_x^2 \rangle = \langle H_y^2 \rangle = \langle H_z^2 \rangle. \quad (2.5)$$

The spin evolution function is found by integrating over the field distributions in all three dimensions.

$$\mathcal{P}_z(t) = \int \int \int \mathcal{P}_z^\mu(t) P(H_x) P(H_y) P(H_z) dH_x dH_y dH_z. \quad (2.6)$$

The result is the well-known Kubo-Toyabe formula for the evolution of a static spin in zero field:

$$\mathcal{P}_z(t) = \frac{1}{3} + \frac{2}{3} \left(1 - \Delta^2 t^2\right) \exp\left[-\frac{1}{2} \Delta^2 t^2\right]. \quad (2.7)$$

The “1/3 tail” corresponds to the fraction of the spin polarization which has its random local field aligned either parallel or anti-parallel with its initial polarization, while the remaining 2/3 of the polarization precesses in the transverse local field components in which it finds itself.

2.1.2 Longitudinal Field

It is possible to extend the above formalism to include an applied magnetic field. In longitudinal field, the situation is similar to the zero field case, although the long time asymptote is at a level greater than 1/3, as one would expect, as in this case more than 1/3 of the initial polarization is aligned with the net local field and thus is not relaxed. For convenience, the applied field is taken to be along the \hat{z} direction. The field distribution along \hat{z} is taken to be

$$P(H_z) = \frac{\gamma_\mu}{\sqrt{2\pi}\Delta} \exp\left[\frac{-\gamma_\mu^2 (H_z - H_0)^2}{2\Delta^2}\right] \quad (2.8)$$

Evaluating $\mathcal{P}_z(t)$ as before, one obtains the result

$$\begin{aligned} \mathcal{P}_z(t) = 1 & - \frac{2\Delta^2}{\omega_0^2} \left[1 - \exp\left(\frac{1}{2}\Delta^2 t^2\right) \cos \omega_0 t\right] \\ & + \frac{2\Delta^4}{\omega_0^3} \int_0^t \exp\left(-\frac{1}{2}\Delta^2 \tau^2\right) \sin \omega_0 \tau d\tau \end{aligned} \quad (2.9)$$

where $\omega_0 = \gamma_\mu H_0$.

The long time behaviour of equation 2.9 is

$$\mathcal{P}_z(\infty) = 1 - \frac{2\Delta^2}{\omega_0^2} + \frac{2\Delta^3}{\omega_0^3} \exp\left(\frac{-\omega_0^2}{2\Delta^2}\right) \int_0^{\omega_0/\Delta} \exp\left(\frac{1}{2}u^2\right) du \quad (2.10)$$

It can be seen from equation 2.10 that $\frac{1}{3} \leq \mathcal{P}_z(\infty) \leq 1$ and that $\mathcal{P}_z(\infty) \rightarrow 1$ as $\omega_0 \rightarrow \infty$.

The behaviour of $\mathcal{P}_z(t)$ is shown in figure 2.1, for zero and various longitudinal fields.

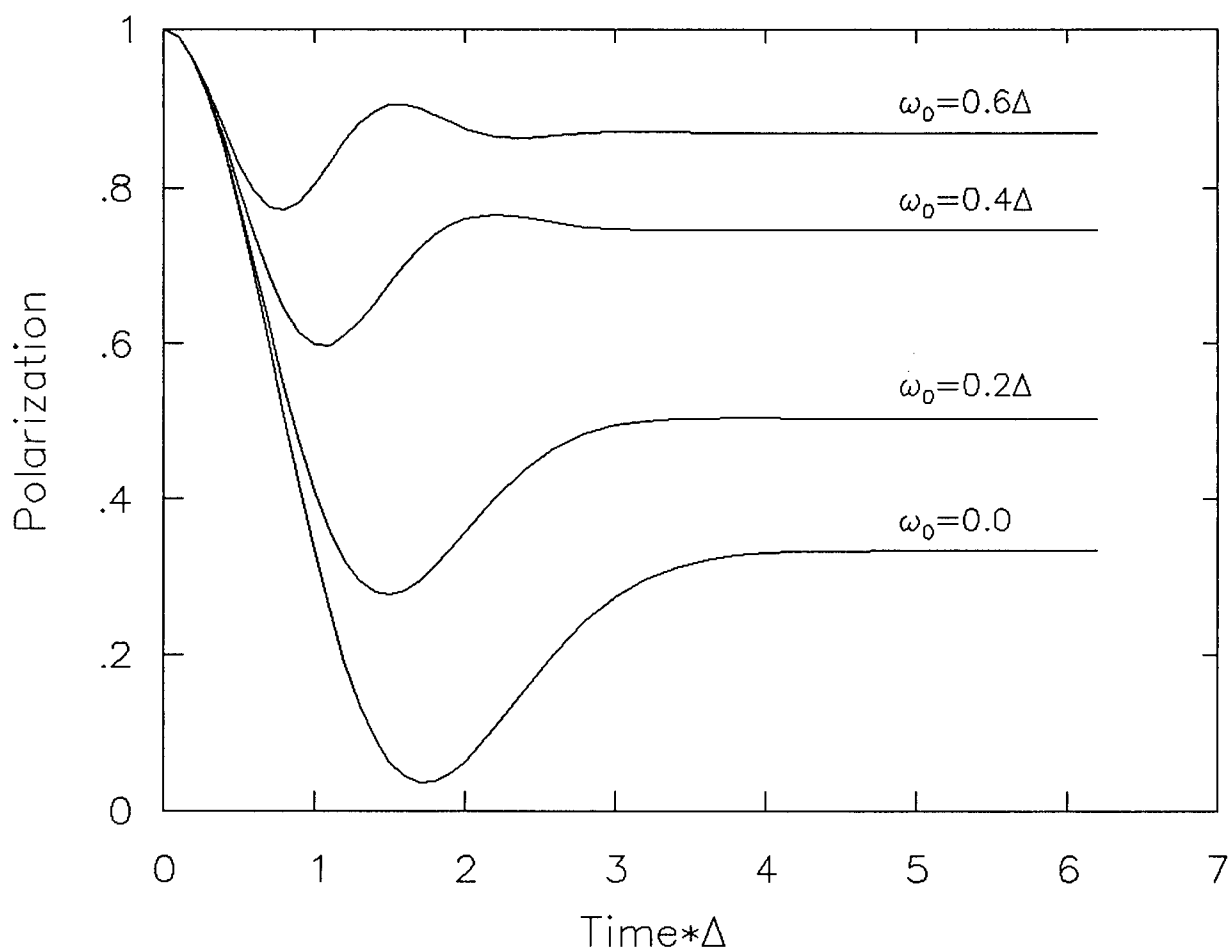


Figure 2.1: Kubo-Toyabe Theory– Static Muon Polarization vs. Time, in zero field and several longitudinal fields ω_0/Δ

2.2 Quantum Mechanical Zero Field Calculations

The first quantum mechanical calculations of the zero field relaxation functions were done by Celio and Meier [67]. They considered the case of a muon interacting with both four and six neighbouring nuclei through the dipolar interaction. The Hamiltonian is sum of the dipolar interactions between the muon ($\mathbf{I} = \frac{1}{2}$) and its N neighbouring spins (\mathbf{J}_i) as well as the muon and nuclear Zeeman interactions (quadrupolar interactions have been disregarded).

$$\mathcal{H} = \mathcal{H}^Z + \sum_{i=1}^N \mathcal{H}_i^D \quad (2.11)$$

$$\mathcal{H}^Z = \hbar\gamma_\mu \mathbf{I} \cdot \mathbf{B} - \sum_{i=1}^N \hbar\gamma_i \mathbf{J}_i \cdot \mathbf{B} \quad (2.12)$$

$$\mathcal{H}_i^D = \frac{\hbar^2 \gamma_\mu \gamma_{Cu}}{r_i^3} [\mathbf{I} \cdot \mathbf{J}_i - 3(\mathbf{I} \cdot \mathbf{n}_i)(\mathbf{J}_i \cdot \mathbf{n}_i)] \quad (2.13)$$

$$= \hbar\omega_i^D [\mathbf{I} \cdot \mathbf{J}_i - 3(\mathbf{I} \cdot \mathbf{n}_i)(\mathbf{J}_i \cdot \mathbf{n}_i)] \quad (2.14)$$

$$= \hbar\omega_i^D \left\{ \left[I^z J_i^z - \frac{1}{4}(I^+ J_i^- + I^- J_i^+) \right] (1 - 3 \cos^2 \theta_i) \right. \\ \left. - \frac{3}{2} \left[(I^+ J_i^z + I^z J_i^+) e^{-i\phi_i} + (I^- J_i^z + I^z J_i^-) e^{i\phi_i} \right] \sin \theta_i \cos \theta_i \right. \\ \left. - \frac{3}{4} \left[I^+ J_i^+ e^{-2i\phi_i} + I^- J_i^- e^{2i\phi_i} \right] \sin^2 \theta_i \right\} \quad (2.15)$$

where \mathbf{n}_i is the unit vector from the μ^+ to the i th copper nucleus, at a distance r_i , radial and azimuthal angles θ_i, ϕ_i . The muon and copper gyromagnetic ratios are γ_μ and γ_{Cu} . The secular part of \mathcal{H}_i^D is comprised of those terms in $I^z J_i^z$ - *i.e.*, those which commute with the Zeeman interaction.

The muon spin polarization is given in general by

$$\mathcal{P}_\mu(t) = \text{Tr}[\rho \exp(i\mathcal{H}t/\hbar) \boldsymbol{\sigma}_\mu \exp(-i\mathcal{H}t/\hbar)] \quad (2.16)$$

where $\boldsymbol{\sigma}_\mu = 2\mathbf{I}_\mu$ are the Pauli matrices. The density matrix ρ in the case of initially

unpolarized nuclei and muon polarization $\mathcal{P}_\mu(0)$ is given by

$$\rho = \frac{1}{2(2J+1)^N} [1 + \mathcal{P}_\mu(0)\sigma_\mu] \quad (2.17)$$

In zero field, the second moment [59] of the muon polarization $M_2 = 2\Delta^2$ may be obtained

$$M_2 = -\frac{\text{Tr}([\mathcal{H}', I^z])}{\text{Tr}(I^z)^2} \quad (2.18)$$

where \mathcal{H}' is the secular part of the Hamiltonian. In the case $J = \frac{3}{2}$, the second moment is [10]

$$M_2 = 5\gamma_\mu^2\gamma_J^2 \sum_j r_j^{-6} \quad (2.19)$$

Equation 2.16 is evaluated by calculating the $2 \times (2J+1)^N$ eigenvalues and eigenvectors of the Hamiltonian \mathcal{H} , and then performing the trace in the basis of the eigenvectors.

Although the calculations became rather time-consuming as the number of nuclei increased, their results demonstrated some of the limitations of the Kubo-Toyabe (K-T) theory. Celio and Meier found marked differences from the K-T results, such as the fact that the polarization didn't reach a constant 1/3 tail, but rather oscillated at long times. These oscillations result from the nonsecular terms in the dipolar interaction (those terms which don't commute with the Zeeman interaction, and cause flip-flops of the muon and nuclear spins).

Rather large deviations from the Kubo-Toyabe theory have been observed in the so-called "F- μ -F" system which forms when muons are injected into most fluorides, such as CaF₂, LiF, or YF₃ [16,79]. In this case, the muon is essentially coupled to only its two neighbouring fluorine nuclei (spin $J=1/2$). In zero field the resulting muon polarization shows extremely large oscillations, as shown in figure 2.2.

Celio and Meier extended their technique to include the interaction with spin ($J=1$) nuclei [80], which experience a quadrupolar interaction with the the electric field gradient caused by the muon's charge as well as the destruction of the cubic symmetry

of the nucleus by the muon-induced lattice distortion. They found that in the case of a strong quadrupole interaction ($\omega^Q > 15\omega^D$), the entire relaxation function became independent of the quadrupole interaction (as only the $\pm 1/2$ states of the nuclear spin remained coupled to the muon spin through the dipolar interaction).

The further application of this method of exact diagonalization to higher dimensional spin systems (either to larger numbers of interacting spins or larger spins \mathbf{J}) became prohibitive due to the amount of computation required. Holzschuh and Meier [53] investigated the spin dynamics of a muon interacting with a number of neighbouring spin $3/2$ nuclei in the limit of a strong nuclear quadrupolar interaction. In this limit, the nuclear spins have a two level energy level spectrum, and they were able to give an analytic expression for the solution of equation 2.16. Again, they found differences from the Kubo-Toyabe theory, which were most pronounced for lower dimensional spin systems. The amplitude of the long time oscillations in reference [67] were reduced when the quadrupole interaction and the interaction with further shells of neighbours were considered.

In the case of a dominant quadrupole interaction, the second moment in a cubic lattice, for spin $3/2$ nuclei, is [10]

$$M_2 = 4\gamma_\mu^2 \gamma_J^2 \sum_j r_j^{-6} \quad (2.20)$$

which is reduced by a factor of 0.8 from the case where there is no quadrupole interaction.

2.3 Exact Static Theory

Although useful in that it is a simple classical model which displays approximately correct behaviour, Kubo-Toyabe theory is not precise enough to permit accurate measurement of subtle differences from the static relaxation function. Various quantum mechanical calculations have been made for the zero-field case, but these methods cannot easily be extended to include the effects of an applied field.

In principle, diagonalizing the full quantum mechanical Hamiltonian is possible for a muon interacting with its 6 nearest neighbours. However, this requires the diagonalization of an 8192×8192 matrix, which is beyond practical computation. Celio [81,82], recently solved the problem of evaluating the theoretical muon polarization as a function of time, allowing an exact treatment of the entire Hamiltonian, even when the various parts don't commute with each other.

In general, the Hamiltonian is given by

$$\mathcal{H}_{tot} = \sum_{i=1}^N \mathcal{H}_i, \quad [\mathcal{H}_i, \mathcal{H}_j] \neq 0 \quad \text{for } i \neq j \quad (2.21)$$

where each term in the sum over N neighbours is the sum of dipolar, quadrupolar and Zeeman terms.

$$\mathcal{H}_i = \mathcal{H}_i^D + \mathcal{H}_i^Q + \mathcal{H}_i^Z \quad (2.22)$$

where

$$\mathcal{H}^Z = \frac{1}{N} \hbar \gamma_\mu \mathbf{I} \cdot \mathbf{B} - \hbar \gamma_{Cu} \mathbf{J}_i \cdot \mathbf{B} \quad (2.23)$$

$$\mathcal{H}_i^D = \hbar \omega_i^D [\mathbf{I} \cdot \mathbf{J}_i - 3(\mathbf{I} \cdot \mathbf{n}_i)(\mathbf{J}_i \cdot \mathbf{n}_i)] \quad (2.24)$$

$$\mathcal{H}_i^Q = \hbar \omega_i^Q [(\mathbf{n}_i \cdot \mathbf{J}_i)(\mathbf{n}_i \cdot \mathbf{J}_i) - J(J+1)/3] \quad (2.25)$$

The quadrupolar term arises from the fact that the muon destroys the cubic symmetry of its neighbouring copper nuclei and exerts an electric field on them. It is assumed in

equation 2.25 that the electric field gradient on each copper nucleus is axially symmetric around \mathbf{n}_i and is the only field gradient present. As the electric field gradient and lattice distortion are dependent on the local geometry, the quadrupole frequency will depend on the muon site. The quadrupole frequency ω^Q is given in terms of the quadrupole moment of the nucleus Q and the electric field gradient eq by:

$$\begin{aligned}\hbar\omega^Q &= \frac{3e^2qQ}{4J(2J-1)} \\ &= \frac{e^2qQ}{4} \quad \text{for } J=3/2\end{aligned}\tag{2.26}$$

One wants to solve for the muon polarization which, in terms of the density matrix ρ is

$$\mathcal{P}_\mu(t) = \text{Tr}[\rho\sigma_\mu(t)]\tag{2.27}$$

where the density matrix ρ is given in terms of the Pauli matrices $\sigma_\mu = 2\mathbf{I}_\mu$ in equation 2.17. One may express $\sigma_\mu(t)$ as a function of time

$$\sigma_\mu(t) = e^{i\mathcal{H}_{tot}t/\hbar}\sigma_\mu(0)e^{-i\mathcal{H}_{tot}t/\hbar}\tag{2.28}$$

Thus, in a representation where σ_μ^z is diagonal, equation 2.27 can be written in the Schrödinger picture:

$$\mathcal{P}_\mu(t) = \sum_{n=1}^d W_n \langle \psi_n(t) | \sigma_\mu | \psi_n(t) \rangle\tag{2.29}$$

where

$$|\psi_n(t)\rangle = e^{-\mathcal{H}_{tot}t/\hbar}|\psi_n(0)\rangle\tag{2.30}$$

The weights W_n in equation 2.29 are given by the elements of the (diagonal) density matrix ρ .

$$\begin{aligned}\rho &= W_n |\psi_n(0)\rangle \langle \psi_n(0)| \\ W_n &= 2/d \quad \text{if } \sigma_\mu^z |\psi(0)\rangle = +|\psi(0)\rangle \\ W_n &= 0 \quad \text{if } \sigma_\mu^z |\psi(0)\rangle = -|\psi(0)\rangle\end{aligned}\tag{2.31}$$

One cannot simply expand the exponentials into sums of simple block diagonal terms, since the various parts of \mathcal{H}_{tot} don't commute with each other. However, one may use the Trotter formula to allow the separation of the exponentials.

$$\begin{aligned} e^{\mathcal{H}_i + \mathcal{H}_j} &= \lim_{n \rightarrow \infty} \left(e^{\frac{\mathcal{H}_i}{n}} e^{\frac{\mathcal{H}_j}{n}} \right)^n \\ &\neq e^{\mathcal{H}_i} e^{\mathcal{H}_j} \end{aligned} \quad (2.32)$$

Thus, equation 2.30 can be written

$$|\psi_n(t)\rangle = \lim_{k \rightarrow \infty} \left[\prod_{j=1}^N \exp(-\mathcal{H}_j(t)/\hbar k) \right]^k |\psi_n(0)\rangle \quad (2.33)$$

The advantage of this procedure is that each of the \mathcal{H}_j describe the interaction a single nuclear spin \mathbf{J}_j with that of the muon and as a result have the simple structure $\mathbf{1}_1 \otimes \mathbf{1}_2 \cdots \otimes \mathcal{H}_j \otimes \cdots \otimes \mathbf{1}_N$, where $\mathbf{1}$ is the unit matrix. In the case of a muon sitting in an octahedral interstitial site (as for the case of copper), this procedure allows one to consider only the 8×8 portions of the Hamiltonian corresponding to the interaction of the muon with one of its spin- $\frac{3}{2}$ neighbours. The problem of diagonalizing a large matrix has been replaced by a large number of multiplications of much smaller ones. In practice, the largest value of k in equation 2.33 is chosen to be large enough such that any error in the resulting polarization is negligible over the time region of interest (usually $t < 16\mu s$).

The second point of Celio's method is to use the Schrödinger picture, that is to place all time dependence of observables in the state vectors, rather than in the operators. This is purely for computational ease, as the number of elements of a vector is only the square root of the number of elements in an operator.

The state vector at time zero (when the muon enters the sample) can be expanded in a basis of states which have the muon initially polarized along the \hat{z} axis.

$$|\phi(0)\rangle = \sum_{i=1}^{\frac{d}{2}} a_i |\psi_i(0)\rangle \quad (2.34)$$

where

$$\sum_{i=1}^{\frac{d}{2}} |a_i|^2 = 1$$

These initial states can then be time-developed in time according to equation 2.30.

Rather than follow this procedure for all $(d/2)$ possible initial states, one chooses a random set of a_i 's, subject to normalization conditions, and repeats this time development a number of times, averaging over the final result. The initial state $|\phi(0)\rangle$ corresponds to a state with the muon polarized along the $+z$ direction with randomly polarized nuclei. This expansion is similar to a random phase approximation.

$$|\phi(t)\rangle = \sum_{m=1}^{\frac{d}{2}} \sqrt{\frac{2}{d}} e^{i\lambda_m} |\psi_m(t)\rangle \quad (2.35)$$

Equation 2.29 can then be expressed in terms of these random phases λ

$$\begin{aligned} \langle \phi(t) | \sigma_\mu | \phi(t) \rangle &= \sum_{m=1}^{\frac{d}{2}} \left(\frac{2}{d} \right) \langle \psi_m(t) | \sigma_\mu | \psi_m(t) \rangle \\ &+ \sum_{m,n=1, m \neq n}^{\frac{d}{2}} \left(\frac{d}{2} \right) e^{i(\lambda_m - \lambda_n)} \langle \psi_n(t) | \sigma_\mu | \psi_m(t) \rangle \end{aligned} \quad (2.36)$$

The second term in equation 2.36 tends to zero in the limit of large d , thus the random phase approximation becomes more exact with the increasing dimensionality of the system.

The advantage of this method of computation is that it is based on the full microscopic Hamiltonian; the only interaction neglected is that between the various copper nuclei, which is extremely small, so that its effects could not be seen in the time scale of μ SR experiments.

The results of the calculation of the muon polarization function is shown in figure 2.3, for longitudinal magnetic fields between 0 and 120 G. The computation for each field value required approximately 1 hour CPU on a VAX-8600.

Measuring the hop rate depends on being able to measure small differences in the polarization function from a theoretical static function. This means that one must have an accurate theoretical function in order to extract accurate hop rates. Clearly Kubo-Toyabe theory, which predicts a $1/3$ tail, is not accurate enough at low hop-rates, as can be seen from figure 2.4, which shows the differences between KT theory and the exact results. In WLF, the calculated polarization is less model-dependent and the hop rate results are thus less dependent upon having an absolutely accurate model for the spin system.

2.4 Level-Crossing Resonance

One of the striking features of figure 2.3 is the enhanced relaxation which occurs around $B_{\text{res}} \approx 80$ G. This level-crossing resonance (LCR) occurs approximately when the quadrupolar splitting of the muon's nearest neighbour copper nuclei is equal to the muon's Zeeman splitting. At this field, the dipolar coupling between the spins causes a cross-relaxation to take place, as energy-conserving flip-flop transitions can occur (where both the muon and nuclear spins change by ± 1 , such that the sum of the spins stays constant).

The effect of the resonance can be demonstrated by considering the simple case of a muon interacting with a single spin- $3/2$ copper nucleus. Half of the matrix elements of the Hamiltonian (those which are involved in the resonance around $\omega^Z = -2\omega^Q$) are shown in figure 2.5. In general, for applied fields greater than the dipolar field of approximately 4 G, the Hamiltonian is essentially diagonal in the direct product representation of muon spin J_z and copper spin I_z , as the diagonal elements of the Hamiltonian are much larger than the off diagonal ones. This means that there are very few transitions between states with different muon spin, and there is little relaxation

of the muon asymmetry. However, near the field where the muon Zeeman frequency equals the copper quadrupole frequency, the diagonal elements become very small, and there is a large mixing of states; the initial state is no longer an eigenstate of the Hamiltonian. Transitions to other states with different \hat{z} -component of muon spin are enhanced and there is an increased muon spin relaxation.

Figures 2.5, 2.6 show that there are in fact four resonances, as there are four values of the applied field where one of the diagonal elements can be zero. This occurs because the energy levels of the copper nuclei, which are split by the quadrupolar interaction are also split by the nuclear Zeeman interaction as shown in figure 2.6. Thus the actual resonance will be a superposition of four lines, whose positions and relative amplitudes depend on the orientation angle θ (between the muon-nuclear axis and the applied field). Each line has a width given by the strength of the coupling between the mixing states, *i.e.*, the dipolar field of approximately 4 G. These four lines will be distributed over a field range of the order of the copper nuclear Zeeman interaction strength ($\sim B_{\text{res}}\gamma_{\text{Cu}}/\gamma_{\mu}$). For a larger number of nuclei (such as six in the case of the muon octahedral site), the resonance contains contributions from copper nuclei at a number of different angles which are convolved together in a complicated manner, which has not been solved analytically. However, the total width of the resonance is still of the order of the copper nuclear Zeeman strength.

Calculations involving larger numbers of copper nuclei become extremely complicated, as the natural quantization direction is different for each of the different copper nuclei. This has the result that as the dimensionality of the Hamiltonian quickly increases with the number of nuclei, so does the complexity, as the Hamiltonian isn't easily diagonalized near resonance. The only accurate calculations are those done as described above, using the Trotter formula.

Because the resonance occurs approximately at a field where the muon Zeeman frequency equals the copper quadrupole frequency and the quadrupole splitting is a result of the electric field gradient produced by the muon, the LCR provides an extremely sensitive probe of the muon site. If the muon were to occupy a different site, with a different muon-copper separation, the position of the resonance would shift. If the number of nuclei involved in the resonance changed, there would be a change in the form of the relaxation function, even if the muon-nuclear distance remained the same. As an example of this sensitivity of the LCR to the detailed nature of the muon site, in a separate application, LCR has been used to prove that one of the muonium centers in silicon is situated exactly between two silicon nuclei [34].

2.5 Strong Collision Model for Diffusion

The above discussion has been restricted to the case where the muon is static, *i.e.* fixed at one site in the lattice. If the muon is diffusing, however, the relaxation of the μ^+ polarization will be modified, as it hops from one site, where it has exchanged some of its polarization with its neighbours, to another site, surrounded by initially unpolarized nuclei. The effects of diffusion are generally described within the framework of the strong collision model [83,49,84]. The term “strong collision” refers to the evolution of the local field experienced by the μ^+ , which is assumed to change discontinuously at the time of a hop and to be uncorrelated with the evolution at the previous site.

In the strong collision model the muon is assumed to be hopping at random times between equivalent sites, with some average frequency ν . The time spent during a jump is taken to be much shorter than the mean residence time at a site. The probability that the muon is still at its initial site after some period of time is simply given by an

exponential decay:

$$P(\text{at initial site}) = e^{-\nu t} \quad (2.37)$$

The model also assumes that there is no correlation between the local field experienced by the muon before and after a hop (other than external fields). Thus the correlation of the local field at some site j at time t with that at time 0 and site i is given by

$$\langle H_i(0)H_j(t) \rangle = \delta_{ij} \langle H_i^2(0) \rangle e^{-\nu t} \quad (2.38)$$

The muon polarization at some time t will then contain contributions from muons which have not hopped at all, those that have hopped once, twice and so on.

$$G_z(t) = \sum_{n=0}^{\infty} g_z^{(n)}(t) \quad \text{where } n = \# \text{ of hops} \quad (2.39)$$

$$\begin{aligned} &= e^{-\nu t} \{ g_z(t) \\ &+ \nu \int_0^t g_z(t_1) g_z(t - t_1) dt_1 \\ &+ \nu^2 \int_0^t \int_0^{t_1} g_z(t_1) g_z(t_2 - t_1) g_z(t - t_2) dt_1 dt_2 \\ &+ \dots \} \end{aligned} \quad (2.40)$$

This can be solved by taking the Laplace transform and summing the infinite series, giving a result which can be inverted numerically. Equation 2.40 can be expressed:

$$G_z(t) = e^{-\nu t} g_z(t) + \nu \int_0^t g_z(\tau) e^{-\nu \tau} G_z(t - \tau) d\tau \quad (2.41)$$

This expression can be solved by numerical integration, allowing one to generate “dynamic” relaxation functions from static ones, as a function of the average hop rate.

In zero field, there are two simple limits where the form of the relaxation function can be seen. In the case of slow hopping and long times, where the mean hop frequency is much smaller than the second moment of the field distribution (*i.e.*, Δ in Kubo-Toyabe theory) and the time is much longer than $1/\Delta$, the effects of hopping are seen

in the 1/3 tail, which relaxes.

$$G_z(t) \simeq \frac{1}{3} \exp\left(\frac{-2}{3}\nu t\right) \quad (\nu \ll \Delta, \quad t \gg \Delta^{-1}) \quad (2.42)$$

This describes the slow decay of the 1/3 tail seen in Kubo-Toyabe theory. It can be seen that in the limit of slow hopping, within the strong collision model and Kubo-Toyabe theory, the decay of the tail becomes independent of Δ , whose value can be deduced from the second moment of the polarization (*i.e.*, from short times), which is independent of the hop rate. In this limit, most of the muons don't hop until times longer than the time at which the polarization has reached its minimum value ($\sim \sqrt{3}/\Delta$) and recovered towards 1/3. Thus the minimum remains, with the main effect of slow hopping being the relaxation of the tail at long times.

In the limit of fast hopping, where the hop rate is much larger than Δ but still smaller than the dominant energy splittings in the system (such as Zeeman or quadrupole), one finds that the relaxation function has the form

$$G_z(t) \simeq \exp\left(\frac{-2\Delta^2 t}{\nu}\right) \quad (\Delta \ll \nu \ll \gamma_I H_z, \omega^Q) \quad (2.43)$$

This corresponds to the extreme motional narrowing limit, at hop rates which are past the “ T_1 -minimum”. The minimum in the relaxation function disappears, as the majority of the muons hop before the polarization reaches its minimum ($t_{\min} \sim \sqrt{3}/\Delta$), which is therefore never reached.

The effect of diffusion on the relaxation function in copper is shown in figure 2.7 for zero field, and in figure 2.8 for weak longitudinal field. In zero field and at low hop rates there is little change in the relaxation function until long times ($t > 8\mu s$), whereas in WLF the changes occur much earlier. This has the potential to make the WLF method more sensitive in measuring very small (but non-zero) hop rates.

There are a number of experimental situations where some of the assumptions of the strong collision model could be violated and thus the model could be expected to

break down. First, the assumption that the local fields experienced by the diffusing particle before and after hopping are uncorrelated does not hold in the case of back diffusion (where the particle hops from one site and then returns to its original site). Second, there is the case of shared neighbours, before and after hopping. Celio [85] considered these effects in a number of numerical simulations of worst-case situations. He found that the general result of the correlations was to modify the extracted value of the hop rate by some constant factor (*i.e.*, independent of the hop rate) of order 1.

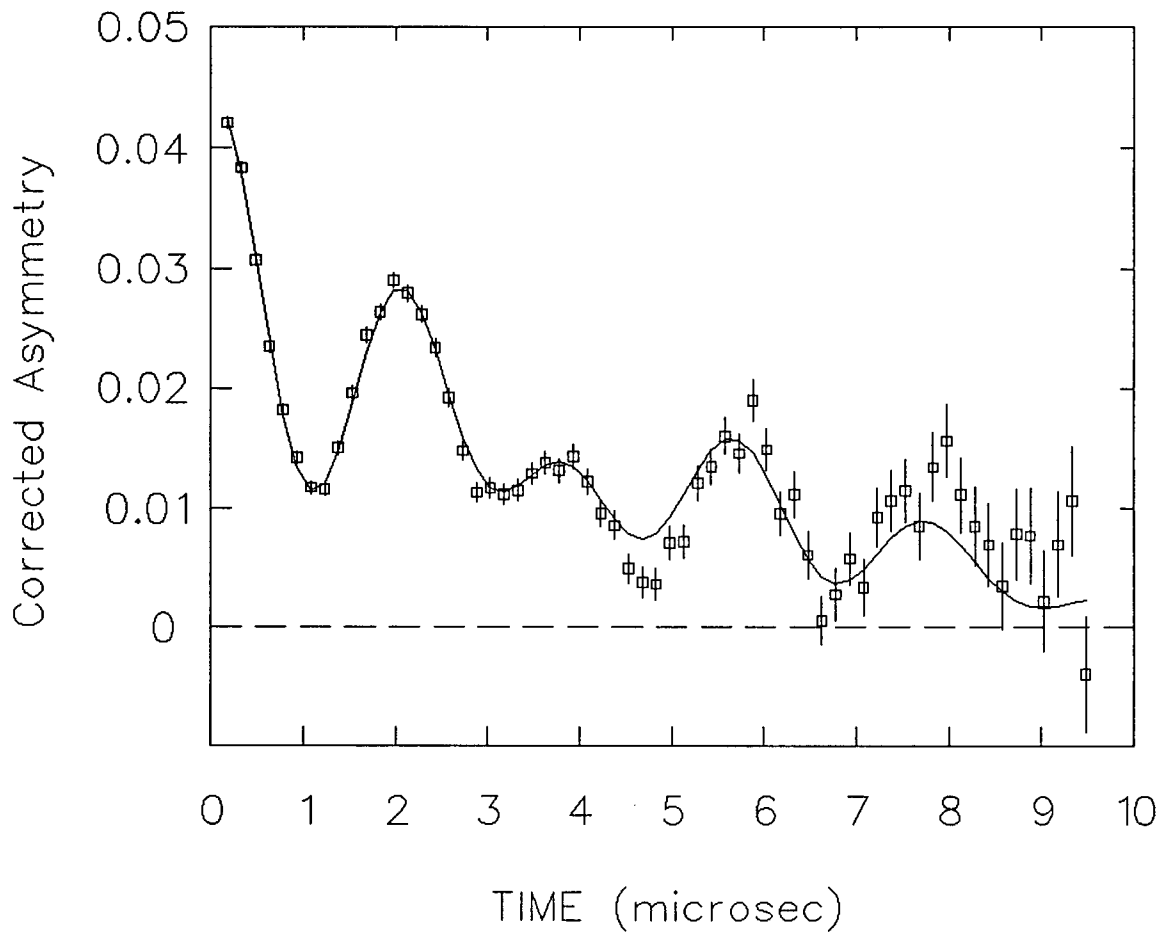


Figure 2.2: Zero field relaxation of muons in NaF, caused by dipolar interactions, showing deviations from Kubo-Toyabe behaviour

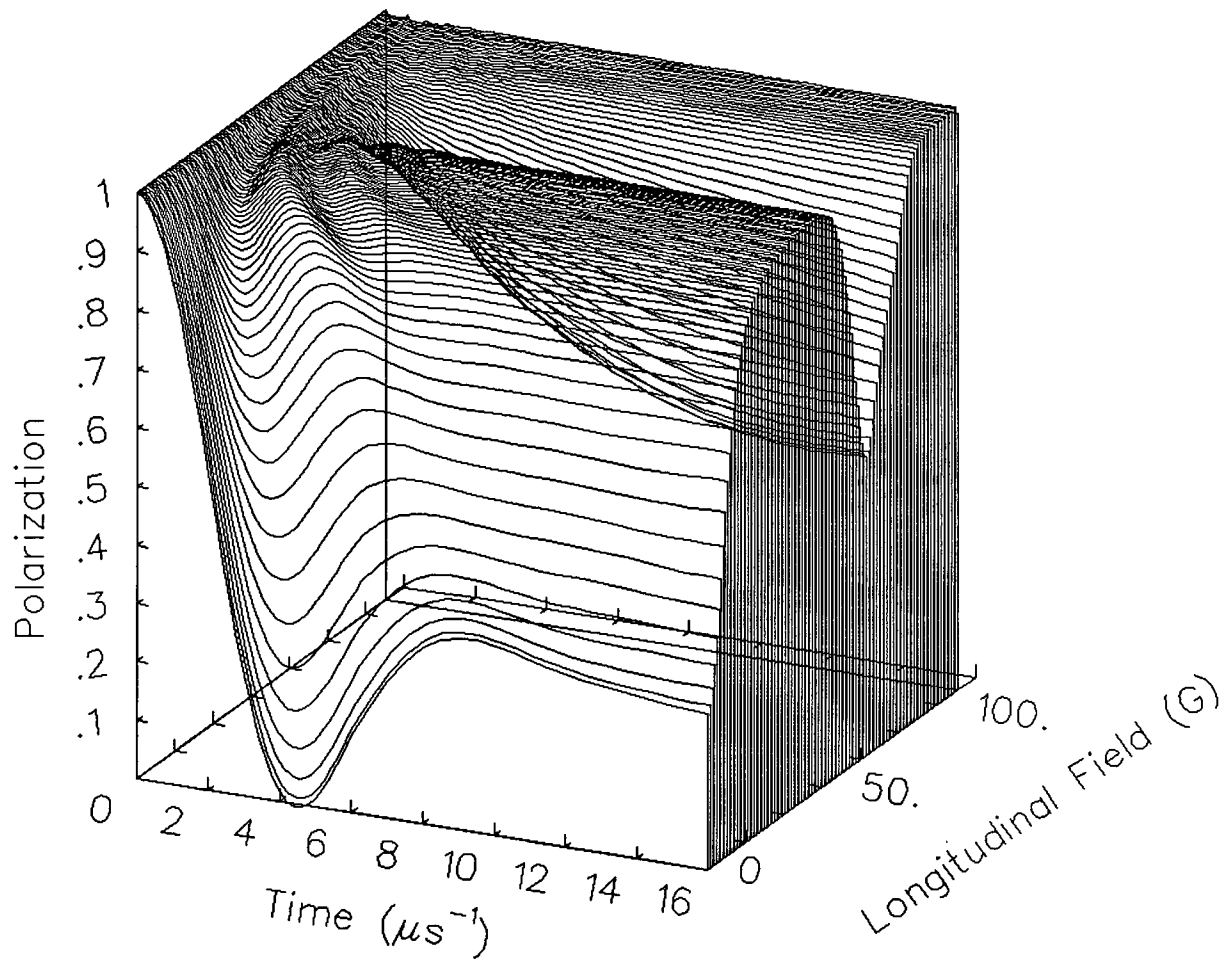


Figure 2.3: Exact Muon Polarization function — 6 nn Cu atoms, $\langle 110 \rangle$ orientation

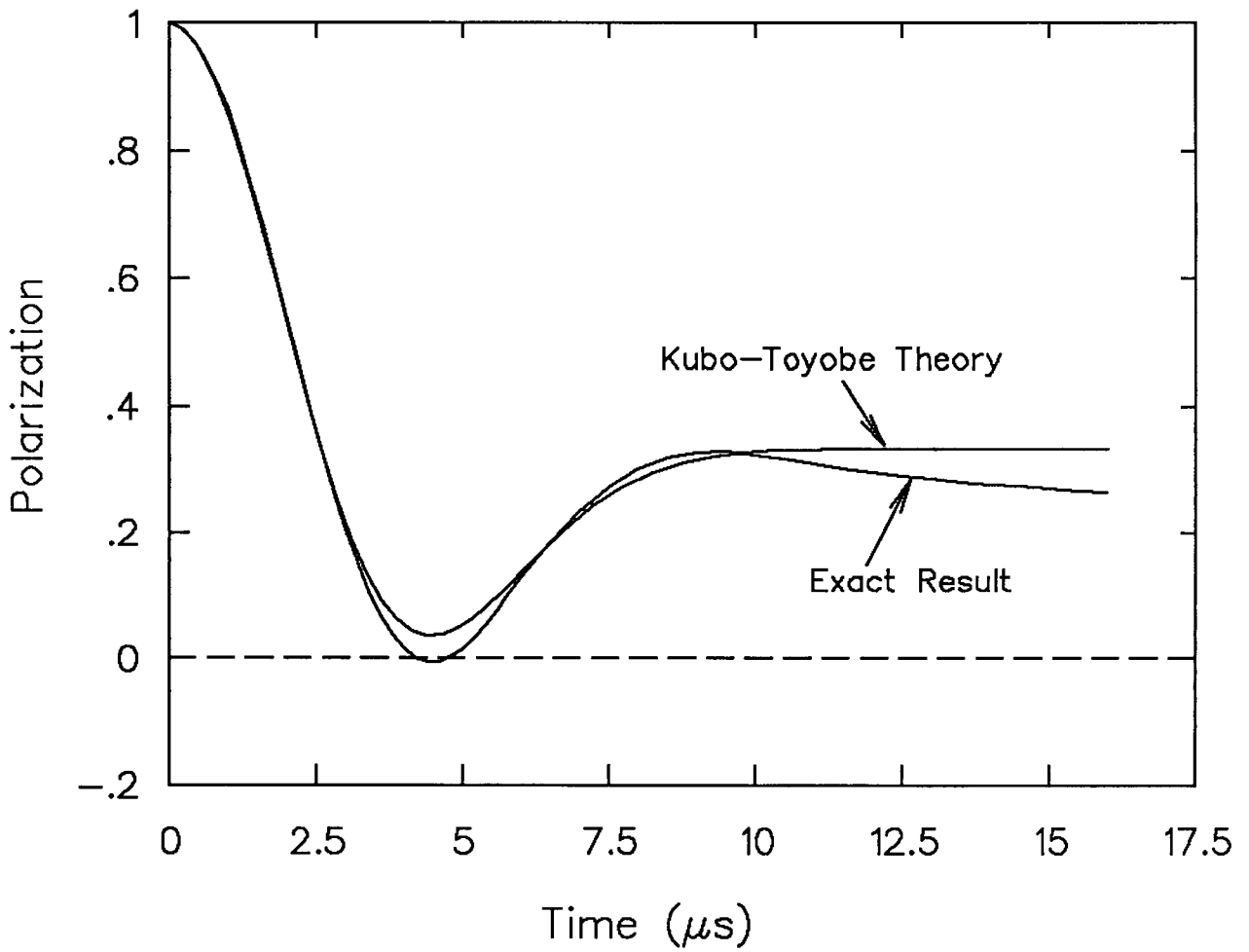


Figure 2.4: Comparison between Kubo-Toyabe and exact theory. Both curves shown for $\Delta = 0.387 \mu\text{s}^{-1}$.

	$ 3/2, \uparrow\rangle$	$ 1/2, \downarrow\rangle$	$ -1/2, \downarrow\rangle$	$ -3/2, \uparrow\rangle$
$ 3/2, \uparrow\rangle$	$(2\omega_i^Q + \omega_\mu^Z)/2 + 3/2\cos\theta(\omega_i^Z - \omega_i^D)$	$\frac{\sqrt{3}}{4}\omega_i^D(\cos\theta - 1)$		
$ 1/2, \downarrow\rangle$	$\frac{\sqrt{3}}{4}\omega_i^D(\cos\theta - 1)$	$-\frac{(2\omega_i^Q + \omega_\mu^Z)}{2} + \frac{1}{2}\cos\theta(\omega_i^Z + \omega_i^D)$	$\frac{(\omega_i^Z + \omega_i^D)}{2}\sin\theta$	
$ -1/2, \downarrow\rangle$		$\frac{(\omega_i^Z + \omega_i^D)}{2}\sin\theta$	$-\frac{(2\omega_i^Q + \omega_\mu^Z)}{2} + \frac{1}{2}\cos\theta(\omega_i^Z + \omega_i^D)$	$\frac{\sqrt{3}}{4}\omega_i^D(\cos\theta - 1)$
$ -3/2, \uparrow\rangle$			$\frac{\sqrt{3}}{4}\omega_i^D(\cos\theta + 1)$	$\frac{(2\omega_i^Q + \omega_\mu^Z)}{2} + \frac{3}{2}\cos\theta(\omega_i^Z - \omega_i^D)$

Figure 2.5: The Hamiltonian matrix displaying a quadrupolar LCR for a single spin 3/2 nucleus interacting with a muon. The quantization axis is along the muon-nuclear axis, except for the muon Zeeman interaction, which is quantized along the direction of the applied field.

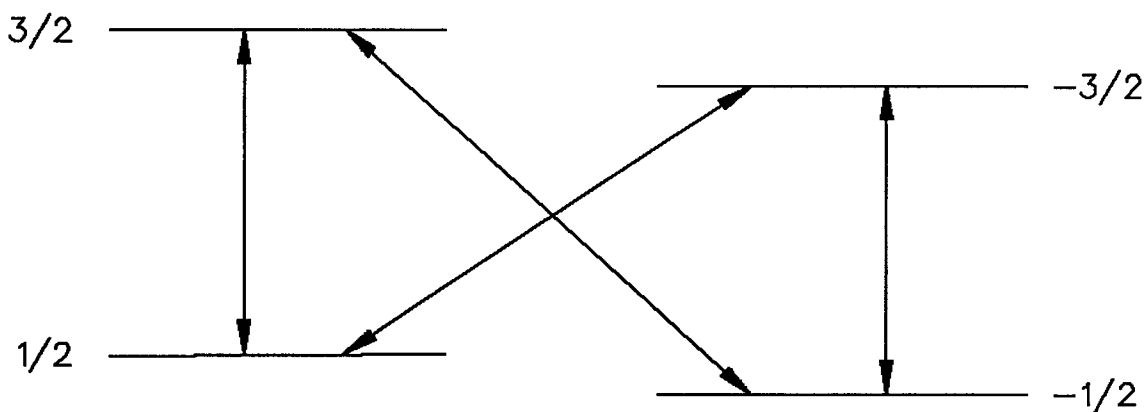


Figure 2.6: Copper energy level diagram for electric quadrupolar and Zeeman interaction.

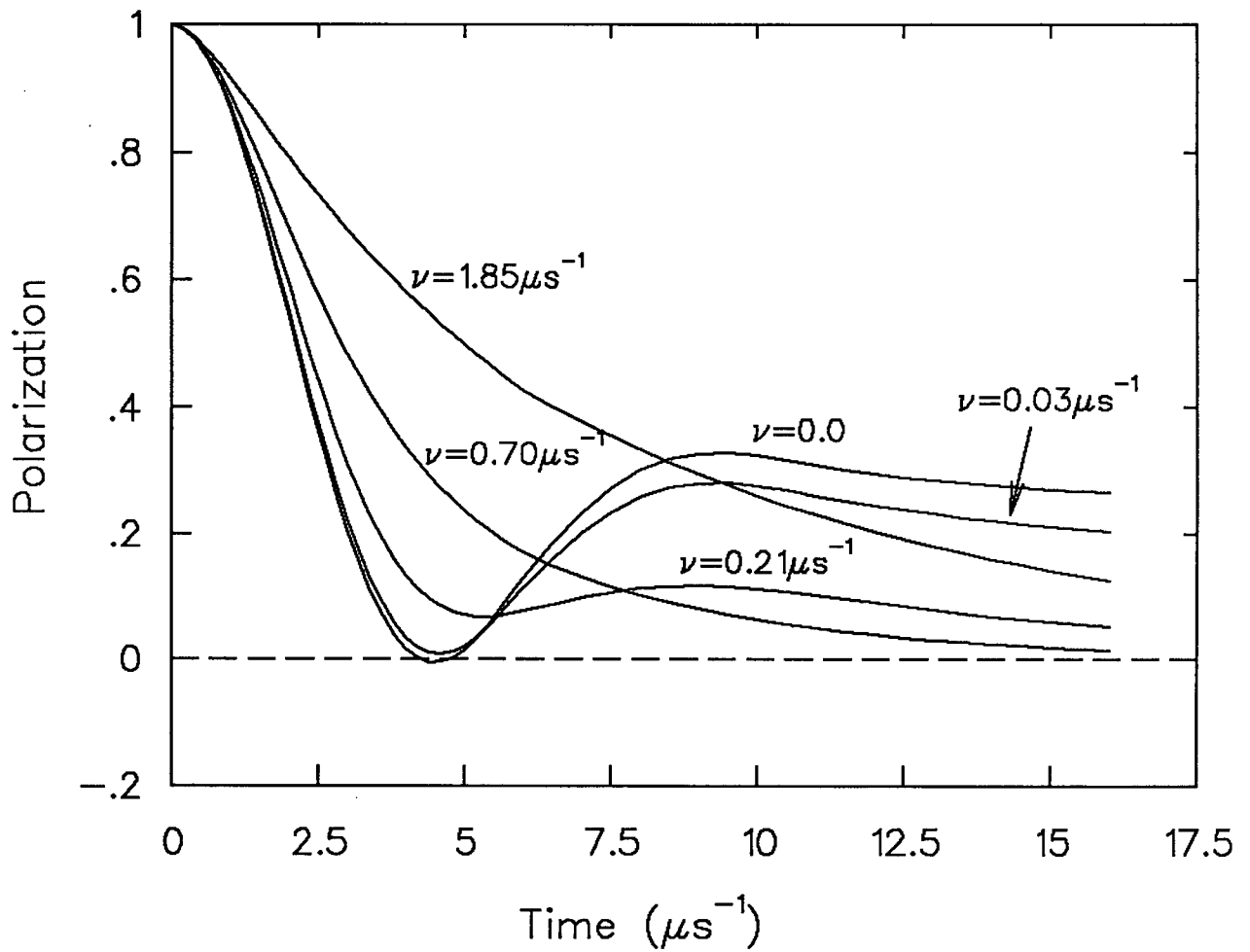


Figure 2.7: Muon Polarization in ZF with hopping

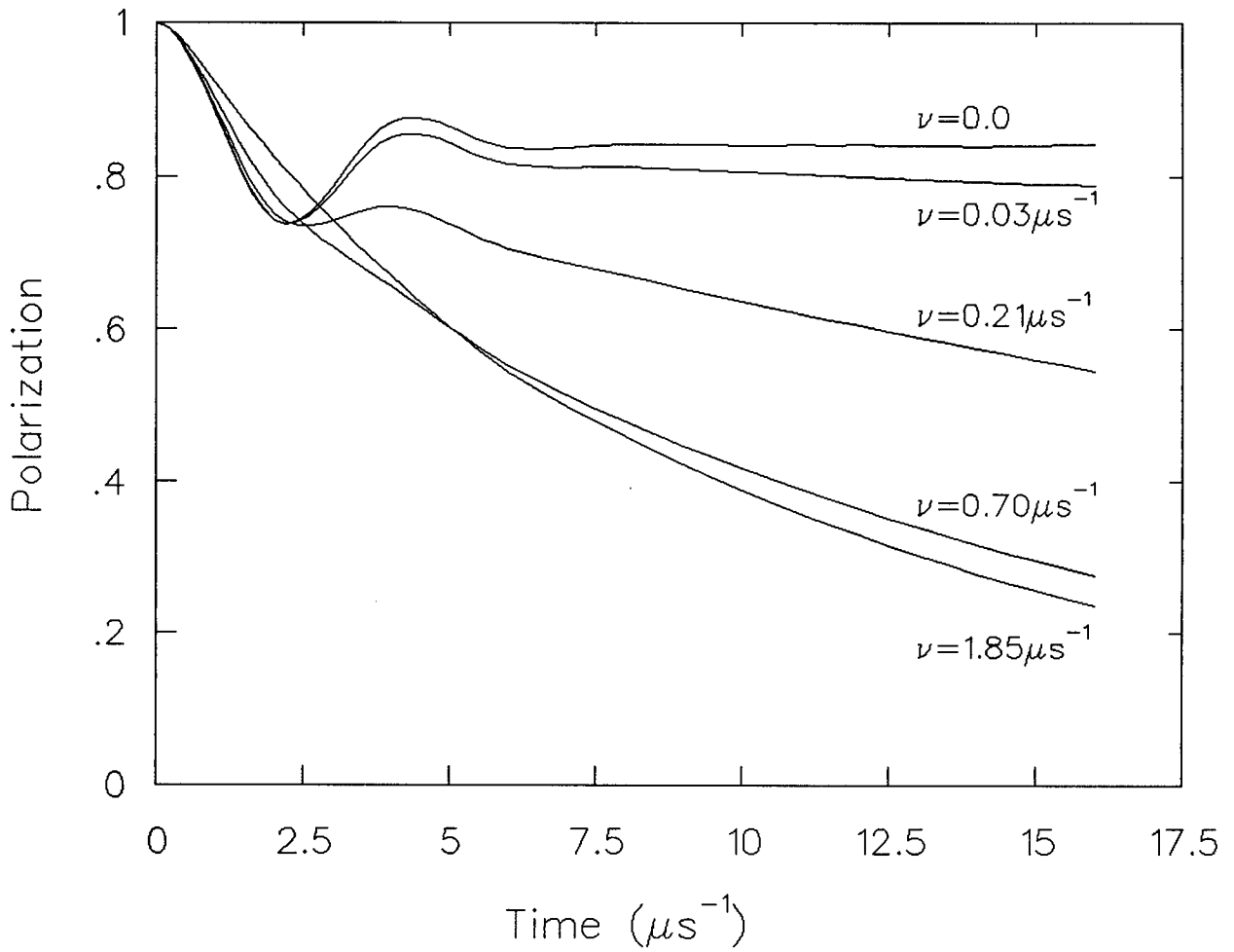


Figure 2.8: Muon Polarization Function in WLF with hopping.

Chapter 3

Diffusion Theories

There have been a number of theoretical attempts to calculate the diffusion rate of light interstitials in metals. The first attempts considered the damping effects of the linear impurity-lattice interaction on the diffusion rate. These calculations gave a temperature dependence in satisfactory agreement with the experimental μ SR results at temperatures above 50 K.

Further effects, including a quadratic lattice interaction and the interaction with the conduction electrons, have extended the theory to explain the muon diffusion data below 50 K. The overall magnitude of the diffusion rate has also proven difficult; only by considering all of these various effects is agreement with experiment reached over the range of temperatures accessible experimentally.

3.1 Flynn and Stoneham Theory

The first theoretical description of the diffusion of light interstitials in metals was due to Flynn and Stoneham [43], extending the polaron formalism of Holstein [42] to the case of light interstitials. They considered the case of so-called thermally activated tunneling, where the motion of the interstitial is slower than that of the phonons, *i.e.*,

when the bare impurity tunneling matrix element (\mathcal{J}) is smaller than the Debye energy.

$$\mathcal{J} \ll \hbar\omega_D \equiv k_B\Theta_D \quad (3.1)$$

They showed that the effect of the interaction between the interstitial and the lattice (the polaron interaction) was to reduce the effective tunneling matrix element

$$\mathcal{J}_{\text{eff}} = \mathcal{J} \exp[-S(T)] \quad (3.2)$$

$$\text{where } S(T) = \sum_q \left(\frac{A_q}{\omega_q}\right)^2 \left(n_q + \frac{1}{2}\right) \quad (3.3)$$

A_q is the interaction strength of a phonon of wavevector q with the interstitial and n_q is the thermal occupation of those phonons.

Treating \mathcal{J} as a perturbation and considering transitions between the ground states at the two sites (before and after hopping), they expressed the hop rate as

$$\mathcal{W} = \frac{\mathcal{J}^2}{\hbar^2} \int_{-\infty}^{\infty} \Phi(t) dt \quad (3.4)$$

$$\text{where } \Phi(t) = \exp[-2S(T)] \exp\left[\sum_q F_q(t)\right] \quad (3.5)$$

$$\text{and } F_q(t) = \left(\frac{A_q}{\omega_q}\right)^2 [n_q \exp(i\omega_q t) + (n_q + 1) \exp(-i\omega_q t)] \quad (3.6)$$

At temperatures greater than the Debye temperature, equation 3.4 reduces to an activated type expression

$$\mathcal{W} = \frac{\mathcal{J}^2}{\hbar} \left(\frac{\pi}{4E_a kT}\right)^{\frac{1}{2}} \exp\left(-\frac{E_a}{k_B T}\right) \quad (3.7)$$

where E_a is an activation energy.

At low temperatures, they found that two phonon processes, where there is an energy-conserving virtual absorption and re-emission of a phonon, was the dominant interaction in the tunneling. For jumps between equivalent sites, they found a T^7 temperature dependence.

$$\mathcal{W} = 1.14 \times 10^6 \left(\frac{E_a^2 \mathcal{J}^2}{\hbar^4 \omega_D^4}\right) \left(\frac{k_B T}{\hbar \omega_D}\right)^7 \quad (3.8)$$

3.2 Teichler Theory

In the first transverse field experiments on muon diffusion, the diffusion was described in terms of an activated process, as an Arrhenius-like temperature dependence of the hop rate was observed. Deviations from the Arrhenius behaviour were described in terms of a temperature dependent pre-exponential factor. Teichler [60] pointed out that in the temperature range where the temperature is comparable to and lower than half the Debye temperature there are few phonons present, and thus an activated process description is inappropriate.

His calculations, valid near $\Theta_D/2$, assume the adiabatic approximation for the electrons to be valid (*i.e.*, the conduction electrons rearrange themselves around the muon after it hops on a much faster timescale than the muon hop rate). The muon-lattice interaction is taken to be linear in the displacements of the host metal atoms. He obtained a temperature dependence which fit the muon hop rate data well in the temperature range between 20 K and 250 K. Above 250 K, he ascribed the muon hop rate as being predominantly due to over barrier diffusion, rather than tunnelling.

The hop rate was given in terms of two auxiliary functions $h_1(T/T_0)$ and $h_2(T/T_0)$ which depend only on the temperature and crystal structure. Both functions tend to T/T_0 for temperatures greater than $T_0 \sim \Theta_D/2$. He found the hop rate to be

$$\mathcal{W} = \frac{\mathcal{J}_{\text{eff}}^2}{\sqrt{h_1(T/T_0)}} \exp \left[\frac{-E_a}{k_B T_0 h_2(T/T_0)} \right] \quad (3.9)$$

$$\text{where } \mathcal{J}_{\text{eff}}^2 = \mathcal{J}^2 \sqrt{\frac{\pi}{4E_a k_B T_0}} \quad (3.10)$$

The activation energy E_a is given in terms of phonon energies and is the energy required to shift the lattice deformation to the neighbouring interstitial site. For temperatures greater than T_0 , equation 3.9 approaches the result of Flynn and Stoneham (equation 3.8).

3.3 Kagan-Klinger Theory

The first microscopic theory to describe the quantum diffusion of light interstitials in crystals was developed by Kagan and Klinger [86]. They gave results for under-barrier coherent and incoherent tunnelling rates, as well as for over-barrier hopping.

Their theory considered the effect of a change in the force constant between atoms near the interstitial position, a quadratic interaction with the lattice. They started with the picture of a localized interstitial and assumed that the adiabatic approximation for electrons was valid.

They showed that the coherent diffusion was disturbed by dynamical destruction of the particle band due to fluctuations in the interstitial energy levels in neighbouring wells, resulting from the interaction of the diffusing particle with phonons.

At low enough temperatures ($T \ll \Theta_D$) the coherent diffusion rate was found to be much greater than the incoherent hopping rate. The temperature dependence of the diffusion rate was given as:

$$\nu_{\text{coherent}} \sim T^{-9} \quad (3.11)$$

$$\nu_{\text{hop}} \sim T^7 \quad (3.12)$$

Their results show that even in temperature ranges where the bands are sufficiently narrow such that the mean free path is smaller than the lattice spacing the coherent transport process still predominates. The relative role of the hopping diffusion is strongly increased due to multiphonon processes with increasing temperature, with increasing strength of the polaron effect (or muon-lattice interaction). Hopping was predicted to become dominant for temperatures of the order of the Debye temperature and higher.

They also point out that a low density of particles and a highly perfect crystal were

necessary in order that the deformation and screened field of the charged impurities and strains due to dislocations do not destroy the coherent diffusion. They postulated that these conditions were not met in the hydrogen in metals experiments performed to that time. μ SR experiments were thought to be a promising field in which to search for the T^{-9} temperature dependence, as these experiments were always performed in the dilute impurity limit. However, no experimental evidence has been reported for a T^{-9} behaviour in the hop rate.

3.4 Kondo Theory

The most successful theory dealing with the quantum diffusion in metals is due to Kondo. He first pointed out the importance of considering the effect that the conduction electrons have on the diffusion of the muon [87]. When the muon is localized at one site, it attracts a screening charge of conduction electrons which surround it. When the muon hops to a neighbouring site, this charge cloud must follow it. Thus, the hop rate will be proportional not only to the overlap integral of the μ^+ wavefunctions at the two sites, but also to the overlap of the Slater determinants for the electrons at the two sites. The Anderson Orthogonality Theorem [88] states that this overlap will be zero at zero temperature, and small for low temperatures. This effect causes a large decrease in the calculated μ^+ hop rate. The orthogonality or infrared catastrophe states that the electronic screening clouds which form around the muon at different positions are orthogonal. This is a result of the fact that in a metal there exist infinitely small electron excitations across the Fermi level, with the result that the conduction electrons react slowly to perturbations (due to the high density of low-lying excitations), and thus can't follow the muon adiabatically.

Kondo considers the effects of four interactions when calculating the muon hop

rate: The muon-electron interaction, linear and quadratic muon-lattice interactions, and inhomogeneous broadening of the muon levels due to imperfections. This theory seems to be able to account for all of the features observed in the muon hop rate in the temperature range $20 \text{ mk} < T < 300 \text{ K}$.

In Kondo's model [77], the Hamiltonian is expressed as the sum of a number of terms. First, \mathcal{H}_0 is the unperturbed Hamiltonian of the phonons and electrons. $\mathcal{V}_L^{(A)}$ is the linear coupling of the muon to the lattice at the octahedral site (A), while $\mathcal{V}_Q^{(A)}$ is quadratic coupling (*i.e.*, a change in the force constant). The contribution of the electrostatic Coulomb potential felt by the muon at position \mathbf{R}_A is denoted $\mathcal{V}_E^{(A)}$. If the muon is static at site A , then the Hamiltonian may be written:

$$\mathcal{H}^{(A)} = \mathcal{H}_0 + \mathcal{V}_L^{(A)} + \mathcal{V}_Q^{(A)} + \mathcal{V}_E^{(A)} \quad (3.13)$$

The unperturbed phonon and electron part is given by:

$$\mathcal{H}_0 = \sum_{\mathbf{q}} \omega_{\mathbf{q}} b_{\mathbf{q}}^{\dagger} b_{\mathbf{q}} + \sum_{\mathbf{k}\sigma} \epsilon_{\mathbf{k}} a_{\mathbf{k}\sigma}^{\dagger} a_{\mathbf{k}\sigma} \quad (3.14)$$

where $\omega_{\mathbf{q}}$ is the frequency of the phonon with wave vector \mathbf{q} , $\epsilon_{\mathbf{k}}$ is the energy of the electron with wave vector \mathbf{k} , $b_{\mathbf{q}}^{\dagger}$ and $b_{\mathbf{q}}$ are creation and annihilation operators for phonons and $a_{\mathbf{k}\sigma}^{\dagger}$ and $a_{\mathbf{k}\sigma}$ are creation and annihilation operators for electrons.

The linear coupling to the lattice is given by:

$$\mathcal{V}_L^{(A)} = -\lambda(u_{1x} - u_{2x} + u_{3y} - u_{4y} + u_{5z} - u_{6z}) \quad (3.15)$$

where u_{ij} is the displacement of the i th nearest neighbour in the direction j .

The quadratic coupling is expressed:

$$\mathcal{V}_Q^{(A)} = \frac{1}{2}\mu \left[(u_{1x} - u_{2x})^2 + (u_{3y} - u_{4y})^2 + (u_{5z} - u_{6z})^2 \right] \quad (3.16)$$

A continuum approximation for the displacement \mathbf{u} at \mathbf{R} gives:

$$\mathbf{u}(\mathbf{R}) = \sqrt{\frac{b^3}{VM}} \sum_{\mathbf{q}} \frac{\mathbf{q}}{q} \frac{1}{\sqrt{\omega_{\mathbf{q}}}} (b_{\mathbf{q}}^{\dagger} + b_{-\mathbf{q}}) e^{i\mathbf{q}\cdot\mathbf{R}} \quad (3.17)$$

where V is the crystal volume, M is the mass of the nearest-neighbour atoms and $2b$ is the unit cell length.

The coulomb potential is given by:

$$\mathcal{V}_E^{(A)} = V_0 \sum_{\mathbf{k}\mathbf{k}'\boldsymbol{\sigma}} a_{\mathbf{k}\boldsymbol{\sigma}}^\dagger a_{\mathbf{k}'\boldsymbol{\sigma}} e^{i(\mathbf{k}'-\mathbf{k})\cdot\mathbf{R}_A} \quad (3.18)$$

corresponding to the scattering of the muon from an electron.

The entire interaction Hamiltonian is given by the sum over all interstitial points at \mathbf{n} :

$$\sum_{\mathbf{n}\boldsymbol{\sigma}} \left(\mathcal{V}_L^{(n)} + \mathcal{V}_Q^{(n)} + \mathcal{V}_E^{(n)} \right) c_{\mathbf{n}\boldsymbol{\sigma}}^\dagger c_{\mathbf{n}\boldsymbol{\sigma}} \quad (3.19)$$

where $c_{\mathbf{n}\boldsymbol{\sigma}}$ destroys a muon of spin $\boldsymbol{\sigma}$ at position \mathbf{n} .

The tunnelling energy of the muon is

$$\mathcal{H}_{\mu 0} = \mathcal{J}_0 \sum_{\mathbf{n}\boldsymbol{\rho}\boldsymbol{\sigma}} c_{\mathbf{n}\boldsymbol{\sigma}}^\dagger c_{\mathbf{n}+\boldsymbol{\rho}\boldsymbol{\sigma}} \quad (3.20)$$

where \mathcal{J}_0 , the bare muon tunnelling matrix element between nearest-neighbouring sites at \mathbf{n} and $\mathbf{n}+\boldsymbol{\rho}$ is treated as a perturbation when calculating the transition rate from site $A \rightarrow B$ and is given by the golden rule, with Φ factored into phonon ($\Phi^{(p)}$) and electron ($\Phi^{(e)}$) parts:

$$\mathcal{W}_{A \rightarrow B} = \mathcal{J}_0^2 \int_{-\infty}^{\infty} \langle e^{i\mathcal{H}^{(A)}t} e^{-i\mathcal{H}^{(B)}t} \rangle_A dt \quad (3.21)$$

where

$$\langle \dots \rangle_A = \frac{\text{Tr}(e^{-\beta\mathcal{H}^{(A)}} \dots)}{\text{Tr}(e^{-\beta\mathcal{H}^{(A)}})} \quad (3.22)$$

Following the treatment of Flynn and Stoneham, this can be written

$$\mathcal{W}_{A \rightarrow B} = \mathcal{J}_0^2 \int_{-\infty}^{\infty} \Phi^{(p)}(t) \Phi^{(e)}(t) dt \quad (3.23)$$

After this separation of the electron and phonon parts, Kondo obtains the result accurate at low temperatures:

$$\mathcal{W}_{A \rightarrow B} = \mathcal{J}_{\text{eff}}^2 \int_{-\infty}^{\infty} e^{-2\pi(K+K')k_B T|t| - i\pi(K+K') \text{sgn}(t)} dt \quad (3.24)$$

where

$$\mathcal{J}_{\text{eff}} = \mathcal{J}_0 e^{-S} \left(\frac{\pi k_B T}{\epsilon_F} \right)^K \left(\frac{\pi k_B T}{\omega_D} \right)^{K'} \quad (3.25)$$

$$S = \frac{\lambda^2 b^2}{6\pi^2 s^2 M \omega_D} \left(\frac{\omega_D b}{s} \right)^5 \quad (3.26)$$

$$K = 2V_0^2 \rho^2 \left(1 - \frac{\sin^2 k_F a}{k_F^2 a^2} \right) \quad a = |\mathbf{R}_A - \mathbf{R}_B| \quad (3.27)$$

$$K' = d \cdot G \left(\frac{T}{\Theta_D} \right) \approx \frac{64d}{15} \left(\frac{\pi T}{\Theta_D} \right)^8 \quad (3.28)$$

$$d = \frac{88}{225\pi^4} \left(\frac{\mu}{M\Theta_D^2} \right)^2 \left(\frac{\Theta_D b}{s} \right)^{12} \quad (3.29)$$

$$G(x) = \frac{x^8}{4} \int_0^{\frac{1}{x}} \frac{y^8}{\sinh^2 \frac{y}{2}} dy \quad (3.30)$$

ϵ_F is the Fermi energy, ρ is the electron density of states per spin and k_F is the Fermi wave number; s is the velocity of sound (we have used $\omega_{\mathbf{q}} = sq$ for the dispersion relation). \mathcal{J}_0 is the bare muon overlap integral between the two sites.

The exponent of equation 3.24 represents a damping of the muon motion from the effects of \mathcal{V}_E and \mathcal{V}_Q , but not from \mathcal{V}_L . The \mathcal{V}_E contribution is proportional to $k_B T$, whereas the \mathcal{V}_Q term varies as T^9 for $T \ll \Theta_D$, as pointed out by Kagan and Klinger. The second term (e^{-S}) in equation 3.25 represents the reduction of the tunnelling matrix due to the phonon cloud around the muon and is present in the results of Flynn and Stoneham (here $S = S(0)$ from equation 3.5). The third term is the overlap integral between the Slater determinants — the effect of the electron cloud around the muon. The last factor comes from \mathcal{V}_Q , and is approximately 1 for $T \ll \Theta_D$ (where $K' \rightarrow 0$).

At low enough temperatures,

$$\mathcal{W}_{A \rightarrow B} = \frac{\mathcal{J}_0^2 e^{-2S}}{\epsilon_F} \sqrt{\pi} \frac{\Gamma(K)}{\Gamma(K + \frac{1}{2})} \left(\frac{\pi k_B T}{\epsilon_F} \right)^{2K-1} \quad (3.31)$$

where Γ is the gamma function. The factor of T^{2K} in equation 3.31 comes from the electron cloud [87] and reflects the effect of the near orthogonality of the conduction

electron wavefunctions at the two sites, reducing the overlap integral. The T^{-1} factor comes from the fact that the energy levels are becoming sharper (with the level broadening being proportional to temperature) with decreasing temperature, and thus the overlap integral increases correspondingly. Equivalently, the final electron density of states is reduced by the smearing of the Fermi surface, which is proportional to T .

This T^{-1} behaviour was derived by Jäckle and Kehr [89], who calculated the effect of muon-electron scattering on the muon diffusion but neglected the effects of orthogonality on the electron overlap integrals.

At this point Kondo considers the effects of inhomogeneous broadening of the muon energy levels [90,77]. This involves the inclusion of a factor $e^{i(E_i - E_f)}$ in the integrand of equation 3.21, giving the calculated hop rate as a function of the energy difference $\mathcal{W}_{A \rightarrow B}(E_i - E_f)$. One then assumes a distribution of the muon energy levels and averages the hop rate over that distribution.

$$\mathcal{W}_{A \rightarrow B} = \frac{1}{Z} \int \int e^{-\beta E_i} p(E_i) p(E_f) \mathcal{W}_{A \rightarrow B}(E_i - E_f) dE_i dE_f \quad (3.32)$$

$$\text{where } Z = \int e^{-\beta E_i} p(E_i) dE_i, \quad \beta = (k_B T)^{-1} \quad (3.33)$$

For simplicity, the distribution of muon energy levels has been taken to be:

$$p(E) \begin{cases} 1/\delta_E & \text{if } 0 < E < \delta_E \\ 0 & \text{otherwise} \end{cases} \quad (3.34)$$

The hop rate in equation 3.32 is evaluated numerically, over all temperatures, as a function of seven parameters.

$$\mathcal{W}_{A \rightarrow B} = \frac{\mathcal{J}_0^2}{\Theta_D} \Xi \left(\frac{T}{\Theta_D}, S, \frac{\epsilon_F}{k_B \Theta_D}, d, \frac{\delta_E}{\Theta_D} \right) \quad (3.35)$$

The results of this calculation for the function Ξ are shown in figure 3.1 for a typical choice of parameters. There are four temperature regions of interest in the hop rate. At

high temperatures, phonon excitations are the most important factor in determining the hop rate of the small polaron. In this region there is an Arrhenius-like temperature dependence of the hop rate.

At intermediate temperatures around $T \sim 40$ K, there is a minimum in the hop rate. The depth of the minimum is increased with increasing quadratic lattice interaction strength d . For large enough d , the T^{-9} behaviour predicted by Kagan and Klinger starts to appear.

At low temperatures, electron-hole excitations (which have a high density of states at zero energy) dominate, causing an increase in the hop rate with decreasing temperature. In this temperature range, the temperature dependence of the hop rate is $\nu \sim T^{2K-1}$ as discussed above. Yamada [91], starting from a band-picture for the muon state, showed that the parameter K is always less than $1/2$; thus the hop rate increases with decreasing temperature in this regime.

As the temperature decreases, the initial and final energy states of the diffusing polaron become sharper, and since the hop rate is proportional to the probability of having the two states equal in energy, this contributes a T^{-1} factor to the hop rate. Lattice strains, caused perhaps by dislocations or by the mixture of isotopes, contribute a small distribution in the energies of polaron states from site to site which remains even at zero temperature. Thus, the hop rate does not increase indefinitely, but instead levels off at temperatures of the order of a characteristic spread in energies δ_E , and then decreases as $\nu \sim T^{2K}$.

Kondo also shows that the correct picture of muon diffusion is that of a localized μ^+ hopping, rather than band-like diffusion of a Bloch state. He estimated that the temperature of the cross-over to such a state would be at approximately 0.5 mK. At this point, the only effect of the muon-electron interaction would be the renormalization of the bandwidth from $\mathcal{J}_0 \rightarrow \mathcal{J}_{\text{eff}}$. Below this temperature, the muon will travel several

atomic distances before being scattered by electrons.

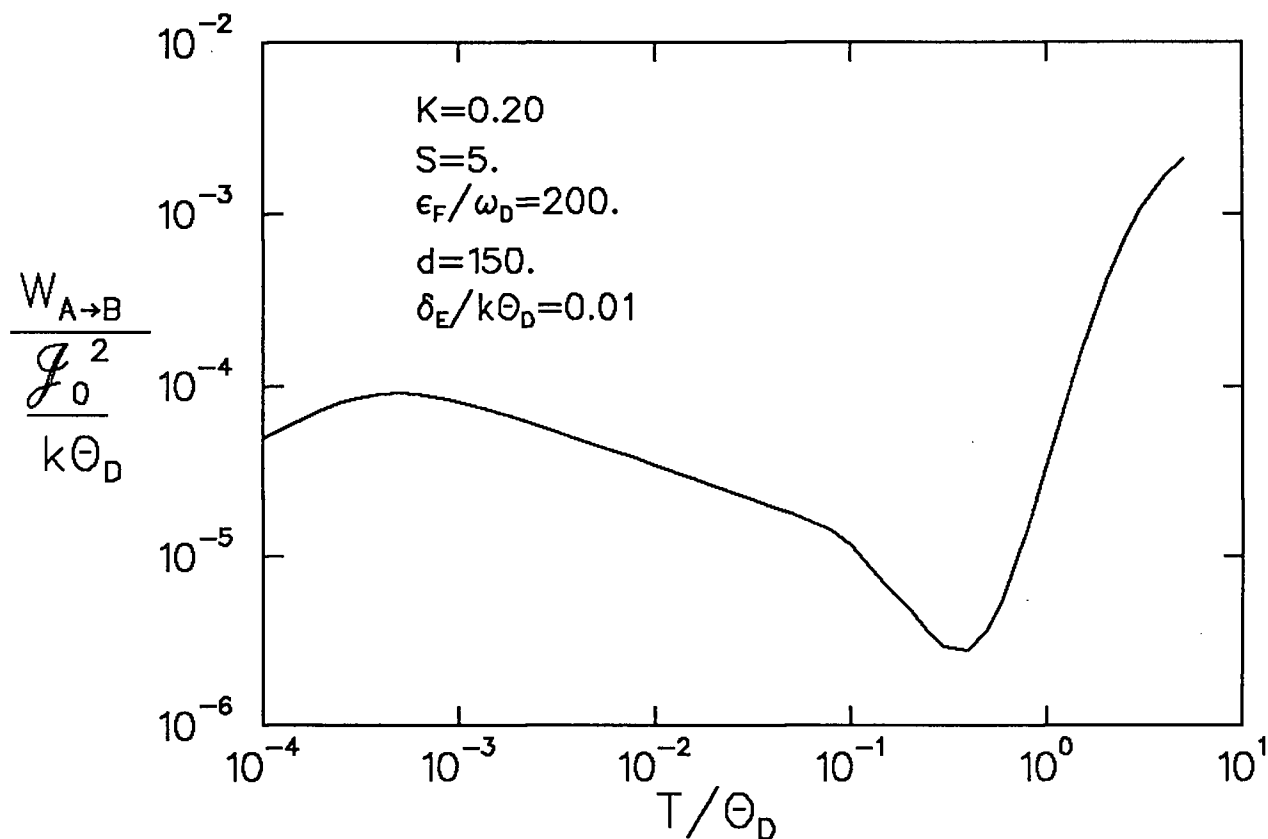


Figure 3.1: Kondo Theory — Hop rate versus temperature.

3.5 Yamada Theory

Yamada *et al.* [92,93] have also calculated the diffusion rate of light interstitials, including the effects of the electron-particle interaction whose importance was pointed out by Kondo. They started from the picture of band-like motion, where the diffusion is

limited by the destruction of the muon band due to scattering by conduction electrons. Their earlier results [94,95] had shown that the overlap between the ground states at two sites i and f , where the interstitial was shielded by s-state electrons, was given by

$$|\langle f|i\rangle| = N^{-2K} \quad (3.36)$$

where N is the number of conduction electrons in the system. This approaches zero as $N \rightarrow \infty$. As a result of this orthogonality, the overlap between the two screening clouds at higher temperatures is

$$\langle f|i\rangle = \left(\frac{\Lambda}{D}\right)^K \quad (3.37)$$

where Λ is a cutoff parameter which is the maximum of the temperature T and the effective lifetime of the interstitial at the site, and D is the conduction band width.

They found the same T^{2K-1} temperature dependence as Kondo in the limit of low temperatures, where K is the exponent of the overlap integral between the initial and final ground states in the conduction electron ground states when the particle changes position. They assumed that the muon diffusion was limited by scattering of the μ^+ by electrons and by the overlap integral between the electron clouds at neighbouring sites.

They first calculated the low temperature diffusion rate considering s-wave scattering of the conduction electrons by the interstitial impurity [92,93]. Their result follows the same temperature dependence as Kondo's result shown in equation 3.31 (in the case where the residual broadening is omitted). However, they are unable to calculate the numerical prefactor scaling the hop rate. The value of K in the exponent of 3.31 is given by

$$K = \frac{2}{\pi^2} \left(\tan^{-1} \frac{\sqrt{1-x} \tan \delta}{\sqrt{1+x \tan^2 \delta}} \right)^2 \quad (3.38)$$

where $x = J_0^2(k_F a)$ is the spherical bessel function for $l = 0$ and δ is the phase shift for s-wave scattering at the Fermi momentum k_F . From equation 3.38, one can see that the maximum of K is $1/2$.

When they extend their theory to include contributions from $l = 1$ scattering [91] following the method of Kagan and Klinger, they obtain the same T^{2K-1} dependence, although again they are unable to estimate the numerical prefactor. This method uses the density matrix for the time development of the system and allows the diffusion rate to be calculated of both cases: hopping and band-like motion. They found a smooth transition from one case to the other, which is taken to occur when the mean free path of the diffusing particle is equal to the lattice spacing.

Other authors [96,97] have subsequently considered the effects of the “electron drag” using a number of different approaches to evaluate the hop rate. They also report a T^{2K-1} temperature dependence for the muon hop rate.

The existence of the low-lying excitations leading to electron “friction” has also been observed by Richter *et al.* [98] in the tunnelling states of hydrogen in NbO_xH_y . They studied the effects of the conduction electrons in destroying the proton tunnelling state above the superconducting transition. Below T_c , there is a gap in the electron density of states, and the orthogonality of electron states no longer applies to the superconducting electrons. The absence of the low energy excitations removes the effect of the electron drag, as the infrared catastrophe no longer applies.

Chapter 4

Experimental Techniques

A number of techniques are used in μ SR experiments. Most common is the time-differential method, which is used to measure the detailed time development of the muon polarization function discussed in chapter 2. Frequently it is sufficient to measure only the integrated value of the polarization function (weighted by the distribution of muon lifetimes) as a function of some externally varied condition, such as temperature or applied field. In such time-integral μ SR methods, the loss of information about the details of the polarization evolution is often compensated for by the vastly higher incoming muon rates which can be accepted in integral experiments. Integral μ SR experiments have recently become widely used for double-resonance experiments. Other techniques, such as stroboscopic μ SR and muon channeling were not used in this work and are described elsewhere (see for example [25]).

In this chapter I will first review the “essentials” of the various standard μ SR techniques and then explain the details of their implementation at TRIUMF; finally, I will describe some of the peripheral experimental apparatus, including the dilution refrigerator used for the millikelvin aspects of this study, and the details of the samples studied.

4.1 Time-Differential μ SR

A time-differential (TD) μ SR experiment measures the polarization of a muon ensemble as a function of the time after the muons are implanted in a sample. In a TD- μ SR experiment, only a single muon is in the sample at a time. Typically, a muon enters the sample after passing through a thin scintillation counter, which signals the start of an event. The muon subsequently decays, emitting two neutrinos (which are not observed) and a positron which is detected in another scintillation counter. A histogram of detected positrons is kept for each detector as a function of the time difference between when the muon enters the sample and when it decays. As mentioned in the introduction, the number of detected positrons in a histogram corresponding to for example, the back (B) counter, will be:

$$N_B(t) = N_0^B (B_B + \exp(-t/\tau_\mu) [1 + S_B(t)]) \quad (4.1)$$

where B_B is the time-independent background and $S_B(t)$ is the “signal” of interest, equal to the product of the muon polarization function and the asymmetry of that counter.

$$S_B = A_0^B \mathcal{P}(t) \quad (4.2)$$

The constant backgrounds ($N_0^B B_B$, $N_0^F B_F$), which are measured during times where no muons are in the sample (as described later in this chapter) are first subtracted to form:

$$\mathcal{B}(t) = N_B(t) - N_0^B(t) \quad (4.3)$$

$$\text{and } \mathcal{F}(t) = N_F(t) - N_0^F(t) \quad (4.4)$$

The experimental asymmetry $\mathcal{A}(t)$ is then defined as:

$$\mathcal{A}(t) \equiv \frac{\mathcal{B}(t) - \mathcal{F}(t)}{\mathcal{B}(t) + \mathcal{F}(t)} \quad (4.5)$$

$$= \frac{(1 - \alpha) + (1 + \alpha\beta)A_0^B \mathcal{P}(t)}{(1 + \alpha) + (1 - \alpha\beta)A_0^B \mathcal{P}(t)} \quad (4.6)$$

$$\text{where } \alpha \equiv \frac{N_0^F}{N_0^B} \quad (4.7)$$

$$\beta \equiv \frac{A_0^F}{A_0^B} \quad (4.8)$$

This can be inverted to give the corrected asymmetry:

$$A_0^B \mathcal{P}(t) = \frac{(\alpha - 1) + (\alpha + 1)\mathcal{A}(t)}{(\alpha\beta + 1) + (\alpha\beta - 1)\mathcal{A}(t)} \quad (4.9)$$

which equals $\mathcal{A}(t)$ when $\alpha = \beta = 1$. A_0^B is the intrinsic maximum asymmetry of the back counter; it is affected by the amount of material (which preferentially absorbs low energy positrons) through which the positrons must pass, the orbits of the positrons in the applied field, if any, and the solid angle subtended by the counter. The corrected asymmetry corresponding to the raw spectrum in figure 1.3 (and its corresponding counter, 180° opposed to it), is shown in figure 4.1.

The quantities α and β reflect the physical experimental layout and are independent of the magnetic interaction of the muon with the target. Although they could in principle be calculated from the experimental geometry, in practice their values are extracted from the data empirically — *e.g.*, by measurement of a “calibration” sample with little muon depolarization.

The ratio of the raw count rates α is extremely sensitive to everything from the applied field to slight changes in the sample position to the position of the proton beam on the production target to intermittent efficiencies of signal discriminators; α is determined empirically as a free parameter when fitting the asymmetry. The parameter β (the ratio of the counter asymmetries) is generally close to 1 for identical counters. However, if the sample is reasonably thick, it acts as an absorber of low energy positrons (which have lower asymmetry), thus increasing the effective asymmetry of that counter

although lowering the raw data rate. This can cause $\beta \neq 1$ if the degrader is anisotropic; it also affects design strategies for the detector layout. A figure of merit for a detector is the product of the count rate and the square of the counter asymmetry. This product is maximized in the design of the counter, within the constraints of the rest of the apparatus. One obtains β by fitting the signals from the two counters separately; its value is then imposed on the asymmetry fit, as a constraint.

4.1.1 Transverse Field

The transverse field experimental geometry is shown in figure 4.2. The muons are injected into the sample with their spins polarized perpendicular to the applied magnetic field. In this case the signal in the left counter $S_L(t)$ is generally given by

$$S_L(t) = A_L G_x(t) \cos(\omega_L + \phi_L)t \quad (4.10)$$

where A_L is the effective asymmetry of the detector, ω_L is the Larmor precession frequency and $G_x(t)$ is a relaxation envelope.

Transverse field experiments are most sensitive to dynamical effects when they occur on a timescale at least as fast as that corresponding to the static relaxation. To illustrate this, the TF function in the absence of dynamical effects is frequently given to a reasonable approximation by $\cos \omega t \exp(-\sigma^2 t^2)$. This is the limit of equation 1.9 when $\tau \rightarrow \infty$. Motion causes a reduction of the gaussian-like damping of the precession; this is most effective when the correlation time τ is of order of $1/\sigma$. In general, this means that the TF relaxation method is not sensitive to very slow hop rates. In the frequency domain, this reduction of the damping corresponds to a narrowing of the Fourier peak, hence this effect is referred to as motional narrowing.

Transverse field measurements were used to calibrate the various magnetic fields in the samples. In order to calibrate the field in a given direction, the muon spins were

rotated perpendicular to that direction, causing them to precess in the applied field at the Larmor frequency. The magnets were controlled by computer through a digital to analog converter (DAC), which allowed for the precise setting of the applied field. The precession frequency was fit to give the field over the volume of the sample, where the muons were stopped. The magnets had homogeneity of better than 10^{-4} over the typical sample volume. The field was then calibrated using either a linear least squares or MINUIT fit of the measured field B versus DAC setting. As a result, all fields are known to within 0.1 G.

With a four positron telescope arrangement, consisting of left/right and backward/forward pairs, it is possible to use TF measurements to provide field calibrations, as well as to measure α , β and the experimental asymmetry, for a successive set of longitudinal and zero field measurements. Muons injected after having their spins rotated into the vertical direction precess around the field applied along the direction of injection. The frequency of the precession provides the calibration of the field strength in the sample. Injecting non-spin-rotated muons into a vertical field causes them to precess in the horizontal plane. The precession amplitude in the F/B counter pair gives the experimental asymmetry for each counter (excluding field-dependent effects due to e^+ orbits or poorly shielded phototubes), as well as the relative asymmetry factor β . The ratio of the normalization rates N_F , and N_B are combined to give α . These values are purely geometrical factors and other than α are mostly field independent, except when the applied fields are large enough to focus either the incoming muon beam or the outgoing positrons, both of which essentially change the effective solid angle of the detectors. These various systematic calibrations are made independently from the actual LF/ZF measurements, and are quite insensitive to the amount or shape of the relaxation of the signal, provided that the precession is sufficiently long-lived to allow a reasonably precise measurement, as is the case in most metals.

4.1.2 Longitudinal and Zero field

The experimental geometry for zero and longitudinal field experiments is shown in figure 4.3. The muons are initially polarized antiparallel to their momentum, along the magnetic field in the case of longitudinal field.

The relaxation seen in longitudinal field occurs when there is an energy reservoir with some spectral density at the muon Zeeman splitting, with which the muon can exchange polarization through energy-conserving transitions. This reservoir can be either some energy splitting in the spin system (which is the basis for the LCR technique), or an externally applied rf field, or fluctuating moments.

Longitudinal and zero field relaxation functions are, in contrast with those in transverse field, extremely sensitive to very slow dynamical effects. This dynamical relaxation can come either from the muon hopping past a series of individually static randomly oriented spins, or through the spins themselves fluctuating. The first effect gives (for slow hopping) an exponential decay to the long-time tail, as discussed in the chapter 2. Dynamical relaxation can be distinguished by the application of a longitudinal field stronger than the oscillating internal (dipolar) fields. If the relaxation is from static spins, the relaxation will be “decoupled”, and a long time non-relaxing tail will be present. Dynamical relaxation, on the other hand, is not decoupled by the application of the field until the field is large relative to $1/\gamma_\mu\tau$, where τ is the correlation time of the fluctuating fields B_{fluct} . These fluctuating fields will cause relaxation if they have a spectral component at the muon Zeeman frequency. At high enough applied fields the fluctuating field will not be able to provide the energy to flip the muon spin and cause relaxation. Measuring the field strength where this relaxation is decoupled can be used to determine the moment fluctuation rate. This has allowed, for example, the detection of the critical slowing down of spins above an antiferromagnetic transition.

At very high fluctuation rates, the ZF and LF relaxation functions approach each other, as the only important relaxation mechanism is that of the dynamical fluctuations of the muon's local spin environment.

4.2 Integral μ SR

In a standard time-differential μ SR experiment, the maximum incoming muon rate which can be used is limited by the requirement that only one muon be in the sample at a time. The optimum rate is found by maximizing the rate of good muon starts (R_g), where only one muon is present during the data gate T ; R_g is given in terms of the raw incoming muon rate R [99] by:

$$R_g = R \exp(-2TR) \quad (4.11)$$

which has a maximum at

$$R = (2T)^{-1} \quad (4.12)$$

For a typical 10 μ s data gate, the maximum rate of good muon starts is $\sim 1.8 \times 10^4 \text{ s}^{-1}$, corresponding to an incoming muon rate of $5.0 \times 10^4 \text{ s}^{-1}$. However, most modern meson factories are capable of producing much more intense beams (for example, the M15 beamline at TRIUMF is capable of over 10^6 muons/second in a 2 cm dia. spot). Clearly it would be advantageous to be able to utilize this extra rate to reduce the time required to perform an experiment with a certain signal to noise ratio. An integral experiment allows one to use all of the incoming beam, giving a correspondingly higher data rate.

In an integral experiment one simply counts all the decay positrons in each detector. One is simply measuring the time integral of each counter's raw spectrum. After a period of time T , much longer than the muon lifetime τ_μ , the number of decay positrons

detected is given by

$$\mathcal{N}_{\pm} = B_{\pm}T + RT\varepsilon_{\pm} + RT\varepsilon_{\pm}A_{\pm}\mathcal{L}(\mathcal{P}_z) \quad (4.13)$$

where R is the muon arrival rate, ε is the efficiency of the electron detector, B is the background rate of the electron detector and A is the effective asymmetry of the detector. The \pm refers to the counter direction relative to the initial muon polarization. Only the LF/ZF geometry is useful for integral μ SR measurements. $\mathcal{L}(\mathcal{P}_z)$ is the Laplace Transform of $\mathcal{P}_z(t)$ defined by

$$\mathcal{L}(\mathcal{P}_z) = \int_0^{\infty} \exp(-t/\tau_{\mu})\mathcal{P}_z(t)dt/\tau_{\mu} \quad (4.14)$$

One can then form an integrated asymmetry

$$\mathcal{A}_{int} \equiv \frac{\mathcal{N}_+ - \mathcal{N}_-}{\mathcal{N}_+ + \mathcal{N}_-} \quad (4.15)$$

$$= \frac{b_- + (1 - \alpha) + (1 + \alpha\beta)A_+\mathcal{L}(\mathcal{P}_z)}{b_+ + (1 + \alpha) + (a - \alpha\beta)A_+\mathcal{L}(\mathcal{P}_z)} \quad (4.16)$$

where

$$b_{\pm} \equiv \frac{B_{\pm} \pm B_-}{R\varepsilon_+}, \quad \alpha \equiv \frac{\varepsilon_-}{\varepsilon_+}, \quad \beta \equiv \frac{A_-}{A_+}$$

With the approximations that $B_{\pm} \approx 0$, $A_{\pm} \approx A$ and $\varepsilon_+ \sim \varepsilon_-$, one obtains the expression

$$\mathcal{A}_{int} \approx \frac{(1 - \alpha)}{(1 + \alpha)} + \frac{2}{(1 + \alpha)}A\mathcal{L}(\mathcal{P}_z) \quad (4.17)$$

The first term essentially forms a baseline, which is is generally both field-dependent and rate-dependent, while the second contains the signal of interest.

If there are fluctuations in the incident muon intensity, they will provide a fluctuation in the integrated signal since in general the efficiency of the positron detectors is rate dependent. These fluctuations may be removed by employing a square-wave modulation of the applied longitudinal field. The largest signal to noise is attained when the modulation amplitude is greater than the width of any features being observed (*e.g.*,

resonances). In addition, the data collection software vetoes data where the incident muon rate varies by more than a certain preset tolerance (typically $\sim 10\%$) from its average value.

The field-dependence of the “baseline” of the integrated signal is due to the field-focussing of the incident muon beam and of the decay positrons, changing the effective asymmetry of the detectors; it can be measured with a blank sample of size similar to that of the sample of interest if it is large enough to obscure the data. Otherwise, this effect is a relatively smooth function of field, and can be easily fit during analysis and discarded.

4.3 Experimental Apparatus

4.3.1 Muon Beamlines

All of the experiments described were performed on either the M15 or the M20 surface μ^+ channel at TRIUMF [100,101]. Both beamlines give a highly focussed beam of positive muons, with a small spot size. For a typical $100 \mu A$ proton current, M15 has a maximum luminosity of $4.3 \times 10^5 \text{ s}^{-1} \text{ cm}^{-2}$, whereas M20's is somewhat poorer, $1.6 \times 10^5 \text{ s}^{-1} \text{ cm}^{-2}$. The final size of the beam is generally controlled through the use of collimators (tungsten, brass or lead) in the beamline, which are designed to ensure that the beam stops only in the sample. These channels deliver a nearly monochromatic (uniform momentum) beam of particles; the momentum can be selected over a wide range by tuning the magnet elements.

The M20 secondary beamline originates at the 1AT2 pion production target, which is generally a strip of Be 10 cm long (in the beam direction). The channel views the target at 55° . It is a general purpose channel, capable of producing forward, backward

or surface muons. There is an alternating gradient decay segment of 10 quadrupole magnets for producing muons from pions which decay in flight. The beamline is divided into two legs, A and B. Leg A is used primarily for backward decay muons with a typical momentum of 86 MeV/c. Simultaneous operation of leg B with 173 MeV/c forward muons and 86 MeV/c backward muons in leg A is possible. Both legs can be used for surface muons, but leg A gives a heavily contaminated beam, as there is no velocity separator (Wien filter) on leg A for removing positrons. Only leg B was used in these experiments; it was always operated in the surface muon mode.

M15 is a relatively new channel; it views the 1AT1 thin target at 150° in the vertical direction. It was designed specifically for surface muons; the first two quadrupoles are permanent samarium cobalt magnets, tuned to 28 MeV/c. This limits the momentum range of the channel, which can be tuned down to approximately 20 MeV/c, maintaining reasonable fluxes. There are three sets of slits along the channel to control the muon rate, beam profile and momentum acceptance. The two spin rotators (see below) are separated by a quadrupole triplet which allows the vertical momentum dispersion caused by the first rotator to be cancelled by the second, making the system achromatic in the vertical plane. The lack of such a feature in the M20 separator causes a loss of approximately 50% in the muon rate when running in spin rotated mode. A considerably smaller loss is encountered in M15.

Positron contamination in the beam is reduced from approximately 10 positrons per muon (in M20) to approximately 1% through the use of a “dc-separator” or Wien filter [102], consisting of crossed magnetic and electric fields, both perpendicular to the beamline axis, which act as a particle velocity selector (whereas the dipole magnet “benders” act as momentum selectors). The crossed magnetic and electric fields in the separator are adjusted such that they exert equal and opposite forces on the muons.

Only particles with a velocity given by

$$\beta_0 = 3.33 \frac{E_0 (kV/cm)}{B_0 (G)} \quad (4.18)$$

(where E_0 and B_0 are the electric and magnetic fields, respectively) will pass through the separator undeflected.

The separator can also be used to rotate the muon spins (since the spins precess in the applied field when in the separator, through an angle proportional to the applied magnetic field strength), allowing the injection of the muon beam into large transverse fields. For large fields (greater than about 200 G) one must inject the beam along the field lines, otherwise the beam will be bent and miss the target. This implies that for a transverse field (TF) geometry, one must have the muon polarization perpendicular to the muon momentum, rather than parallel to it as created in pion decay. By using a large enough magnetic field, the muons precess by 90 degrees while travelling through the separator, and emerge with their spins perpendicular to their momentum.

When operating the separator in “non spin-rotated mode” the μ^+ spins are rotated by ~ 10 degrees from horizontal, antiparallel to their momentum, towards the vertical. In the LF configuration, the component of the muon polarization perpendicular to the field gives a precession signal in the side counters at the frequency corresponding to the total applied field. This signal sometimes provided a useful check on field calibrations during the experiment.

4.3.2 μ SR Spectrometers

Two nearly identical spectrometers, referred to as OMNI and OMNI', were used. Both employ multiple orthogonal Helmholtz coil designs, which allow a main field of 4.0(3.4) kG along the direction of beam travel and smaller fields up to approximately

100 G in perpendicular directions (both vertical and transverse horizontal on OMNI; only vertical in OMNI').

Incoming muons are detected using a thin (.13 mm to .26 mm) plastic scintillator. This counter is thin enough not to stop the muon beam and to give only a very small signal from the $\sim 30 - 50$ MeV muon-decay positrons, which are minimum-ionizing. This positron signal is discriminated against in the constant fraction discriminator, shown in figure 4.5.

Decay positrons are observed with thick (~ 1 cm) plastic scintillator detectors coupled to photomultiplier tubes through plexiglass light guides, arranged in a box around the sample space. Generally 4 or 6 positron counters are used, covering approximately $2\pi - 3\pi$ steradians. The areas not covered are used to provide cryostat access as well as a beam entry point.

The counter telescopes were either single counters or pairs. With a pair of counters, one requires a coincidence in the detection of a positron to count as a good event. This has the effect of eliminating one source of background, namely random triggering due to noise in the photomultipliers. Frequently, this was not a problem, and single counters were used, as this simplified the electronics somewhat and was much simpler to align in the spectrometer.

When the dilution refrigerator was used, however, two counter telescopes were always used. This was a result of the fact that a $^{60}\text{Co}^{59}\text{Co}$ γ -ray source was mounted next to the sample for temperature measurement. The ~ 1 MeV γ 's emitted can cause scintillation if they Compton scatter, which they do with some (small) probability[103]. The plastic scintillator is not an efficient detector of these γ 's, but they do provide an unwanted time-independent background. Requiring a coincidence lowers the rate to an acceptably small value ($\sim 25/\text{second}$).

A typical LF/ZF experimental arrangement of the OMNI spectrometer is shown in

figure 4.4.

4.3.3 Data Acquisition System

In a μ SR experiment, data is collected at a reasonably high rate; up to 10^5 events/second are frequently accumulated. This necessitates the sorting of data as it is collected, to reduce the amount of storage needed. This data sorting is accomplished in hardware.

The information of interest in an experiment is the event rate in each scintillator and the direction and time of each decay positron, relative to the time of arrival of the corresponding μ^+ . The data acquisition system must therefore accomplish a number of tasks. It generates histograms of muon decays for each counter. It must also veto events where there were two muons in the sample at a time (otherwise one doesn't know which positron corresponds to which muon). In addition, it must veto events when two counters detect positrons when there was supposedly only one muon in the sample (double hits).

The electronics setup is shown in figure 4.5. Attached to each photomultiplier tube is a coaxial cable to the electronics counting room. The signal first passes through a variable delay, used to synchronize the various counters. Following this, each signal enters a constant fraction discriminator (CFD), which, in the case of the muon counter, rejects positron events and noise (dark current). The output from the CFD is a well defined negative pulse of constant amplitude (-0.7 V) and width (~ 30 ns). Following this stage, counters which form a telescope are logically "anded" to give an event only when they are in coincidence, reducing the effects of noise in the individual detectors.

The μ^+ counter signal is scaled as the μ_{inc} rate. It also generates the pileup gate. If another muon enters the sample during this gate, both events will be discarded. If

the muon has arrived when the pileup gate was not triggered, then the clock (time-to-digital convertor or TDC) is started; a valid start has occurred. The start signal triggers the data gate, which is generally 500 ns shorter than the pileup. The data gate determines the time period when a valid clock stop can be detected.

If a positron is detected at a time when there is no pileup and during the data gate, its logic pulse is sent to the NIM/ECL converter, which routes the signal to the stop input of the clock, a LeCroy 4604 TDC. To one input, not used for a telescope, is fed the pileup signal, which allows the TDC to reject these events and restart. The clock is programmed through CAMAC from the data acquisition computer and automatically rejects double hit events (one of which could indicate pileup). Valid events are stored in a CAMAC histogramming memory (CES HM-2161), which is periodically read by the acquisition computer, that handles the display and storage of the data.

The signals for the various positron counters are all delayed by approximately 200–300 ns relative to the μ^+ counter. This permits the examination of times before the arrival of the muon, allowing one to measure the positron rates when it is known that no muons are in the sample. As a result, one is able to measure the time-independent background counting rate, so that it can be subtracted from the data during analysis. The relative timing of these various signals is shown in figure 4.6.

4.3.4 Cryogenics — Above 4.2 K

In the temperature range from 4.2 K to 300 K, the samples were mounted in a cold-finger helium flow cryostat, either a Janis Research model ST or a Cryo Industries model RC-110. The cryostats were fitted with thin (0.002 in) Kapton windows to allow for beam access. The sample was attached using low-temperature varnish to a high purity (five nines) aluminum disc, which was then bolted to the copper cold-finger

using Apiezon N-type grease for improved thermal contact. An aluminum backing was chosen since muons diffuse approximately 1000 times faster in Al than in copper and so no relaxation is seen in zero or longitudinal field due to muons stopping in the backing.

The temperature of the sample was monitored using a combination of Si and Ge calibrated diodes, as well as calibrated carbon-glass and platinum resistors. These sensors were mounted in the sample holder. Temperature control was provided either by a homemade PID controller or by a commercial controller (Lakeshore DRC 82C), connected to a bifilar wound resistance heater mounted in the copper cold finger.

4.3.5 Cryogenics — Dilution Refrigerator

All of the experiments performed below 4.2 K were done using an Oxford model 400 top-loading $^3\text{He}/^4\text{He}$ dilution refrigerator. The principles involved in the operation of dilution refrigerators are well known and are described in a number of books on low temperature physics (see for example references [104,105]). This refrigerator had a base temperature slightly below 10 mK, and a cooling power of approximately 100 μW at 100 mK. The layout of the refrigerator is shown in figure 4.7.

The design of the refrigerator allows the introduction of samples into it without disassembly of the unit. As a consequence, circulation of the mixture is only slightly interrupted and the mixing chamber remains below 2.0 K. A complete cycle of sample removal, changing and cooling down to 100 mK takes approximately two hours, an important consideration at an accelerator facility. If the refrigerator must be opened, there is a four day turnaround time, assuming that no leaks are introduced into the system during the process.

The refrigerator was fitted with thin windows in each of the concentric tails around the mixing chamber extension, to which the sample was attached. The two vacuum

windows were made of aluminized mylar, of 0.01 in and 0.005 in respectively. The other two windows were used as thermal radiation shields and were at 77 K and 50 mK respectively. The 50 mK shield was originally made from aluminum (as provided by Oxford), but was replaced by gold-coated mylar, as aluminum superconducts and thus distorts the applied field at the sample below approximately 1 K.

The sample changing technique involves precooling the sample to 4.2 K before attaching it to the mixing chamber using a combination of right- and left-handed threads which allow it to be detached from the loading syphon and attached to the mixing chamber extension. The sample (maximum dimensions 20 mm \times 30 mm) was attached to the copper sample holder by means of non-superconducting solder.

Temperature measurement was provided by the use of a calibrated carbon resistor mounted on the mixing chamber and an AVS-45 resistance bridge using a standard four-wire technique. Below 50 mK, the temperature was also measured using nuclear orientation thermometry [106]. The thermometer used was a single hcp crystal of cobalt which had been activated to contain approximately 5 μ Ci of ^{60}Co .

A nuclear orientation thermometer is a primary thermometer, in that it gives an absolute measure of the temperature, without the need for calibration. The crystal fields in a non-cubic crystal polarize the cobalt nuclei. When the unstable ^{60}Co nuclei decay, there are two γ 's emitted in the decay of the daughter nucleus. The angular distribution of these γ 's is anisotropic at low temperatures where the nuclei are polarized by the hyperfine field. The degree of anisotropy reflects the level of nuclear polarization, and thus the temperature through the Boltzmann distribution.

The cobalt crystal was soldered to the back of the sample holder using Woods metal. The domain structure of the crystal is such that, although the crystal is ferromagnetic, most of the flux is contained within the crystal, so long as it is not exposed to large polarizing fields, especially along the easy axis. In the experiment, the applied fields

were kept either vertical or longitudinal, both directions which are perpendicular to the easy c -axis. These fields were kept less than 200 G. Fields from the crystal on the sample were less than 20 mG, as measured at room temperature by a Hall probe.

The γ particles were detected using a NaI crystal mounted 20 cm from the sample, in the direction of the crystal c -axis; the spectrum was displayed and analyzed on a standard multi-channel analyzer. Temperatures were calculated from the decrease in counting rate relative to high (> 100 mK) temperatures.

4.3.6 Data Analysis

All data analysis was performed on VAX computers at TRIUMF, using MINUIT χ^2 minimization software [107]. All of the errors quoted from fits are full MINOS errors, which give the statistical “ 1σ ” error, *i.e.*, the change in the fit parameter such that the value of χ^2 increases by one, taking correlations between the various parameters into account.

4.4 Samples

Most of the work described here was done on a single copper crystal of nominal 5 nines purity (99.999%). This sample had a residual resistivity ratio of 4000 and was oriented with its $\langle 110 \rangle$ axis normal to its surface. The sample area was approximately 1 in². In the dilution refrigerator, only 1/2 of the sample was used. (It had been cut into 4 pieces using spark erosion). Many of the LCR measurements were done on the $\langle 110 \rangle$ sample; the rest were done on other 5 nines crystals obtained from the Monocrystals Company of Cleveland, Ohio, oriented with the magnetic field along the $\langle 100 \rangle$ and $\langle 111 \rangle$ directions. The accuracy of the various sample orientations was $\pm 2^\circ$.

Finally, a polycrystalline sample of ultra-high purity ($\text{rrr}=18000$) copper was used in some of the lowest temperature runs. This sample had been used previously in experiments by Kadono *et al.* [12,11]. A small amount of material was cut from the 5 mm diameter sample rod and arranged to form a mosaic, covering an area of 30 mm \times 20 mm. Although the sample was polycrystalline, the various crystallites were clearly visible in the freshly cut surfaces and were several millimetres in size.

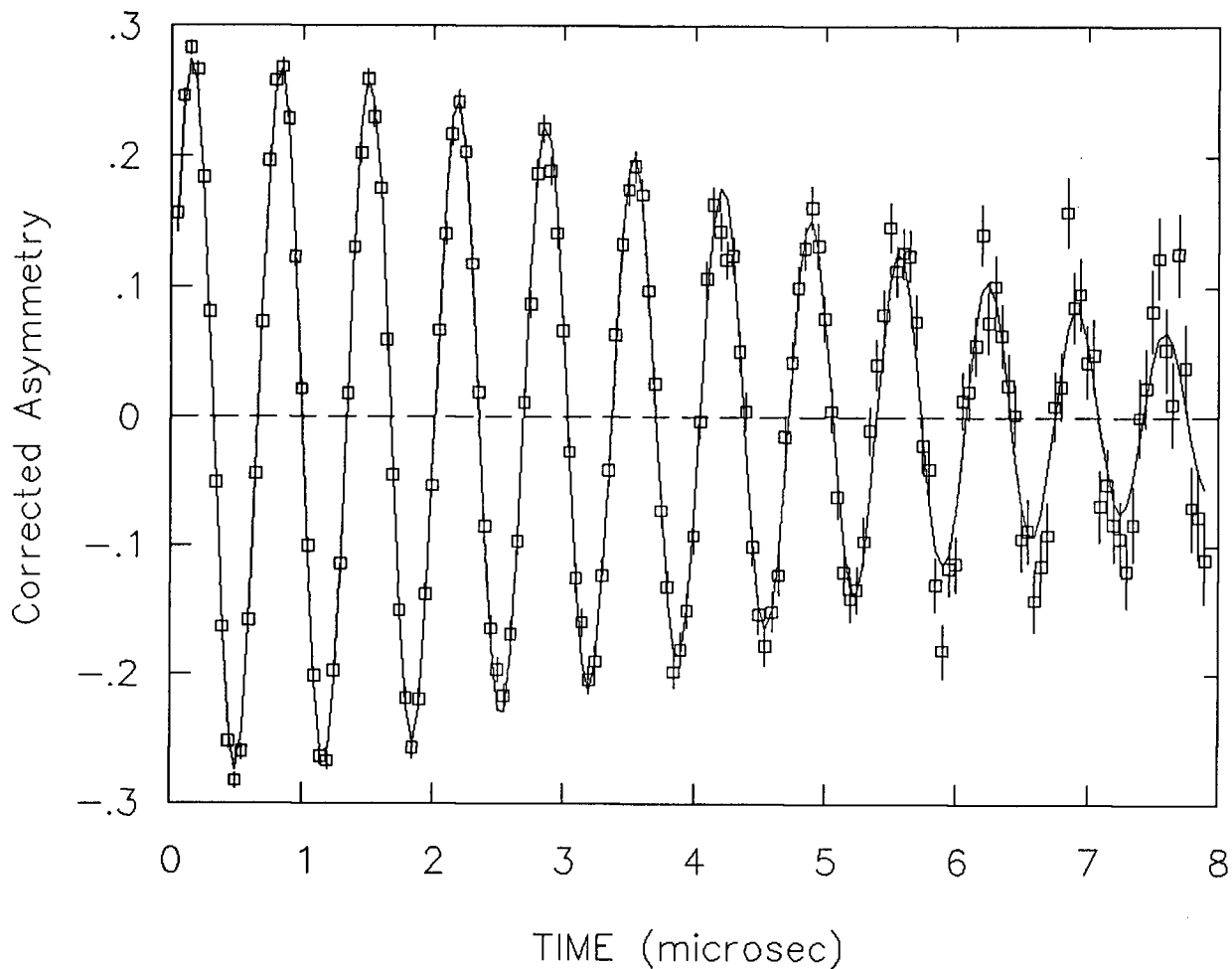


Figure 4.1: Corrected asymmetry for a typical transverse field experiment, showing muon precession as well as relaxation.

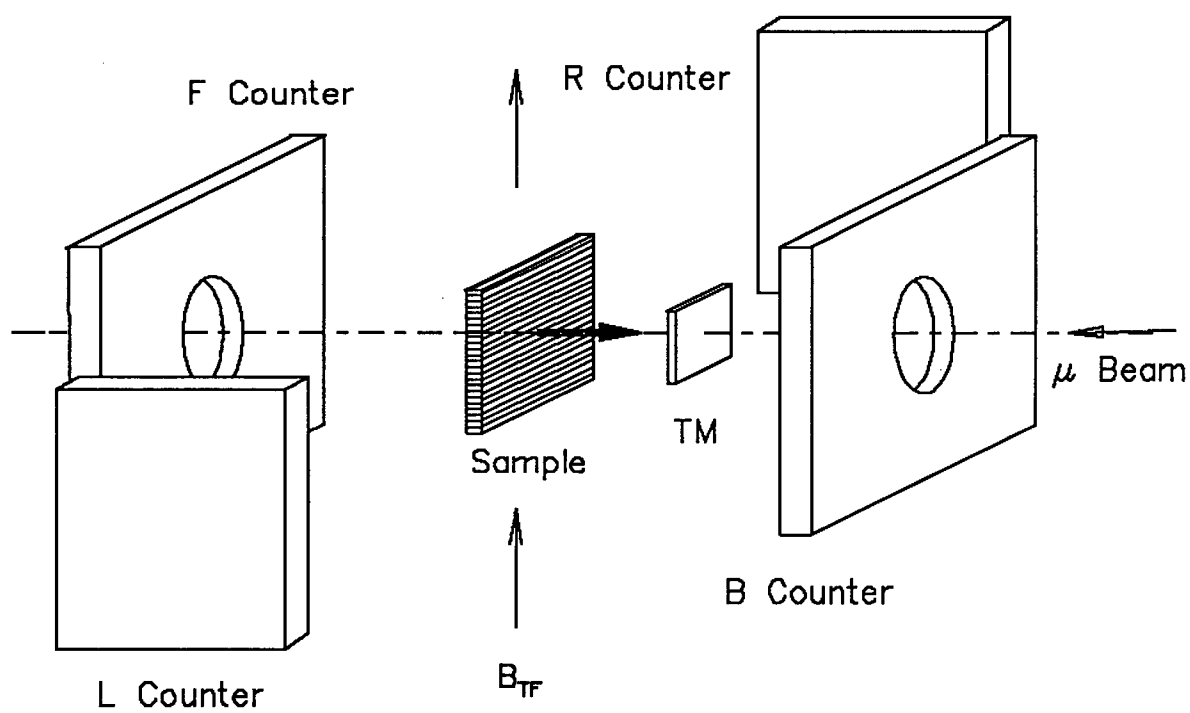


Figure 4.2: Weak transverse field geometry.

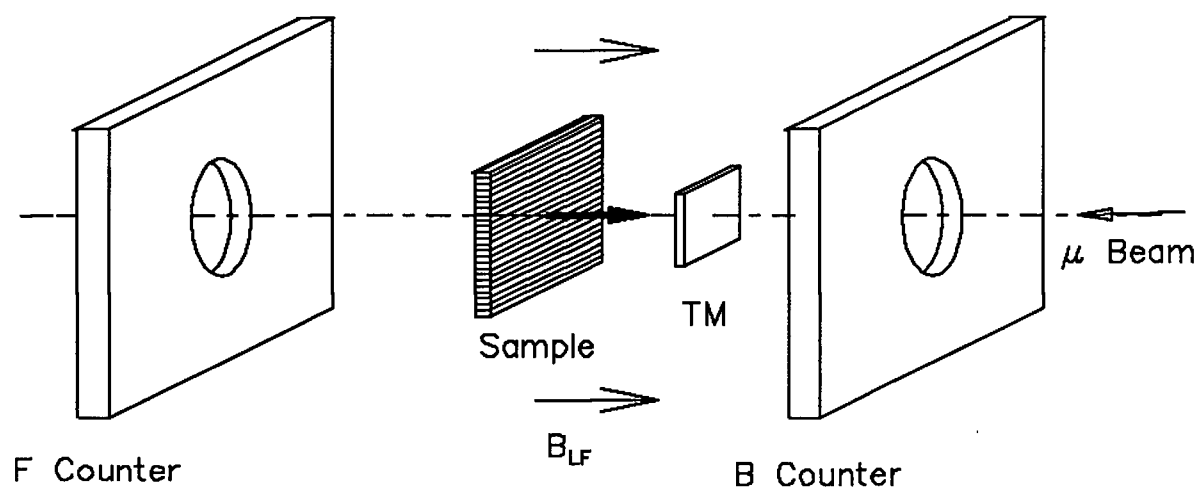


Figure 4.3: Longitudinal and zero field geometry

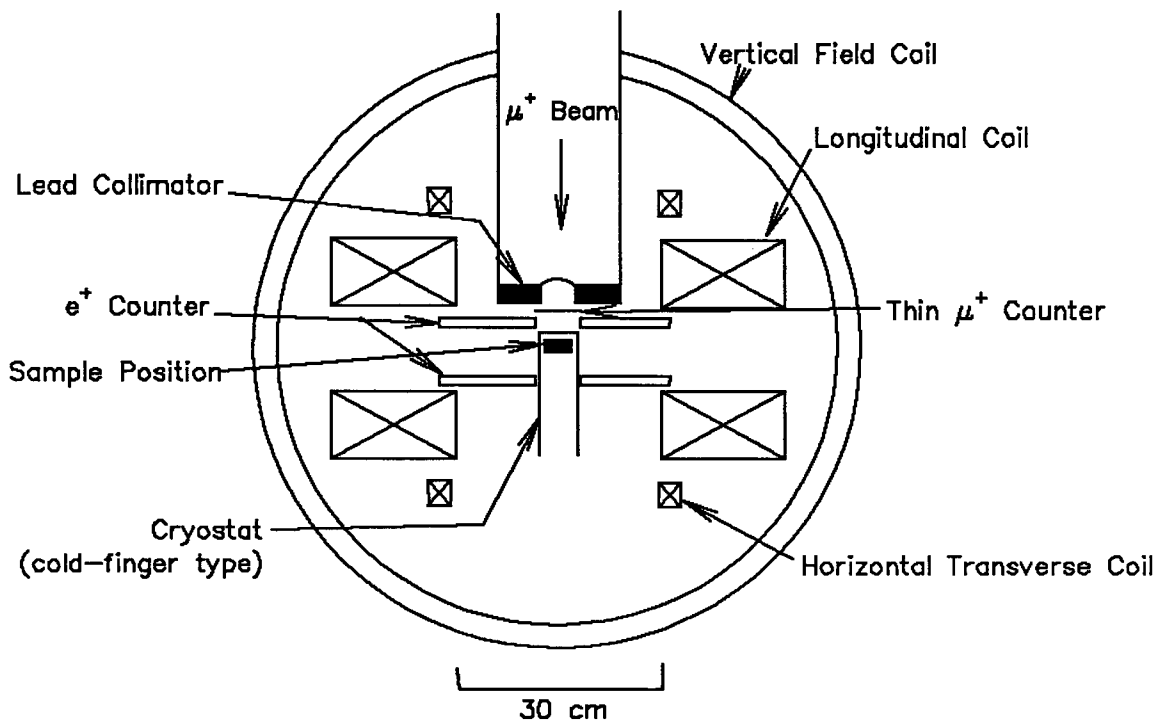


Figure 4.4: Omni - μ SR spectrometer, showing counter-cryostat geometry used for ZF and LF measurements.

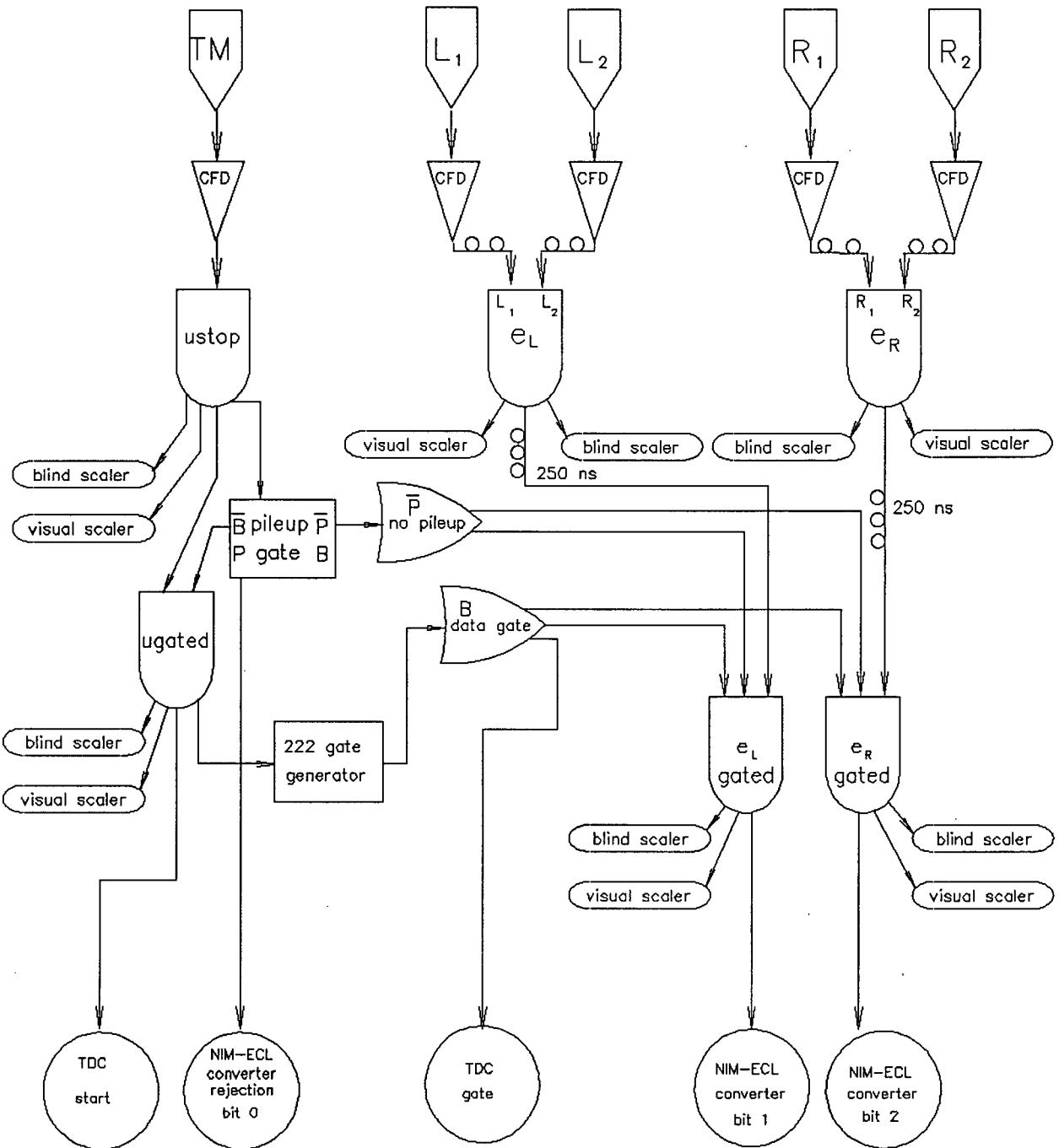


Figure 4.5: Electronics arrangement for time-differential μ SR experiments. Two e^+ telescopes of 2 detectors each, plus the thin counter (TM) are shown.

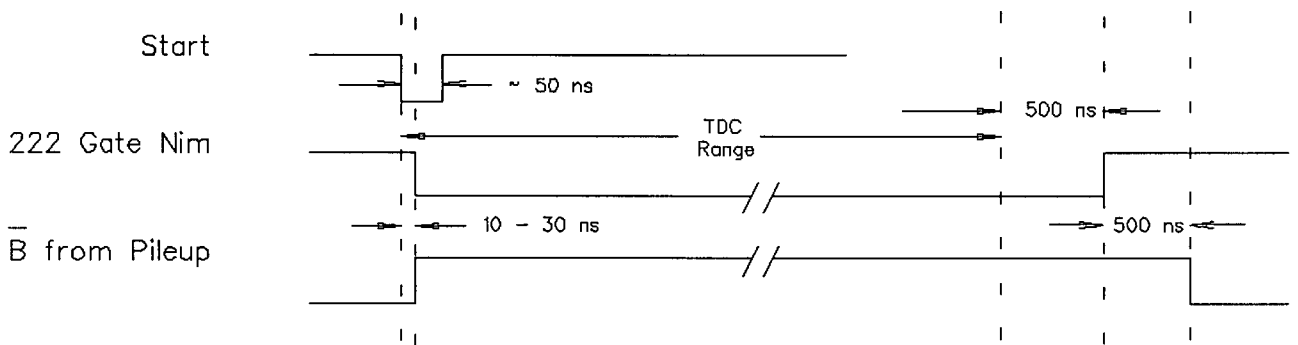


Figure 4.6: Timing of data acquisition events

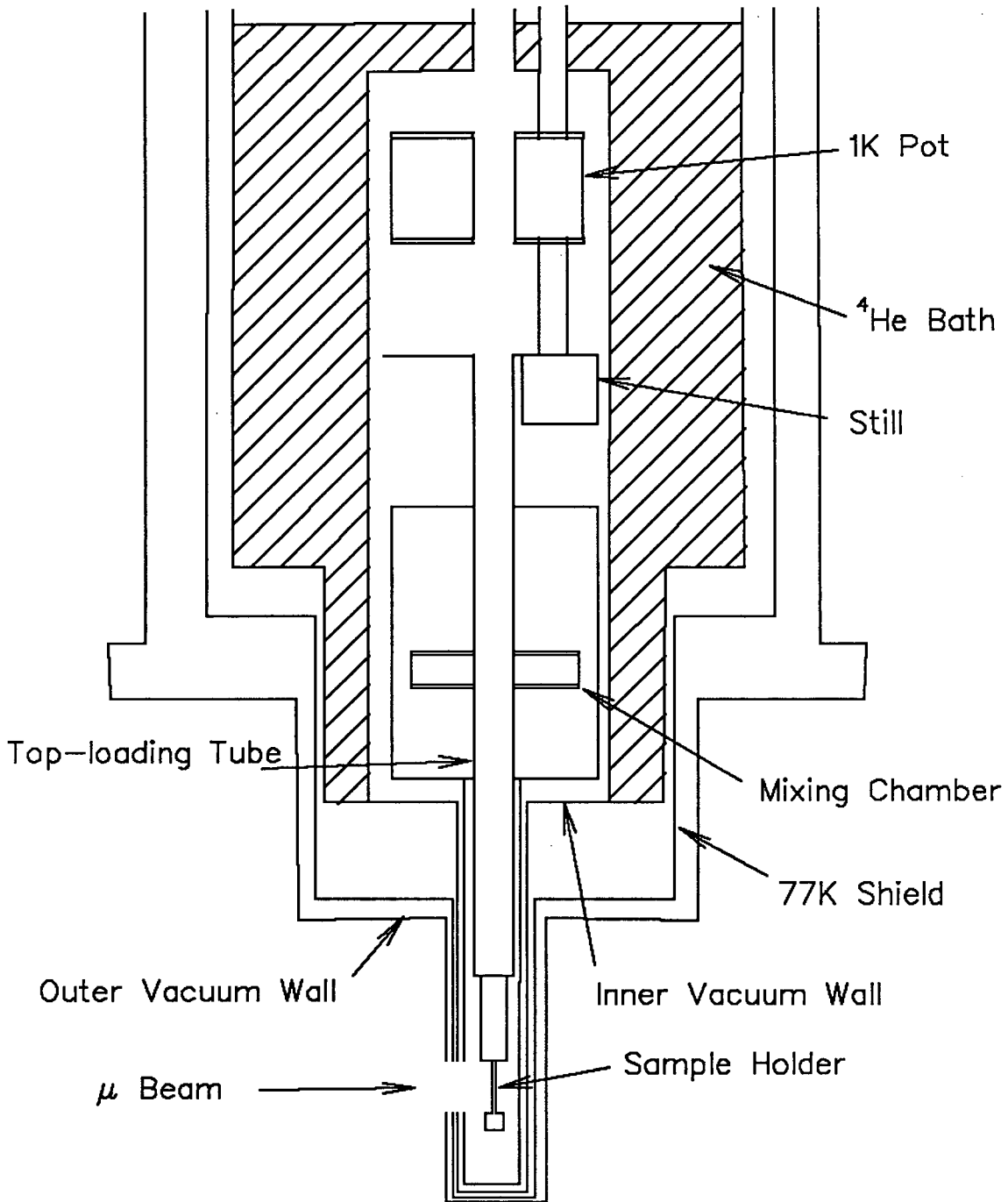


Figure 4.7: Dilution refrigerator—Oxford Model 400 (top-loading)

Chapter 5

Results

5.1 Quadrupolar LCR

The main advantage of a level-crossing scheme is that it is a double-resonance technique and as such allows the direct measurement of various host spin interactions, whether they are induced by the muon (as in the case of quadrupolar LCR in copper), or intrinsic to the material (such as the hyperfine interaction in radicals). This direct measurement gives much more accurate values for the various interactions than can be estimated from non-resonant methods, such as line-broadening in transverse field.

The easiest and fastest way to locate any LCR is by using time-integral μ SR. The results of such an experiment are shown in figure 5.1 for muons in copper in longitudinal fields from zero to 100 G at two different temperatures. The location of the resonance (maximum asymmetry loss other than as $B \rightarrow 0$) around 80 G is evident, as is the width of the resonance and the difference between nearly static and diffusing muons. However, since an exact theoretical model for the relaxation function was available, we chose to determine the important physical parameter, the copper quadrupole interaction with the EFG of the muon, using time-differential μ SR.

5.1.1 Quadrupolar Interaction

The level-crossing in copper occurs when the muon Zeeman energy splitting is roughly equal to the copper quadrupolar splitting. This occurs in an applied longitudinal field of approximately 80 G. We were able to accurately measure both the magnitude and sign of the quadrupole interaction, which had previously been reported [5] to be:

$$|\omega^Q| = 3.02 \pm 0.4 \mu\text{s}^{-1} \quad (5.1)$$

This was done by collecting a series of spectra at the minimum in the hop rate, around $T = 45$ K, in longitudinal fields where there was the maximum relaxation, as well as halfway down the resonance curve, both above and below the center of the resonance. The fields used were 70.1 G, 79.5 G and 86.9 G. These runs were then all fit together, in a global fit to theoretical functions calculated using the Trotter formalism for various values of the quadrupole frequency ω^Q . A typical fit is shown in figure 5.2 for the three applied fields at $T = 50$ K. Other than normalizations between counters (constant for each of the three runs at a given temperature), the only free parameter was the quadrupole frequency. Although both positive and negative signs for the quadrupole frequency give a resonance at approximately 80 G (corresponding to $\omega_\mu^Z \approx \pm 2\omega^Q$), the resonance is asymmetric about its center and the total amplitude is slightly larger for the case of negative sign. This asymmetry is a result of the fact that the resonance does not occur exactly at $\omega_\mu^Z = \pm\omega^Q$, but is actually split into four (unresolved) lines by the copper nuclear Zeeman interaction. The intensities of these various line (and thus the overall lineshape) depends upon the relative orientation of the applied field and the muon-nuclear axis as well as the relative signs of the quadrupole, Zeeman and dipolar frequencies.

We found that it was only possible to fit the data by using a negative sign for the quadrupole frequency; it was not possible to get a large enough amount of relaxation

using the positive sign. This could not be an effect of hopping; even assuming the muon to be completely static there was not enough amplitude in the theoretical resonance for the positive sign case – and hopping serves to *diminish* the amplitude of the resonance, as can be seen in figure 5.1.

Abraham [59] has shown that it is impossible in an NMR experiment to determine the sign of the quadrupole frequency except at extremely low temperature, when the nuclei become polarized through the Boltzmann distribution. The fact that the muon spin is significantly (initially 100%) polarized, corresponding to an extremely low spin temperature allows us to differentiate between positive and low quadrupole frequencies.

Our final result for the quadrupole frequency is:

$$\omega^Q = -3.314(7) \mu\text{s}^{-1} = \frac{e^2 q Q}{4\hbar} \quad (5.2)$$

From this result, we can extract the electric field gradient q . The value of the copper quadrupole moments are slightly different; we use a weighted average for the two isotopes. Effenberger *et al.* [108] found $|Q| = 0.220(15) \times 10^{-24} \text{ cm}^2$ for ^{63}Cu . Sternheimer [109] gives $Q = -0.209(5) \times 10^{-24}$ for ^{63}Cu and $Q = -0.194(4) \times 10^{-24}$ for ^{65}Cu . Using the average value of $Q = -0.205(5) \times 10^{-24} \text{ cm}^2$, we obtain

$$q = 0.296(7) \text{ \AA}^{-3} \quad (5.3)$$

This value may be compared with the theoretical result of Jena *et al.* [110], who obtained $q = 0.26 \text{ \AA}^{-3}$ for the electric field gradient at copper nuclei due to an interstitial positive muon.

5.1.2 Muon Site

The level-crossing resonance data allow us to lay to rest the discussion as to whether any of the apparent features observed at low temperatures are in fact due to a muon site

change. If the muon were to change to another type of site, or spend any significant time in some metastable site, such as the tetrahedral interstitial site, there would be a change in the position of the level-crossing. This is because the resonance position is given by the strength of the quadrupole interaction of the nearest-neighbour copper atoms, which experience an electric field gradient (EFG) caused by the muon's presence. A different site would be characterized by a different electric field gradient, shifting the resonance position. Additionally, the number of neighbours participating in the resonance would change in a different site, changing the amount of polarization involved in the resonance.

A series of time differential measurements were made at a series of longitudinal fields around the LCR position at 10 mK. It was found that all of these runs could be fit simultaneously using the value of the hop rate extrapolated from figure 5.6 to 10 mK. The only free parameters were the asymmetry and α .

We see no evidence of any significant occupation of the tetrahedral site. Recalling that Flik *et al.* [57] and Seeger [111] reported metastable occupation by π^+ 's in the tetrahedral site at $T = 150$ K, we can reconcile these two seemingly contradictory observations. The pion has a much shorter lifetime than the muon, therefore the muon would have to hop a factor of ~ 1000 more slowly than the pion, for a similar occupation of the metastable site to be equally apparent. Since they have similar masses and the same charge, we would expect the muon and pion diffusion rates to be similar and thus we conclude that the muon is never hopping infrequently enough in the temperature range available to us to observe possible occupation of the metastable site. The muon may well occupy the t-site for a few ns at high temperature; but subsequent diffusion is between o-sites. If the muon occupied the t-site at low temperature there would be a genuine contradiction of the π^+ results; but it does not.

It should be pointed out that the LCR is quite insensitive to small hop rates. This has been described by Kreitzman [112] as being a consequence of the non-averaging of

the quadrupolar interaction due to slow hopping. The fact that the resonance does not quickly disappear due to hopping can be visualized by considering the effect of hopping in longitudinal field. After a hop, the component of the muon polarization which is perpendicular to the net field (random local field and applied longitudinal field) precesses. This perpendicular component is lost from the longitudinal polarization. After each hop to a different site with a different random field, this component is again lost and so on, as the total polarization is gradually relaxed away. This process only causes relaxation when there is hopping and is therefore quite sensitive to the magnitude of the hop rate. On the other hand, in the situation of the LCR, the muon polarization is lost through the resonant exchange with neighbouring copper nuclei. Even if the muon is static, it is constantly losing polarization, whereas in weak longitudinal field the situation is quickly reached where there is no further loss of polarization with time until the muon hops again (in the long-time tail). On resonance, the muons are constantly being depolarized, regardless of whether or not they are hopping. As a result, one would not expect the relaxation function around the LCR to be especially sensitive to the hop rate.

We have observed the level-crossing at temperatures up to 200 K, where the muon is hopping at approximately $1.5 \mu\text{s}^{-1}$. The amplitude of the resonance at that temperature is slightly greater than expected on the basis of the strong collision model. This results from the violation of the assumption that the hop rate is smaller than the dominant (in this case quadrupolar) spin interaction of the copper nuclei. In the field region away from the LCR, the second moment of the relaxation is different, depending on whether there is a strong or weak quadrupolar interaction. As the hop rate approaches the quadrupole frequency, the quadrupole interaction begins to be averaged out, causing a transition from the strong to the weak quadrupole limit. As this happens, the second moment of the relaxation increases (as discussed in chapter 2). Around the LCR,

half of the main diagonal elements of the Hamiltonian are much smaller than away from the resonance; the hop rate approaches the magnitude of those elements much more quickly. The effective dipolar coupling (which gives the second moment) is then stronger, increasing the amount of relaxation. This acts to oppose the reduction in the resonance amplitude with hopping. The net result is that the hop rate that would be extracted on resonance by assuming $\omega^Q \gg \nu$ is smaller than the actual value of ν . As a result, the level-crossing persists to higher hop rates than predicted by the strong collision model.

5.2 Hop Rate

In measuring the muon hop rate in copper, we used the weak longitudinal field (WLF) technique [15,113]. This technique has a number of advantages over both the transverse field and zero-field methods in determining hop rates.

As previously mentioned, the first transverse field results were subject to a number of alternate interpretations for the change in the relaxation rate at low temperature, including the muon site changing to one of different symmetry and trapping at defects. Transverse field measurements also suffered from a lack of sensitivity to changes in hop rate at very low hop rates. There is the additional difficulty in distinguishing the effects of small hop rates from the effects of a small ($\leq 5\%$) lattice dilation. In transverse field, many different physical interactions affect the amount of spin relaxation, often in ways which are virtually indistinguishable from each other.

Zero field measurements of the hop rate are difficult near the minimum in the hop rate due to the fact that the decay of the “1/3-tail” doesn’t show much effect until long times ($t \geq 8 \mu\text{s}$), where there are few muons still remaining in the sample. This problem is most pronounced at a “continuous” beam facility, such as TRIUMF or PSI,

where one is limited to a certain incoming muon rate by the requirement that only one muon be present in the sample at a time. The maximum allowable rate decreases as one observes each muon out to longer times, as discussed in chapter 4. A further limitation of the ZF method is that the $1/3$ tail does not actually exist; the muon polarization does in fact decay slightly at long times, even when the muons are static. If one used Kubo-Toyabe theory for the static muon polarization function, this would show up as an apparent small hop rate. This is no longer as large a problem as a number of years ago, now that the exact solution for the static polarization function can be calculated, but it does demonstrate the sensitivity of results obtained in zero field to the fine details of the assumed static relaxation behaviour.

The application of longitudinal field increases the amount of polarization that is available to relax (due to hopping) from its approximate $1/3$ value in ZF, increasing the sensitivity of the WLF technique. In longitudinal field, the action moves to earlier times, where there are correspondingly more muons and any systematic distortions of the spectra are smaller and therefore less significant. This can be seen in figures 2.7 and 2.8 which show theoretical static and dynamic relaxation functions for both zero field and 15 G longitudinal field. The WLF polarization functions exhibit more significant differences at earlier times than do the zero field ones. This increases the accuracy with which one can extract information from the data, since the error associated with any measurement of the polarization function increases exponentially with the time region in which it is studied due to the decreasing number of muons left in the sample.

Clearly, ZF measurements are extremely sensitive to small stray fields; a small transverse field component can increase the apparent amount of recovery of the polarization, causing one to underestimate the muon hop rate. Thus, great pains must be taken to accurately cancel any stray fields in ZF studies.

At a given temperature a series of spectra were taken, at a series of applied longitudinal fields. Generally these fields were 8 G, 16 G and 24 G. Typical spectra are shown in figures 5.3 and 5.4 where the muons are nearly static and diffusing rapidly, respectively.

There are a number of advantages in taking a series of runs at various fields at each temperature. First, being able to fit the relaxation functions at a number of different fields with all free parameters common to all the runs (*i.e.*, hop rate, asymmetry etc.) gives one added confidence that one has a correct functional form and interpretation of the relaxation functions. Secondly, data at a series of fields extends the advantage that the WLF method has over zero field in that the applied field can be chosen such that one is most sensitive to small changes in ν_{hop} . This can be seen most clearly by referring to figure 5.5, which shows theoretical relaxation functions for various hop rates in zero field and in a longitudinal field of 15 G. It can be seen that there is a range of hop rates where the relaxation functions aren't very sensitive to small changes in the hop rate, around the "T₁ minimum"[45]. The hop rate where this takes place is field dependent, allowing one to use a field placing one well away from the T₁ minimum. Using a series of fields guarantees that at worst one field will suffer from this lack of sensitivity.

The experimental asymmetry of the apparatus was determined in two ways. Transverse field spectra, taken by applying a field perpendicular to the direction in which the longitudinal field was applied, provided one measure of the asymmetry. Furthermore, in fitting the WLF runs themselves the asymmetry was fit. The results were always consistent with each other, as expected.

At this point the spectra were fit simultaneously (data from all 3 fields), either fixing the asymmetry to the value measured in transverse field (occasionally these runs were fit together with the WLF runs in a larger global fit) or fitting it as well,

as described above. The only free parameters in these fits were the asymmetry, α (the relative efficiency of the two counters) and the hop rate. The results obtained in these fits were also checked against the results from fitting the runs separately and were found to be consistent, within the fit uncertainties. In a series of spectra at different temperatures taken under otherwise identical experimental conditions, the data were often fit simultaneously. For example, the points marked by diamonds in figure 5.6, taken at ten different temperatures and representing thirty different spectra, were fit together in a single global fit. In this way, the experimental asymmetry and the parameters α and β were held equal for all runs. The only other free parameters in the fits were the extracted hop rates for each temperature. The curves drawn through the data in figures 5.3, 5.4 are the fits obtained for that data.

The tables used for fitting the LF data were calculated assuming the values of the μ^+ -Cu dipole interaction appropriate to the case where there is no lattice dilation and using the average gyromagnetic ratio $\gamma_{Cu}/2\pi = 1.154$ kHz/G for the two isotopes. The dipole frequency, given by equation 2.13, was

$$\omega^D = 0.11 \mu s^{-1} \quad (5.4)$$

This was calculated for a muon-copper distance of one half of the copper fcc lattice constant of 3.62 Å. The possible effects of dilation were allowed in the fitting procedure through the use of a parameter "SCALE" which scaled the time axis, giving the first order effect of a lattice dilation on the relaxation function. The value of this parameter in all of the fits was consistent with virtually no dilation and inconsistent with the previously quoted 5% dilation. The fitted value of the "SCALE" parameter is 1.00(5). Since the dipole frequency is proportional to r^{-3} , this implies that the lattice dilation is less than 2%.

The second moment of the numerically computed relaxation functions was obtained

by numerical differentiation giving an effective $\Delta = 0.387 \mu s^{-1}$, which can be compared to the experimental results of Clawson [9] $\Delta = 0.389(3) \mu s^{-1}$ and Kadono [11,114] $\Delta = 0.390(1) \mu s^{-1}$. These results are clearly inconsistent with a 5% lattice dilation.

In interpreting this discrepancy between our results and the previous transverse field results, we note that the previous measurements were made at 20 K and 80 K. Since they obtained the same results at the two temperatures, they assumed that the muons were static. In fact, as can be seen in figure 5.6 these two temperatures happen to be on opposite sides of the minimum in the hop rate; the muons are hopping at about $0.06 \mu s^{-1}$. If this small hop rate is included in the calculation of the dilation, an upper limit of approximately 2% is obtained [115].

The quadrupole frequency ω^Q was also held to a constant value of $-3.2 \mu s^{-1}$ for the hop rate analysis. The fact that this value is slightly different than the value eventually extracted for the quadrupole frequency from the analysis of the level-crossing is unimportant, as the relaxation functions in fields away from the LCR are quite insensitive to the magnitude of the quadrupole splitting, so long as it is significantly greater than the Zeeman splitting.

The extracted hop rates have been fit in terms of Kondo's model for the diffusion rate of the muon as a function of the various parameters described in section 3.4. Since the calculation of the hop rate in terms of these parameters requires reasonably intensive computations, the fitting was performed in stages. First, the region where the hop rate follows a $T^{-\alpha}$ relation was fit to extract a value of the coupling constant K . This value was then held fixed throughout the remaining analysis.

Following this, a series of theoretical hop rates were computed as a function of the remaining parameters, with the exception of the residual broadening δ_E , which was

held to zero.

$$\mathcal{W}_{A \rightarrow B} = \frac{\mathcal{J}_0^2}{\Theta_D} \Xi \left(\frac{T}{\Theta_D}, S, \frac{\epsilon_F}{k_B \Theta_D}, d, 0 \right) \quad (5.5)$$

These results were stored in a multi-dimensional table and a MINUIT fit was performed to extract results for the parameters in the temperature range above 500 mK. Finally, the effects of broadening were taken into account and the value of δ_E necessary to provide the turning over in the hop rate below 500 mK was extracted.

The fitted hop rates are shown in figure 5.6 over the temperature range $20 \text{ mK} < T < 150 \text{ K}$. It can be seen in figure 5.6 that there are a number of temperature regions exhibiting different hop rate behaviour.

At the highest temperatures studied, $40 \text{ K} < T < 150 \text{ K}$, the muon diffuses by through-the-barrier phonon-assisted tunnelling. The dominant process is that involving two phonons. The role of the phonons is to bring the energy levels between the two self-trapped states (before and after hopping) into coincidence, allowing a tunnelling transition. We did not extend the study to higher temperatures, as the muon diffuses so rapidly that the strong collision model no longer gives accurate results for the hop rate (as discussed in chapter 2). At such high rates, the most reliable method for deducing hop rates is through the use of high transverse fields.

In the intermediate temperature range, around the minimum in the hop rate, we see the effect of the quadratic muon-lattice interaction, which causes a deepening of the minimum.

At lower temperatures $1.0 \text{ K} < T < 10 \text{ K}$, the hop rate increases with decreasing temperature. In this region, the hop rate has a power law temperature dependence $\nu_{hop} \sim T^{-\alpha}$. We extract a value of $-0.553(7)$ for the exponent α . In terms of the predicted temperature dependence of Kondo and Yamada, the parameter $K = 0.224(4)$. This value was held fixed for the remaining analysis.

If we consider Yamada's equation for the electron-muon coupling parameter K given by

$$K = \frac{2}{\pi^2} \left[\tan^{-1} \frac{\sqrt{1-x} \tan \delta}{\sqrt{1+x \tan^2 \delta}} \right]^2 \quad (5.6)$$

we can estimate a theoretical value for K . The phase shift δ is given by the Friedel sum rule [116] in terms of the screened charge ($Z = 1$ in the case of the muon)

$$Z = \frac{2}{\pi} \sum_l (2l+1) \delta_l \quad (5.7)$$

In the case where the muon is screened by s -electrons ($l = 0$), we have $\delta = \frac{\pi}{2}$. The value of $x = J_0^2(k_F b)$ can be calculated using $k_F = 1.36 \times 10^8 \text{cm}^{-1}$ and $b = a/\sqrt{2}$ where $a = 3.62 \times 10^{-8} \text{cm}$ is the fcc lattice constant. This gives an estimate of 0.28 for K , which is close to our measured value. The difference between the two values is presumably due to deviations from s character in the screening electron cloud. Hartmann *et al.* [69] interpolated the results of Puska and Nieminen [117], who calculated the Fermi-level phase shifts for atoms in a homogeneous electron gas, obtaining $K = 0.33$ for copper and $K = 0.27$ for aluminum. Their experimental value for aluminum was $K = 0.15$. The smaller value for K is a result of aluminum's greater electron density relative to copper.

Below $T = 500$ mK, the value of the hop rate turns over and starts to decrease with decreasing temperature. This effect is explained by Kondo in terms of a phenomenologically introduced broadening of the energy levels before and after hopping. As a result of this residual broadening, the hop rate no longer increases with decreasing temperature, but rather turns over at a temperature which corresponds roughly to the size of the residual broadening. Below this turnover, Kondo predicts that the hop rate will follow a T^{2K} temperature dependence. Sugimoto [118] has also considered the effects of a distribution of final states which remains in the limit $T \rightarrow 0$. He finds the same results as Kondo when the occupation probability of sites reaches thermal equilibrium. In

Table 5.1: Parameters extracted from hop rate results, for Kondo's model for the muon hop rate.

\mathcal{J}_0	37.1 ± 2.6 K
θ_D	184.6 ± 2.0 K
ϵ_F/θ_D	$340. \pm 20.$
S	7.15 ± 0.1
d	171.1 ± 2.4
δ_E	0.37 K
$\mathcal{J}_{\text{eff}} = e^{-S} \mathcal{J}_0$	0.029 K

the opposite limit, where the site occupation probability is independent of the various site energies, he finds that the hop rate becomes temperature independent. Thus, one would expect the exponent in the hop rate to fall in the range $0 < \alpha < 2K$. One additional explanation for the discrepancy with the value of K extracted from the higher temperature region could be a range of residual broadening, depending for example on the distance from impurities or dislocations. As a result, at lower temperatures (*e.g.*, lower than all of these residual broadening energies) the hop rate will decrease more quickly.

The full results in terms of the various coupling parameters in Kondo's model are given in table 5.1. As can be seen, reasonable values of the various physical parameters are sufficient to fit our experimental results. The errors quoted are the statistical errors only and do not include any systematic uncertainties. Presumably, the actual uncertainty is somewhat larger. The value of $\Theta_D = 185$ K is in reasonable agreement with the quoted value (315 K), when it is considered that Θ_D enters the calculations for the hop rate as an effective cutoff in the phonon spectrum.

The temperature where the turnover takes place agrees well with the results previously reported by Kadono *et al.* [11,114], who observed only a leveling off in the hop rate. We note however, that the slope extracted is quite small. The fact that they were only able to measure down to $T = 69$ mK and that the zero-field technique is inherently less sensitive than the WLF method employed here may explain the fact that they were only able to observe a leveling off.

In comparing our results with those previously reported by Kadono *et al.*, we note that the greatest difference appears in the temperature range near the minimum in the hop rate. Their results are consistent with zero hopping at the minimum, whereas we report a minimum hop rate of $\sim 0.03 \mu\text{s}^{-1}$.

The source of this discrepancy may lie with their use of a pulsed muon beam. Following a pulse, there are a number of distortions which affect the spectra. The early time region is distorted by beam positrons which scatter from the sample into the forward counter. This distortion was severe enough to force the discarding of the forward spectra.

Second, since all of the muons enter at once, the instantaneous positron counting rate just following a pulse is large enough that there is some counting inefficiency in the detectors. This problem was addressed by numerically correcting the spectra for this counting loss. Typically, differences in the spectra before and after this correction were $\sim 1\%$, which is certainly significant relative to the precision of these experiments. They note [11,12] that these corrections tend to emphasize the static character of the relaxation functions.

Finally, most of the experiments were performed using backward decay muons. With such a beam, it is impossible to reject events originating from muons stopping outside of the sample. Any muons which stop in the aluminum sample holder will provide a non-relaxing background signal, which will also tend to indicate that the diffusion rate

is lower than is actually the case (through the appearance of a long-lived tail).

Experiments with a “continuous” surface muon beam such as performed here at TRIUMF avoid these difficulties. Instantaneous beam rates in time-differential experiments are never high enough that the counting efficiency varies significantly and most of the beam positrons are removed through the use of the dc-separator. The small beam spot of the surface beam helps ensure that most of the beam stops in the sample. The further requirement that each positron be correlated with an incident muon (which has entered through the thin muon counter) ensures that the detected positron came from a muon inside the sample.

Data was taken at two temperatures (13 mK and 35 mK) for the high purity polycrystalline Cu sample. These runs were fit using the static relaxation functions generated for the $\langle 110 \rangle$ orientation. The data could only be fit using a value of 1.13 for the “SCALE” parameter. This corresponds to reduction of the second moment, illustrating the orientation dependence of the relaxation functions. Other primary orientations ($\langle 100 \rangle$ and $\langle 111 \rangle$) gave similar results. The data at the two temperatures had slightly higher hop rates than extracted for the $\langle 110 \rangle$ crystal. This may be an effect of the choice of static relaxation functions. Another possible explanation is that this sample had a smaller residual energy disorder (δ_E) as a result of its greater purity, causing the turnover in the hop rate to occur at a slightly lower temperature.

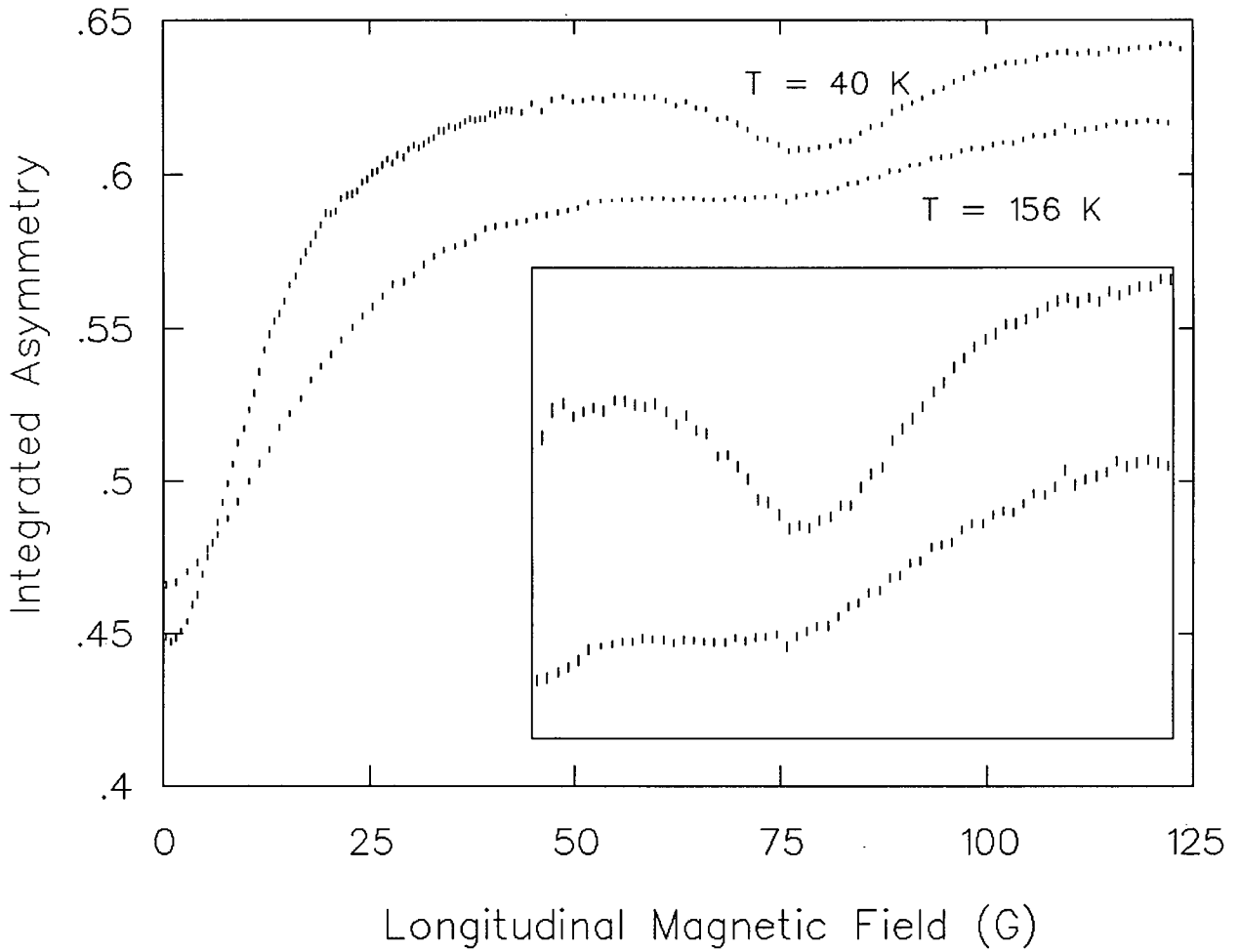


Figure 5.1: Integral measurement of longitudinal relaxation. Field applied along the $\langle 110 \rangle$ direction. Inset: expanded vertical scale

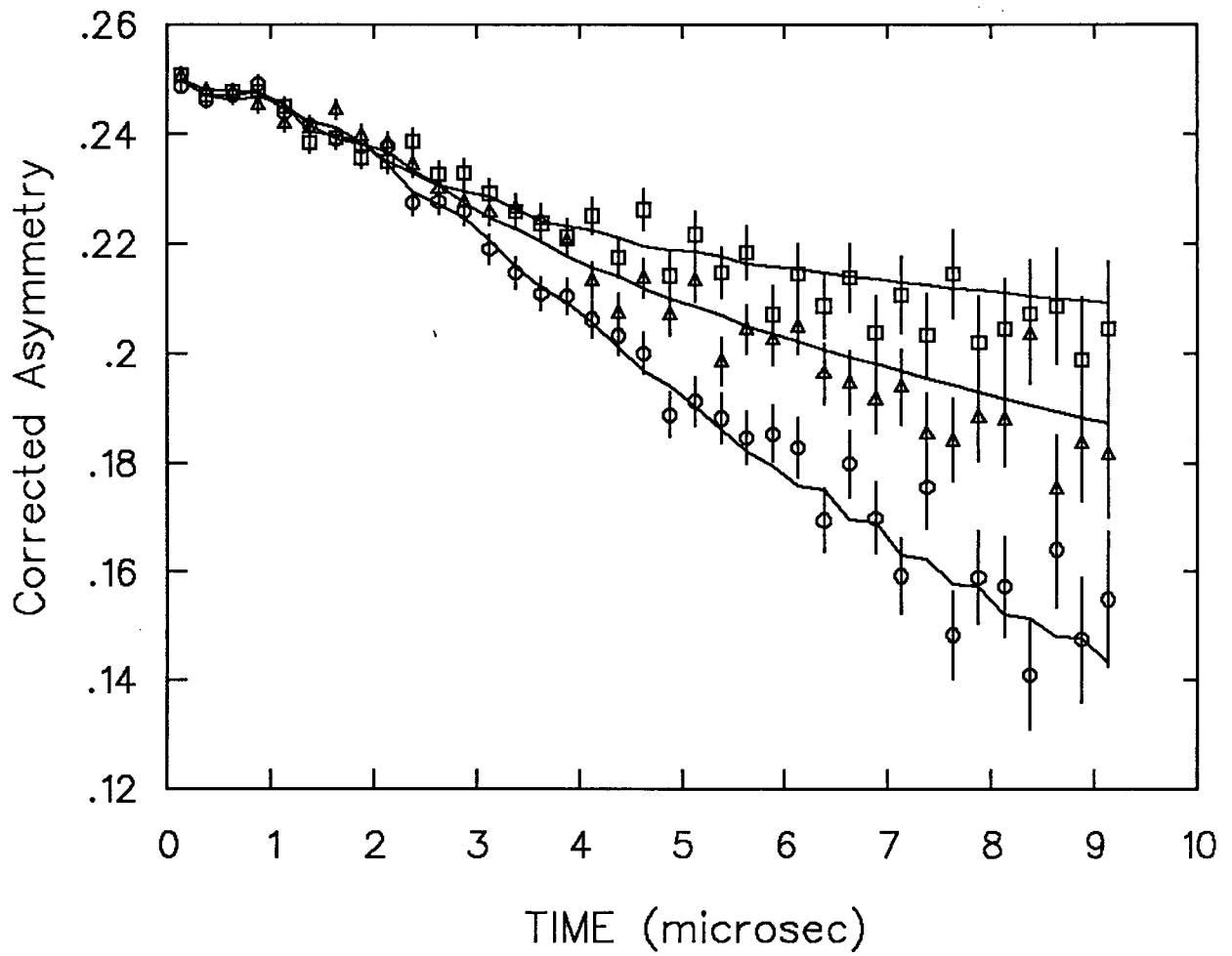


Figure 5.2: Time-differential spectra around level-crossing resonance. Longitudinal fields are 70.1 G (triangles), 79.5 G (circles) and 86.9 G (squares).

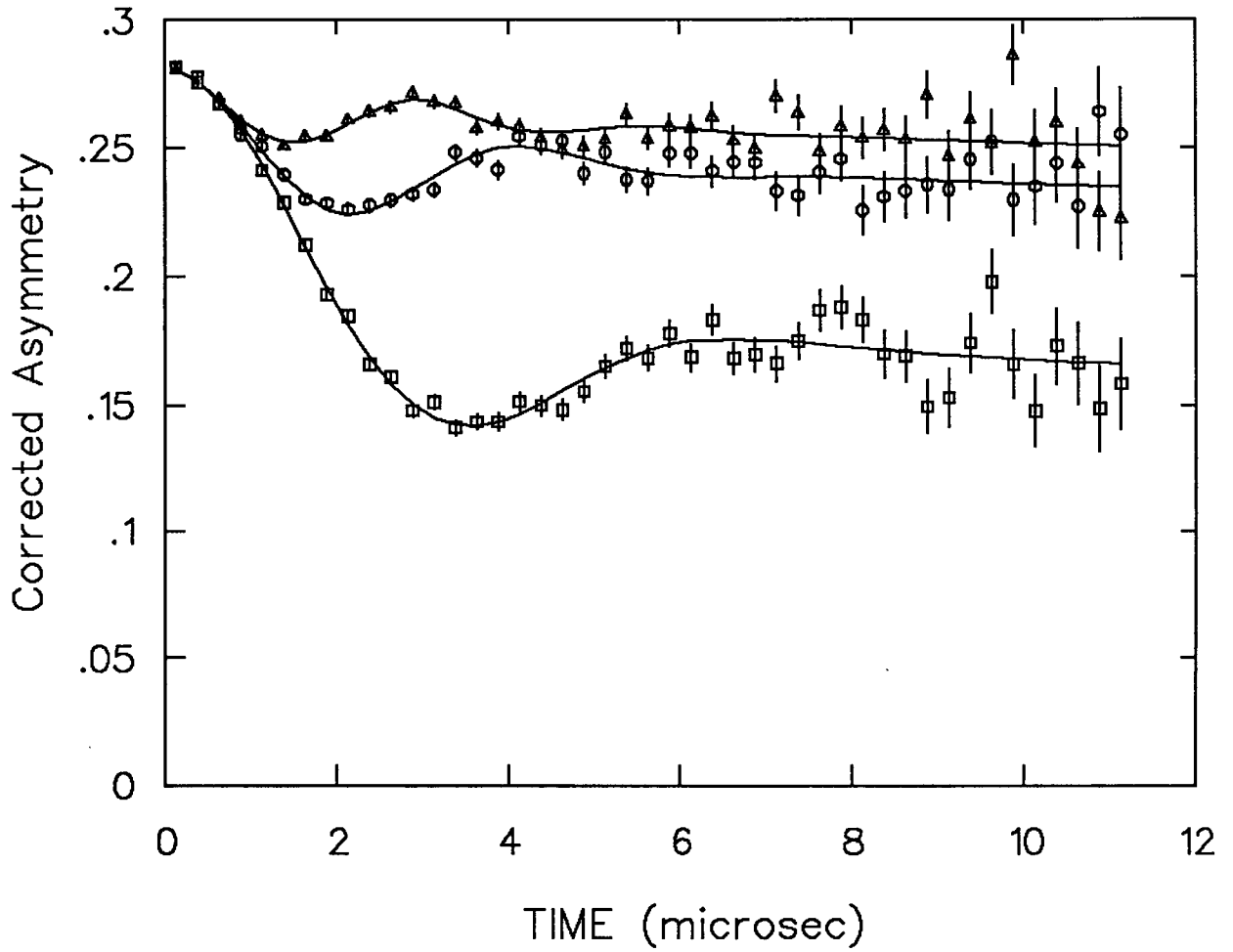


Figure 5.3: WLF TD- μ SR Spectra for applied fields 8 G (squares), 16 G (circles) and 24 G (triangles). Muons are nearly static - $T=45\text{K}$

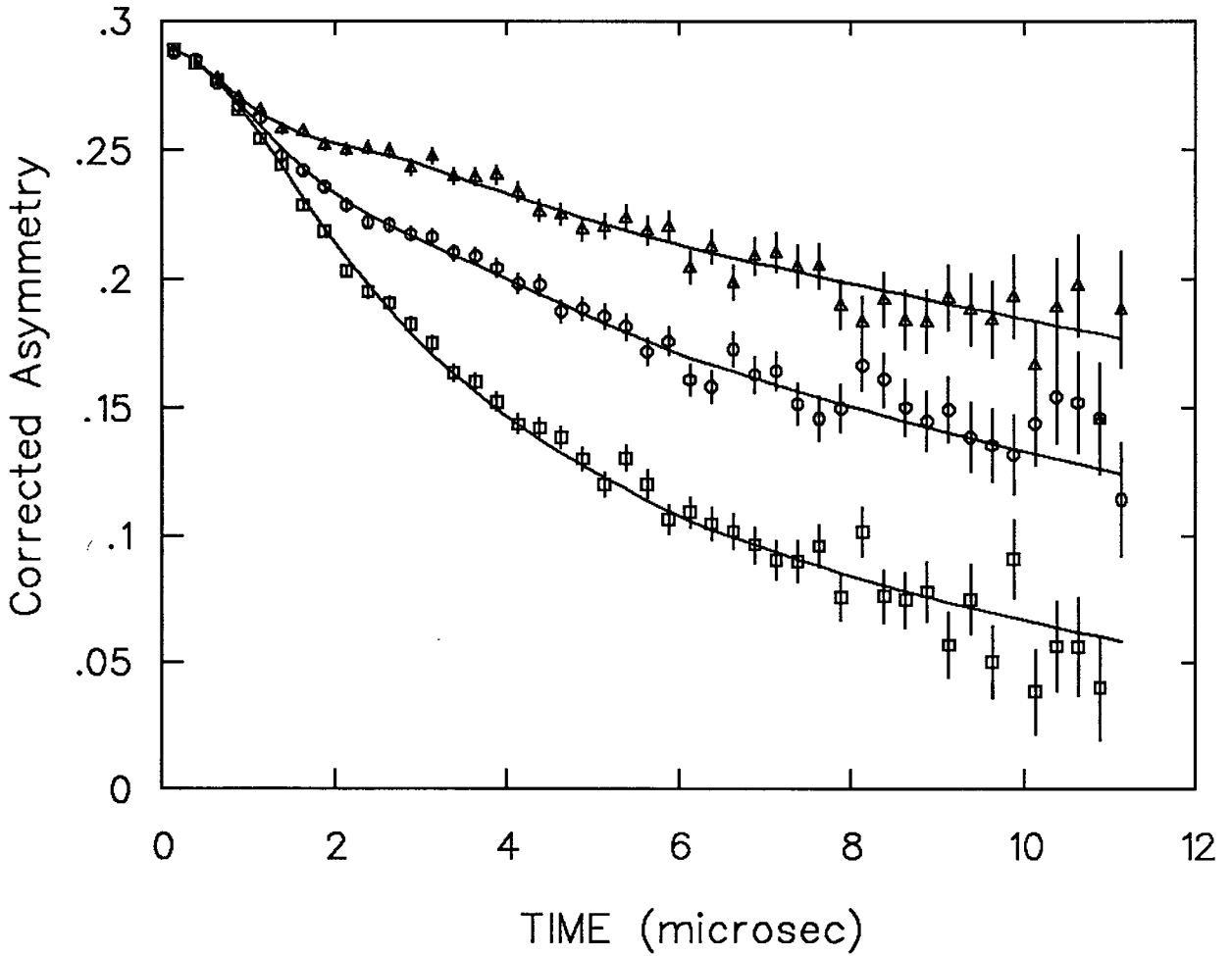


Figure 5.4: WLF TD- μ SR Spectra for applied fields 8 G (squares), 16 G (circles) and 24 G (triangles). Muons are diffusing rapidly - $T=150$ K

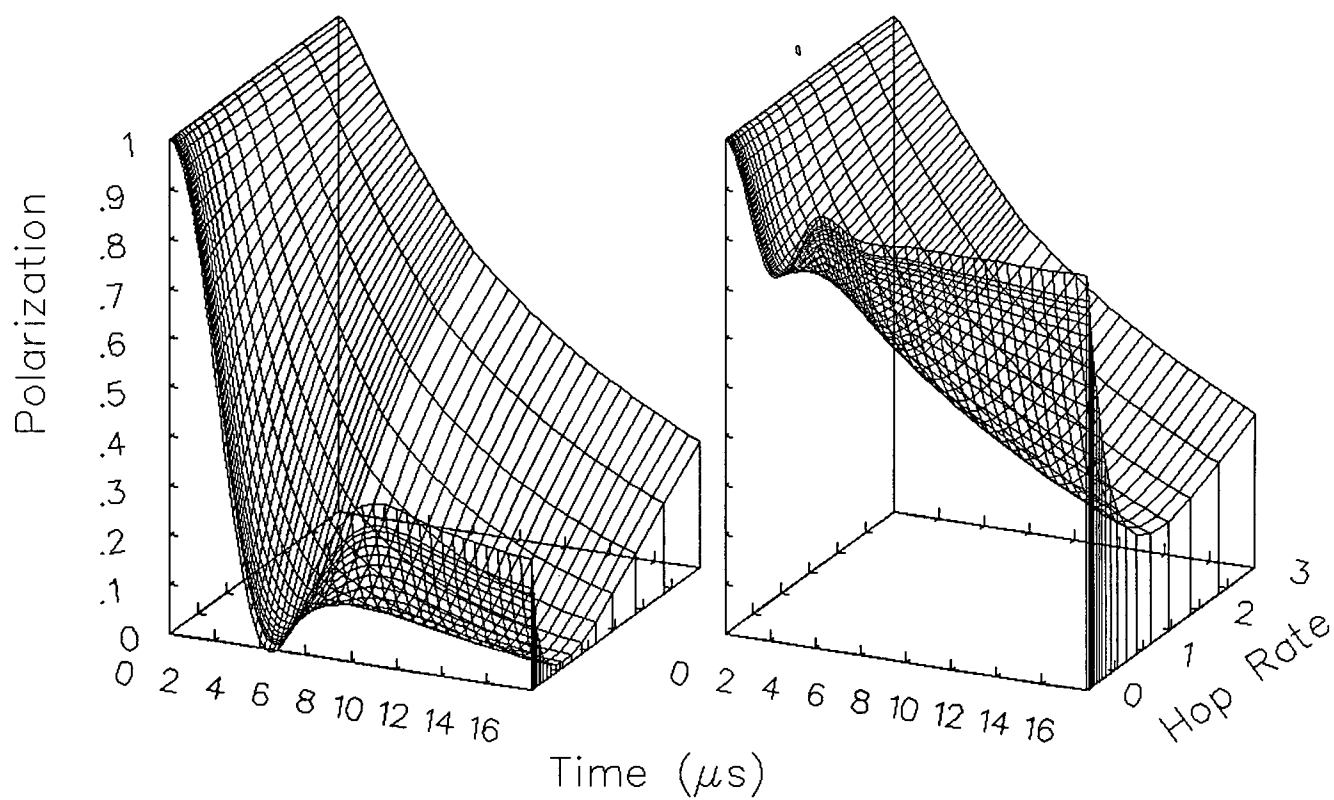


Figure 5.5: Dynamic relaxation functions in ZF and 15 G longitudinal field, with hop rate ν_{hop} between 0 and $3 \mu\text{s}^{-1}$.

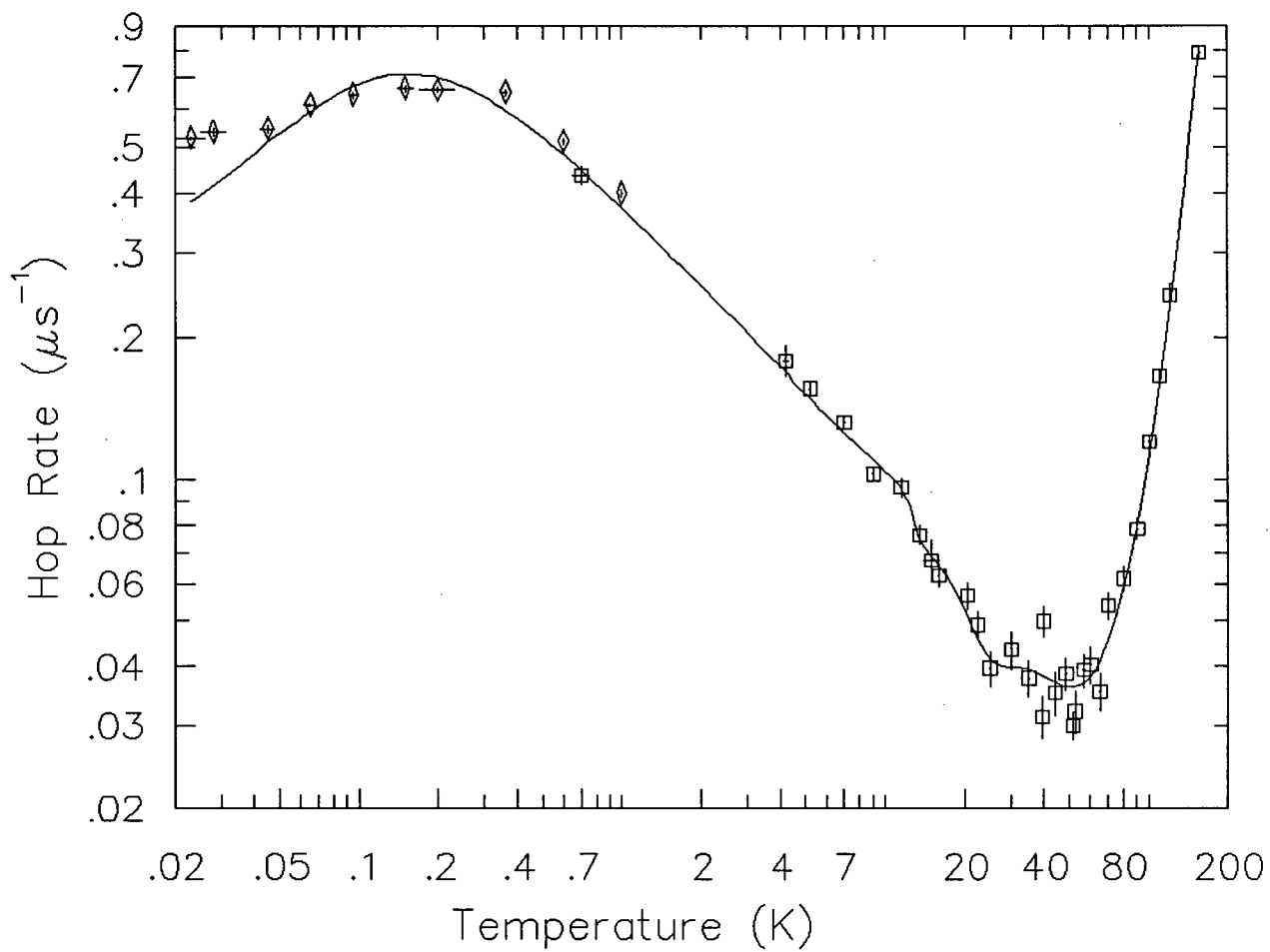


Figure 5.6: Muon hop rate over the temperature range $20 \text{ mK} < T < 200 \text{ K}$.

Chapter 6

Conclusions

We have studied the diffusive motion of positive muons implanted in high purity copper in the temperature range $20 \text{ mK} < T < 150 \text{ K}$. The muon hop rate has been extracted through its effect on the time evolution of the muon polarization. This technique has been found to be the most sensitive to slow hopping when the spin relaxation is studied in a weak longitudinal magnetic field. The static muon polarization has been calculated exactly for the microscopic spin Hamiltonian, considering the muon interacting with its six nearest neighbours and the applied magnetic field through the Zeeman, electric quadrupole and dipolar interactions.

We find that the temperature dependence of the muon hop rate can be well described by Kondo's theory of quantum diffusion. This theory describes four different interactions of the muon with the host metal, each of which affects the hop rate. The apparently anomalous increase of the diffusion rate with decreasing temperature has been seen to result from "electron drag" which follows from the near-orthogonality of the screening conduction electron wavefunctions at different sites. The eventual decrease in the muon hop rate at the lowest temperatures studied provides evidence for a residual broadening of muon energy levels of order 0.4 K which is apparently temperature independent. Such a broadening could arise from the spread in energies of the

muon self-trapped state, associated with the $^{63}\text{Cu}/^{65}\text{Cu}$ isotope mixture. Experiments on single crystals of isotopically pure copper would be of interest in clarifying the origin of this residual energy broadening.

We have also determined that the muon only occupies the octahedral site at the center of the copper unit cell over all temperatures studied. The electric quadrupole frequency of the nearest neighbour copper nuclei has been found to be $\omega^Q = -3.314(7)\mu\text{s}^{-1}$ using level-crossing resonance. Time differential measurements of the level-crossing have allowed us to determine the sign as well as the magnitude of the Cu electric quadrupole frequency, in contrast to transverse field measurements which are only sensitive to its magnitude. This demonstrates the extreme sensitivity of the LCR technique to the details of the microscopic spin environment of the muon.

Bibliography

- [1] O. Hartmann. Quadrupole Influence on the Dipolar-Field Width for a Single Interstitial in a Metal Crystal. *Physical Review Letters*, **39**:832, 1977.
- [2] K. W. Kehr. Theory of the Diffusion of Hydrogen in Metals. In *Hydrogen in Metals I*. Springer-Verlag, 1978.
- [3] Y. Fukai and H. Sugimoto. Diffusion of Hydrogen in Metals. *Advances in Physics*, **34**:263, 1985.
- [4] I. I. Gurevich, E. A. Mel'eshko, I. A. Muratova, B. A. Nikol'sky, V. S. Roganov, V. I. Selivanov, and B. V. Sokolov. Dipole Interactions and Diffusion of μ^+ Meson in Copper. *Physics Letters*, **40A**:143–144, 1972.
- [5] M. Camani, F. N. Gyax, W. Ruegg, A. Schenck, and H. Schilling. Positive Muons in Copper: Detection of an Electric Field Gradient at the Neighbor Cu Nuclei and Determination of the Site of Localization. *Phys. Rev. Lett.*, **39**:836, 1977.
- [6] M. Camani, D. G. Fleming, F. N. Gyax, W. Ruegg, A. Schenck, , and H. Schilling. New Results on the Depolarisation of Positive Muons in Copper. *Hyperfine Interactions proceedings μ SR1*, **6**:265–270, 1979.
- [7] O. Hartmann, L. O. Norlin, A. Yaounac, J. Le Hericy, E. Karlsson, and T. O.

- Niinikoski. Low Temperature Studies of Muon Localization in Copper. *Hyp.Int. ,Proceedings of μ SR2*, 8:533–538, 1981.
- [8] J-M. Welter, D. Richter, R. Hempelmann, O. Hartmann, E. Karlsson, L. O. Norlin, T. O. Niinikoski, and D. Lenz. Muon Diffusion in Copper Below 2K. *Z. Phys. B*, 52:303, 1983.
- [9] C. W. Clawson, K. M. Crowe, S. E. Kohn, S. S. Rosenblum, C. Y. Huang, J. L. Smith, and J. H. Brewer. Low Temperature Diffusion of Positive Muons in Copper. *Physica*, 109:2164–2167, 1982.
- [10] C.W. Clawson. *Zero-field Spin Relaxation of the Positive Muon in Copper*. PhD thesis, University of California at Berkely, 1982.
- [11] R. Kadono, T. Matsuzaki, K. Nagamine, T. Yamazaki, D. Richter, and J. M. Welter. Diffusion of Positive Muons in Copper Detected by Zero Field μ SR. *Hyperfine Interactions (proceedings of μ SR4)*, 31:???, 1986.
- [12] R. Kadono. *Quantum Diffusion of Positive Muon in Copper*. PhD thesis, University of Tokyo, 1987.
- [13] A. Seeger. *Physics Letters*, 93A:33, 1982.
- [14] A. Seeger. Low-temperature Mobility of Positive Muons in Pure Copper. *μ SR Newsletter*, 27:1356–1366, 1982.
- [15] J. H. Brewer, M. Celio, D. R. Harshman, R. Keitel, S. R. Kreitzman, G. M. Luke, D. R. Noakes, R. E. Turner, E. J. Ansaldo, c. W. Clawson, K. . Crowe, and C. Y. Huang. Determination of Very Slow μ^+ Hop Rates in Cu by LLF- μ SR. *Hyperfine Interactions (proceedings of μ SR4)*, 31:191–197, 1986.

- [16] J. H. Brewer, S. R. Kreitzman, D. R. Noakes, E. J. Ansaldo, D. R. Harshman, and R. Keitel. Observation of Muon-Fluorine “Hydrogen Bonding” in Ionic Crystals. *Physical Review*, **33**:7813, 1986.
- [17] S. R. Kreitzman, J. H. Brewer, D. R. Harshman, R. Keitel, D. Ll. Williams, K. M. Crowe, and E. J. Ansaldo. Longitudinal-Field μ^+ Spin Relaxation via Quadrupolar Level-Crossing Resonance in Cu at 20K. *Phys. Rev. Lett.*, 56:181, 1986.
- [18] S. H. Neddermeyer and C. D. Anderson. Note on the Nature of Cosmic-Ray Particles. *Physical Review*, **51**:884, 1937.
- [19] J. C. Street and E. C. Stevenson. New Evidence for the Existence of a Particle of Mass Intermediate Between the Proton and Electron. *Physical Review*, **52**:1003, 1937.
- [20] T. D. Lee and C. N. Yang. Parity Non-Conservation and a Two-Component Theory of the Neutrino. *Physical Review*, **105**:1671, 1957.
- [21] L. M. Lederman R. L. Garwin and M. Weinrich. Observations of the Failure of Conservation of Parity and Charge Conjugation in Meson Decays: the Magnetic Moment of the Free Muon. *Physical Review*, **105**:1415, 1957.
- [22] J. I. Friedman and V. L. Telegdi. Nuclear Emulsion Evidence for Parity Nonconservation in the Decay Chain $\pi^+ - \mu^+ - e^+$. *Physical Review*, **105**:1681, 1957.
- [23] J. H. Brewer and K. M. Crowe. Advances in Muon Spin Rotation. *Ann. Rev. Nucl. Par. Sci.*, **28**:239, 1978.
- [24] J. Chappert and R. I. Grynspan, editors. *Muons and Pions in Materials Research*. North-Holland, 1987.

- [25] A. Schenck. *Muon Spin Rotation Spectroscopy*. Adam Hilger Ltd., 1985.
- [26] S. F. J. Cox. Implanted Muon Studies in Condensed Matter Science. *J. Phys. C.*, **20**:3187, 1987.
- [27] D. E. Casperon *et al.* New Precise Value for the Muon Magnetic Moment and Sensitive Test of the Theory of the hfs Interval in Muonium. *Physical Review Letters*, **38**:956, 1977.
- [28] K. M. Crowe, J. F. Hague, J. E. Rothberg, A. Schenck, D. L. Williams, R. W. Williams, and K. K. Young. Precise Measurement of the Magnetic Moment of the Muon. *Physical Review*, **D5**:2145, 1972.
- [29] J. Bailey *et al.* Precise Measurement of the Anomalous Magnetic Moment of the Muon. *Nuovo Cimento*, **9A**:369, 1972.
- [30] Y. J. Uemura. Probing Spin Glasses with Zero Field μ SR. *Hyperfine Interactions*, **8**:739, 1981.
- [31] R.F. Kiefl, S.R. Kreitzman, M. Celio, R. Keitel, G.M. Luke, J.H. Brewer, D.R. Noakes, P.W. Percival, T. Matsuzaki, and K. Nishiyama. Resolved nuclear hyperfine structure of a muonated free radical using level-crossing spectroscopy. *Physical Review*, **A34**:681, 1986.
- [32] P.W. Percival, R.F. Kiefl, S.R. Kreitzman, D.M. Garner, S.F.J. Cox, G.M. Luke, J.H. Brewer, K. Nishiyama, and K. Venkateswaren. Muon Level-Crossing Spectroscopy of Organic Free Radicals. *Chemical Physics Letters*, **133**:465, (1987).
- [33] R.F. Kiefl, M. Celio, T. L. Estle, G.M. Luke, S.R. Kreitzman, J.H. Brewer, D.R. Noakes, E. J. Ansaldo, and K. Nishiyama. GaAs LCR. *Physical Review Letters*, **58**:1780, (1987).

- [34] R. F. Kiefl, M. Celio, T. L. Estle, S. R. Kreitzman, G. M. Luke, T. M. Riseman, and E. J. Ansaldo. ^{29}Si Hyperfine Structure of Anomalous Muonium in Silicon: Proof of the Bond-Centered Model. *Physical Review Letters*, **60**:224, 1988.
- [35] G. Aeppli, R. J. Cava, E. J. Ansaldo, J. H. Brewer, S. R. Kreitzman, G. M. Luke, D. R. Noakes, and R. F. Kiefl. Magnetic Penetration Depth and Flux-Pinning Effects in High- T_c Superconductor $\text{La}_{1.85}\text{Sr}_{0.15}\text{CuO}_4$. *Physical Review B*, **35**:7129, 1987.
- [36] D. R. Harshman, G. Aeppli, E. J. Ansaldo, B. Batlogg, J. H. Brewer, J. F. Carolan, R. J. Cava, M. Celio, A. C. D. Chaklader, W. N. Hardy, S. R. Kreitzman, G. M. Luke, D. R. Noakes, and M. Senba. Temperature Dependence of the Magnetic Penetration Depth in the High- T_c Superconductor $\text{Ba}_2\text{YCu}_3\text{O}_{9-\delta}$: Evidence for Conventional S-Wave Pairing. *Physical Review B*, **36**:2386, 1987.
- [37] J. H. Brewer *et al.* μ^+ SR Study of Antiferromagnetism and Superconductivity in Oxygen Deficient $\text{YBa}_2\text{Cu}_3\text{O}_x$. *Physical Review Letters*, **60**:1073, 1988.
- [38] G. M. Luke, R. F. Kiefl, J. H. Brewer, T. M. Riseman, D. Ll. Williams, J. R. Kempton, S. R. Kreitzman, E. J. Ansaldo, N. Kaplan, Y. J. Uemura, W. N. Hardy, J. F. Carolan, M. E. Hayden, and B. X. Yang. Antiferromagnetism and Superconductivity in $\text{YBa}_2\text{Cu}_3\text{O}_x$ Studied by μSR . *Physica*, **C153-155**, 1988.
- [39] A. E. Pifer, T. Bowen, and K. R. Kendall. A High Stopping Power μ^+ Beam. *Nuclear Instruments and Methods*, **135**:39, 1976.
- [40] T. Bowen. The Surface Muon Beam. *Physics Today*, July:23, 1985.
- [41] J. H. Brewer, K. M. Crowe, F. N. Gygax, and A. Schenck. *Muon Physics*, volume 3, chapter 7. Academic Press, 1975.

- [42] T. Holstein. Studies of Polaron Motion. *Ann. of Physics*, **8**:343, 1959.
- [43] Flynn and Stoneham. Quantum Theory of Diffusion with Application to Light Interstitials in Metals. *Phys. Rev.*, **B1**:3966, 1980.
- [44] D. Emin. The Positive Muon as a Small Polaron. *Hyperfine Interactions*, **8**:515, 1981.
- [45] C. P. Slichter. *Principles of Magnetic Resonance*. Springer-Verlag, 1978.
- [46] S. R. Kreitzman, D. Ll. Williams, N. Kaplan, J. Kempton, and J. H. Brewer. Spin Echoes for μ^+ SR Spectroscopy. *preprint*, 1988.
- [47] J. M. Rowe, J. J. Rush, L. A. de Graaf, and G. A. Ferguson. Neutron Quasielastic Scattering Study of Hydrogen Diffusion in a Single Crystal of Palladium. *Physical Review Letters*, **29**:1250, 1972.
- [48] J. H. Van Vleck. The Dipolar Broadening of Magnetic Resonance Lines in Crystals. *Physical Review*, **74**:1168, 1948.
- [49] R. S. Hayano, Y. J. Uemura, J. Imazato, N. Nishida, T. Yamazaki, and R. Kubo. Zero- and Low-field Spin Relaxation Studied by Positive Muons. *Phys. Rev.*, **B20**:850, 1979.
- [50] C. W. Clawson, K. M. Crowe, S. S. Rosenblum, S. E. Kohn, C. Y. Huang, J. L. Smith, and J. H. Brewer. Low-Temperature Mobility of Positive Muons in Copper. *Phys. Rev. Lett.*, **51**:114, 1983.
- [51] R. Kadono, J. Imazato, K. Nishiyama, K. Nagamine, T. Yamazaki, D. Richter, and J. M. Welter. μ^+ Diffusion in Copper Studied by Zero Field μ SR. *Hyperfine Interactions*, **17-19**:109, 1983.

- [52] R. Kadono, K. Nishiyama, K. Nagamine, and T. Matsuzaki. Muon Diffusion in Pure Bismuth: Evidence for an Extended Muon State. *preprint*, 1988.
- [53] E. Holzschuh and P. F. Meier. Zero-Field Spin Relaxation of Positive Muons. *Physical Review*, **B29**:1129, 1984.
- [54] A. Abragam. Magnetic Resonance – Spectrometry Through Level Crossing in Muon Physics. *C.R. Acad. Sci. Paris Ser. 2*, 299:95, (1984).
- [55] S.R. Kreitzman, J.H. Brewer, D.R. Harshman, R. Keitel, D.Ll. Williams, K.M. Crowe, and E.J. Ansaldo. LCR in Cu. *Phys. Rev. Letters.*, 56:181, (1986).
- [56] M. Heming, E. Roduner, B.D. Patterson, W. Odermatt, J. Schneider, Hp. Baumeler, H. Keller, and M. Savic. Detection of muonated free radicals through the effects of avoided level-crossing. *Chem. Phys. Letters*, 128:100, (1986).
- [57] G. Flik, J. Bradbury, W. Cooke, M. Leon, M. Paciotti, M. Schillaci, K. Maier, and A. Seeger. Pion Decay Site Spectroscopy in Copper. *Hyperfine Interactions (proceedings of μ SR4)*, 31:61–67, 1986.
- [58] V. G. Grebinnik, I. I. Gurevich, V. A. Zhukov, A. P. Manych, E. A. Meleshko, I. A. Muratova, B. A. Nikol'skii, V. I. Selivanov, and V. A. Suetin. Sub-Barrier Diffusion of μ^+ Mesons in Copper. *Sov. Phys. JETP*, 41:777–780, 1976.
- [59] A. Abragam. *Principles of Nuclear Magnetism*. Oxford, 1971.
- [60] H. Teichler. On the Theory of Muon Diffusion in Metals. *Physics Letters*, **64A**:78, 1977.
- [61] J. M. Welter, D. Richter, R. Hempelmann, O. Hartmann, E. Karlsson, L. O. Norlin, , and T. O. Niinikoski. Mobility of Muons in Cu Below 2K. *Hyp.Int.*

- (*Proceedings μ SR3 vol. 1*), 17-19:117–124, 1984.
- [62] O. Echt, H. Graf, E. Holzschuh, E. Recknagel, A. Weidingeer, and Th. Wichert. μ SR Study of Proton-Irradiated Aluminum and Copper at Low Temperatures. *Physics Letters*, **67A**:427, 1978.
- [63] T. Natsui, T. Hatano, Y. Suzuki, R. Yamamoto, M. Doyama, K. Nishiyama, J. Imazato, and K. Nagamine. Evidence against μ^+ Trapping in In and Deformed Cu Above Room Temperature. *Physics Letters*, **93A**:137, 1983.
- [64] R. Kadono, J. Imazato, K. Nishiyama, K. Nagamine, T. Yamazaki, D. Richter, and J. M. Welter. μ^+ Diffusion in Copper Studied by Zero Field μ SR. *Hyp.Int. (Proceedings μ SR3 vol.1)*, 17-19:109–116, 1984.
- [65] K. G. Petzinger. Zero Field Spin Relaxation Studies as a Probe of Positive Muon Diffusion Mechanisms. *Physics Letters*, **75A**:225, 1980.
- [66] K. G. Petzinger. The Effect of Traps on the Muon Spin Relaxation Function. *Hyperfine Interactions*, **8**:639, 1981.
- [67] M. Celio and P. F. Meier. Spin Relaxation of Positive Muons due to Dipolar Interactions. *Phys. Rev.*, **B27**:1908, 1983.
- [68] O. Hartmann, E. Karlsson, E. Wäckelgård, R. Wäppling, D. Richter, R. Hempelmann, and T. O. Niinikoski. Low Temperature Diffusion and Trapping of Muons in Aluminum: New Experiments and Comparison with Theory. *Hyperfine Interactions*, **31**:223, 1986.
- [69] O. Hartmann, E. Karlsson, E. Wäckelgård, R. Wäppling, D. Richter, R. Hempelmann, and T. O. Niinikoski. Diffusion and Trapping of Muons in Aluminum: New

- Experiments and Comparison with Kondo Theory. *Physical Review*, **B37**:4425, 1988.
- [70] J. A. Brown, R. H. Heffner, R. L. Hutson, S. Kohn, M. Leon, C. E. Olsen, M. E. Schillaci, S. A. Dodds, T. L. Estle, D. A. Vanderwater, P. M. Richards, and O. D. McMasters. Muon Depolarization by Paramagnetic Impurities in Nonmagnetic Metals. *Physical Review Letters*, **47**:261, 1981.
- [71] O. Hartmann, E. Karlsson, R. Wäppling, D. Richter, R. Hempelmann, K. Schulze, B. Patterson, E. Holzschuh, W. Kündig, and S. F. J. Cos. Trap Identification and Impurity-Induced Localization of Muons in Nb. *Physical Review*, **B27**:1943, 1983.
- [72] W. Schwarz, E. H. Brandt, K.-P. Döring, K. FÜRDERER, M. Gladisch, D. Herlach, G. Majer, H.-J. Munding, H. Orth, A. Seeger, and M. Schmolz. Muons in Type II Superconductors: μ^+ Diffusion in Ultra-Pure Niobium. *Hyperfine Interactions*, **31**:247, 1986.
- [73] E. H. Brandt. Private Communication, 1988.
- [74] H. Graf, G. Balzer, E. Recknagel, A. Weidinger, and R. Y. Grynszpan. *Physical Review Letters*, **44**:1333, 1980.
- [75] E. Yagi, H. Bossy, K. P. Döring, M. Gladisch, D. herlack, H. Matsui, H. Orth, G. zu Putlitz, A. Seeger, and J. Vetter. Longitudinal Muon Spin Relaxation in α -Iron in High Magnetic Fields. *Hyperfine Interactions*, **8**:553, 1981.
- [76] E. Yagi, G. Flik, K. FÜRDER, N. Haas, D. Herlach, J. Major, A. Seeger, W. Jacobs, M. Krause, M. Krauth, H. J. Munding, and H. Orth. Quantum Diffusion of Positive Muons in Iron. *Physical Review*, **B30**:441, 1984.

- [77] J. Kondo. Muon Diffusion in Metals. *Hyperfine Interactions*, **31**:117, 1986.
- [78] R. Kubo and T. Toyabe. A Stochastic Model for Low field Resonance and Relaxation. In Blinc, editor, *Magnetic Resonance and Relaxation*, page 810, 1966.
- [79] J. H. Brewer, D. R. Harshman, R. Keitel, S. R. Kereitzman, G. M. Luke, D. R. Noakes, R. E. Turner, and E. J. Ansaldo. Thermal Hopping of μ^+ Between F- μ -F Centres in NaF. *Hyperfine Interactions*, **32**:677, 1986.
- [80] M. Celio and P. F. Meier. Exact Calculation of the Muon Polarization Function. *Hyperfine Interactions*, **17-19**:435, 1983.
- [81] M. Celio. New Method to Calculate the Muon Polarization Function. *Physical Review Letters*, **56**:2720, 1986.
- [82] M. Celio. A New Technique to Calculate the Muon Polarization Function. *Hyperfine Interactions*, **31**:41, 1986.
- [83] K. W. Kehr, G. Honig, and D. Richter. Stochastic Theory of Spin Depolarization of Muons Diffusing in the Presence of Traps. *Zeitschrift für Physik B*, **32**:49, 1978.
- [84] Y. J. Uemura. Spin Relaxation of Positive Muon in ZrH₂ and MnO. Master's thesis, University of Tokyo, 1979.
- [85] M. Celio. Corrections to the Strong Collision Model. *Hyperfine Interactions*, **31**:153, 1986.
- [86] Yu. Klinger and M. I. Klinger. Theory of Quantum Diffusion of Atoms in Crystals. *J. Phys. C: Solid State Physics*, **7**:2791, 1974.
- [87] J. Kondo. Localized Atomic States in Metals. *Physica*, **84B**:40, 1984.

- [88] P. W. Anderson. Infrared Catastrophe in Fermi Gases with Local Scattering Potentials. *Physical Review Letters*, **18**:1049, 1967.
- [89] J. Jäckle and K. W. Kehr. Calculation of the Diffusion Constant of Muon in Metals at Low Temperatures. *Journal of Physics F: Metal Physics*, **13**:753, 1983.
- [90] J. Kondo. Diffusion of Light Interstitials in Metals. *Physica*, **126B**:377, 1984.
- [91] K. Yamada, A. Sakurai, S. Miyazima, and H. S. Hwang. Application of the Orthogonality Theorem to the Motion of a Charged Particle in Metals. II. *Progress of Theoretical Physics*, **75**:1030, 1986.
- [92] K. Yamada. Diffusion of Positive Muon and Orthogonality Theorem. *Progress of Theoretical Physics*, **72**:195, 1984.
- [93] K. Yamada, A. Sakurai, and S. Miyazima. A Closed Form Solution for the Hopping Rate of Charged Particles in Metals. *Progress of Theoretical Physics*, **73**:1342, 1985.
- [94] K. Yamada and K. Yosida. Orthogonality Catastrophe for a System of Interacting Electrons III. *Progress of Theoretical Physics*, **68**:1504, 1982.
- [95] K. Yamada, A. Sakurai, and M. Takeshige. Application of the Orthogonality Theorem to the Motion of a Charged Particle in Metals. *Progress of Theoretical Physics*, **70**:73, 1983.
- [96] Per Hedegård. Path Integral Approach to Quantum Diffusion in Metals. *Hyperfine Interactions*, **31**:135, 1986.
- [97] H. Grabert, U. Weiss, and H. R. Schober. Quantum Tunneling of Light Particles in Metals. *Hyperfine Interactions*, **31**:147, 1986.

- [98] D. Richter. The Motion of Light Interstitials in Metals: Recent Experiments. *Hyperfine Interactions*, **31**:169, 1986.
- [99] D. M. Garner. *Application of the Muonium Spin Rotation Technique to a Study of the Gas Phase Chemical Kinetics of Muonium Reactions with the Halogens and Hydrogen Halides*. PhD thesis, University of British Columbia, 1979.
- [100] J. L. Beveridge, J. Doornbos, and D. M. Garner. Muon Facilities at TRIUMF. *Hyperfine Interactions*, **32**:907, 1986.
- [101] R. Keitel and J. T. Worden. The μ SR Facility at TRIUMF. *Hyperfine Interactions*, **32**:901, 1986.
- [102] J. L. Beveridge, J. Doornbos, D. M. Garner, D. J. Arseneau, I. D. Reid, and M. Senba. A Spin Rotator for Surface μ^+ Beams on the New M20 Muon Channel at TRIUMF. *Nuclear Instruments and Methods in Physics Research*, **A240**:316, 1985.
- [103] G. F. Knoll. *Radiation Detection and Measurement*. John Wiley & Sons, 1979.
- [104] O. V. Lounasmaa. *Experimental Principles and Methods below 1K*. Academic Press, 1974.
- [105] G. K. White. *Experimental Techniques in Low-Temperature Physics*. Oxford University Press, 1979.
- [106] H. Marshak. Nuclear Orientation Thermometry. *Journal of Research of the National Bureau of Standards*, **88**:175, 1983.
- [107] F. James and M. Roos. MINUIT—Function Minimization and Error Analysis. Technical report, CERN, 1985.

- [108] B. Effenberger, W. Kunold, W. Oesterle, M. Schneider, L. M. Simons, R. Abela, and J. Wüest. Determination of the Spectroscopic Quadrupole Moments of $^{75}_{33}\text{As}$ and $^{63}_{29}\text{Cu}$. *Zeitschrift für Physik A*, **309**:77, 1982.
- [109] R. M. Sternheimer. Quadrupole Shielding and Antishielding Factors for Several Atomic Ground States. *Physical Review*, **A6**:1702, 1972.
- [110] P. Jena, S. G. Das, and K. S. Singwi. Electric-Field Gradient at Cu Nuclei Due to an Interstitial Positive Muon. *Physical Review Letters*, **40**:264–266, 1978.
- [111] A. Seeger. Diffusion and Localization of Positive Muons and Pions in Copper. *μSR Newsletter*, **34**:1880, 1988.
- [112] S. R. Kreitzman. Muon Level Crossing Resonance Resonance in Diamagnetic Systems – General Considerations. *Hyperfine Interactions*, **31**:13, 1986.
- [113] J. H. Brewer, S. R. Kreitzman, K. M. Crowe, C. W. Clawson, and C. Y. Huang. μ^+ Diffusion in Copper Below 4K Reconfirmed by LF- μ^+ SR. *Phys. Lett. A*, **120**:199, 1987.
- [114] R. Kadono, J. Imazato, T. Matsuzaki, K. Nishiyama, K. Nagamine, T. Yamazaki, D. Richter, and J. M. Welter. Quantum Diffusion of Positive Muon in Copper. *preprint*, 1988.
- [115] M. Celio. Private Communication, 1986.
- [116] J. M. Ziman. *Principles of the Theory of Solids*. Cambridge University Press, 1972.
- [117] M. J. Puska and R. M. Nieminen. Atoms Embedded in an Electron Gas: Phase Shifts and Cross Sections. *Physical Review*, **27**:6121, 1983.

- [118] H. Sugimoto. Effects of Energy Disorder on the Quantum Diffusion of Light Interstitials in Metals: Average Jump Rate. *Journal of the Physical Society of Japan*, **55**:1687, 1986.

Appendix A

Muon Diffusion Rates in Copper

Temperature (K)	Hop Rate (μs^{-1})
0.023(2)	0.522(4)
0.045(3)	0.55(1)
0.028(3)	0.538(9)
0.065(3)	0.611(4)
0.095(3)	0.64(1)
0.15(1)	0.66(1)
0.20(3)	0.66(1)
0.360(5)	0.65(1)
0.60(1)	0.514(8)
0.70(5)	0.44(2)
1.00(1)	0.399(7)
4.2(1)	0.18(1)
5.18(3)	0.156(6)
7.00(5)	0.132(4)
9.00(5)	0.103(4)
11.50(5)	0.096(4)
13.50(5)	0.076(4)
15.0(10)	0.068(7)
16.0(1)	0.062(3)
20.50(5)	0.056(4)
22.50(5)	0.049(3)
25.0(1)	0.040(3)
30.00(5)	0.043(4)
35.0(1)	0.038(3)
39.50(5)	0.031(3)
40.00(5)	0.050(4)
44.00(5)	0.035(4)
48.50(5)	0.039(3)
51.5(1)	0.030(2)
52.5(1)	0.032(3)
56.5(5)	0.039(3)
60.0(1)	0.040(4)
65.0(5)	0.035(3)
70.0(2)	0.054(4)
80.0(1)	0.062(4)
90.0(1)	0.079(4)
100.0(5)	0.121(4)
109.8(3)	0.165(6)
119.7(3)	0.25(1)
156.0(10)	0.79(2)